

# Caderno de RESUMOS

XLV Congresso Brasileiro de Aplicações de Vácuo na Indústria e na Ciência

> Balneário Camboriú - SC 11 a 13 de Novembro de 2024

> > ISBN: 978-65-01-61693-3 DOI: 10.17563/cbravic.2024





Dados Internacionais de Catalogação na Publicação (CIP)

C749 Congresso Brasileiro de Aplicações de Vácuo na Indústria e na Ciência (45. : 2024 : Balneário Camboriú, SC).

Caderno de resumos do XLV CBrAVIC [recurso eletrônico] / organizadores: Luiz Antonio Alves, Nazir Monteiro dos Santos, Julio César Sagás. – Balneário Camboriú, SC: UDESC, 2023.

ISBN: 978-65-01-61693-3 DOI: 10.17563/cbravic.2024

1. Ciências aplicadas. 2. Indústria. 3. Tecnologia. I. Alves, Luiz Antonio. II. Santos, Nazir Monteiro dos. III. Sagás, Julio César. IV. Congresso Brasileiro de Aplicações de Vácuo na Indústria e na Ciência. V. Universidade do Estado de Santa Catarina.

CDU 6 CDD 60

Ficha elaborada pela bibliotecária Priscila Rodrigues dos Santos CRB1/3381





# **PatrOcinadOres**



### SILVER





# **APOIO**





# ORGANIZAÇÃO







# Comitê Organizador

Luiz Antonio Alves | UDESC - CESFI Oséias Alves Pessoa I UDESC - CESFI Luiz Adolfo Hegele Jr. | UDESC - CESFI Fábio Ullmann Furtado de Lima | UDESC - CESFI José Carlos de Souza I UDESC - CESFI Muriel de Pauli | UDESC - CESFI Luis César Fontana I UDESC - CCT Julio César Sagás | UDESC - CCT Teresa Tromm Steffen | UDESC - CCT Júlia Karnopp | UDESC - CCT Francisco Tadeu Degasperi | Fatec-SP / CEETEPS Nazir Monteiro dos Santos I IEAv Pedro Augusto de Paula Nascente | UFSCar Carlos Roberto Grandini | UNESP - Campus Bauru/SP Joel Stryhalski | IFSC - Jaraguá do Sul Francisco Alfaro I UFSC - Joinville Rodrigo Perito Cardoso | UFSC - Florianópolis Cristiani Campos Plá Cid | UFSC - Florianópolis

# Diretoria Executiva SBV

Presidente: Nazir Monteiro dos Santos (FATEC)

1º Vice Presidente: Luis Cesar Fontana (UDESC)

2º Vice Presidente: Maria Lucia Pereira da Silva (USP/FATEC)

1º Diretor Secretário: Carlos Roberto Grandini (UNESP)

2º Diretor Secretário: Francisco Tadeu Degasperi (FATEC)

1º Diretor Tesoureiro: Rogério Pinto Mota (UNESP)

2º Diretor Tesoureiro: Antonio Renato Bigansolli (UFRRJ)

Diretor Científico: Luciana Sgarbi Rossino (FATEC)

Diretor Cultural: Júlio César Sagas (UDESC)





# Comitê Científico

Dra. Adriana Silva | INPE - Campus São José dos Campos/SP

Dr. Adriano Gonçalves dos Reis | UNESP - Campus São José dos Campos/SP

Dra. Ana Neilde R Silva | USP - Campus São Paulo/SP

Dr. André Ricardo Marcondes | INPE – Campus São José dos Campos/SP

Ms. Ângelo Luiz Gobbi | LNNano - Campinas/SP

Dr. Antonio Renato Bigansolli | UFRRJ - Campus Seropédica/RJ Dr.

Carlos Roberto Grandini | UNESP - Campus Bauru/SP

Dr. Cícero Rafael Cena da Silva | UFMS - Campus Campo Grande/MS

Dr. Clodomiro Alves Júnior | UFERSA - Campus Mossoró/RN

Dra. Cristiane Costa Wachesk | UNIFESP - Campus São Paulo/SP

Dra. Danieli Aparecida Pereira Reis | UNIFESP - Campus São José dos Campos/SP

Dra. Deborah Cristina Ribeiro dos Santos | SBV - Guaratinguetá/SP

Dr. Durval Rodrigues Júnior | EEL/USP - Campus Lorena/SP

Dra. Elaine Conceição de Oliveira | Fatec-So / CEETEPS

Dra. Elidiane Cipriano Rangel | UNESP - Campus Sorocaba/SP

Dra. Érica Freire Antunes | INPE - Campus São José dos Campos/SP

Dr. Evaldo José Corat | INPE - Campus São José dos Campos/SP Dr.

Felipe Carneiro da Silva | Fatec-Cotia / CEETEPS

Dr. Fernando Luiz de C. Carvalho | UNESP – Campus São José dos Campos/SP

Dr. Francisco Tadeu Degasperi | Fatec-SP / CEETEPS

Dra. Gabriela Araújo Ranieri | UNIFEI - Campus Itajubá/MG Dr.

Gelson B. de Souza | UEPG - Campus Ponta Grossa/PR

Dr. Gilberto Petraconi Filho | ITA/CTA - São José dos Campos/SP

Dra. Graziela da Silva Savonov | INPE - Campus São José dos Campos/SP

Dr. João Moro | IFSP - Campus Bragança Paulista/SP

Dr. José Lucena Barbosa Júnior | UFRRJ - Campus Seropédica/RJ





# Comitê Científico

Dr. Julio César Sagás | UDESC - Campus Joinville/SC

Dr. Konstantin G. Kostov | UNESP - Campus Guaratinguetá/SP Dra.

Luciana Sgarbi Rosisno | Fatec-So / CEETEPS

Dr. Luis César Fontana | UDESC - Campus Joinville/SC

Dra. Maria Lúcia Pereira da Silva | USP - Campus São Paulo/SP

Dra. Maria Margareth da Silva | ITA/DCTA - São José dos Campos/SP

Dra. Marina Fuser Pillis | IPEN/CNEN - Campus São Paulo/SP

Dr. Mario Ueda | INPE - Campus São José dos Campos/SP

Dr. Mauricio Antônio Algatti | UNESP - Campus Guaratinguetá/SP Dr.

Michel Felipe Lima de Araújo | UDC - Campus Foz do Iguaçu/PR Dr.

Milton Eiji Kayama | UNESP - Campus Guaratinguetá/SP

Dr. Milton Sergio Fernandes de Lima | IEAv/ITA/DCTA - São José dos Campos/SP

Dr. Nilson Cristino Cruz | UNESP - Campus Sorocaba/SP

Dr. Pedro Augusto de Paula Nascente | UFSCar - Campus São Carlos/SP

Dr. Rafael Humberto Mota de Siqueira | IEAv/ITA/DCTA - São José dos Campos/SP

Dra. Renata Antoun Simao | UFRJ - Campus Rio de Janeiro/RJ

Dr. Roberto Yzumi Honda | UNESP - Campus Guaratinguetá/SP

Dr. Rodrigo Sávio Pessoa | ITA/CTA - São José dos Campos/SP

Dr. Rogério de Almeida Vieira | UNIFESP - Campus São Paulo/SP

Dr. Rogério Pinto Mota | UNESP - Campus Guaratinguetá/SP

Dr. Ronaldo Camara Cozza | FEI - Campus São Bernardo do Campo/SP / Fatec-Mauá

Dr. Rui de Góes Casqueira | UFRRJ - Campus Seropédica/RJ

Dra. Samantha de Fátima Magalhães Mariano | INPE - Campus São José dos Campos/SP

Dra. Silvia Pierre Irazusta | Fatec-So / CEETEPS

Dr. Steven Frederick Durrant | UNESP - Campus Sorocaba/SP





# Programação

HORÁRIO	SABADO 09/11	DOMINGO 10/11	SEGUNDA-FEIRA 11/11	TERÇA-FEIRA 12/11	QUARTA-FEIRA 13/11
08:00		30.11		1211	10/11
08:10					
08:30					
08:40					Palestra
08:50			ABERTURA DA SECRETARIA	PALESTRAS TÉCNICAS	The challenges of hydrogen in modern metallurgy
			(50 min)		The challenges of hydrogen in modern metallurgy
09:00	¢.		(800)0000	VÁCUO NA INDÚSTRIA (2h10m)	Matheus Tunes (University of Leoben)
09:10					Online - (50 min)
09:20			Palestra		Palestra
09:30				*Minicurso "Aprender ciência pode ser gostoso" Início: 9:00 h	
09:40			Magnetron Sputtering Coatin Technologies	inicio. 9.00 n	Surface Characterization of Energy Related
			Applied for Hydrogen Aircraft and Electrochromic Devices		Materials
09:50			Little and in only be field		Richard Haasch (University of Illinois Urbana-
10.00			Diao Xungang (Beihang University)		Champaign)
			(50 min)		(50 min)
10:10			COFFEE BREAK (20 min)	COFFEE BREAK (20 min)	COFFEE BREAK (20 min)
10:20				out the strain per trany	0011 00 01 00 11 (00 1111)
10:30			Palestra		
10:40			A dinâmica dos gases rarefeitos para o		
10:50			cálculo de condutâncias nos sistemas de		Apresentações orais (40 min)
10.00			vácuo	PALESTRAS TÉCNICAS	
11:00			- 1 - 1 - 1 - 1	VÁCUO NA INDÚSTRIA (1h55m)	
11:10			Felix Sharipov (UFPR) (50 min)	VACOO NA MOOSTRIA (1110011)	Palestra
11:20			(as min)		IEMIE/DONIES Vacuum Sustam Dasign
	1			*Minicurso "Aprender clência pode ser gostoso" Final: 12:00 h	IFMIF/DONES Vacuum System Design
11:30			Apresentações orais (40 min)	Final: 12:00 h	Marcelo Juni Ferreira (Lund University)
11:50					(50 min)
12:00					
12:10			100000000000000000000000000000000000000		ALMOÇO (1h30m)
12:25			ALMOÇO (2 h)		AEMOÇO (TIBOTI)
12:50	MINICURSOS	MINICURSOS		ALMOÇO (1h45m)	
13:30				National Section (Section )	
14:00			Palestra		
14:10			raicsua	Palestra	
14:20			The upgrade of the TCABR Tokamak and		
14.30			the need for a new wall conditioning system		PALESTRAS TÉCNICAS
14:40			Gustavo Paganini Canal (IFUSP)	Beam Welding	
14.40			(50 mln)	Milton Sergio Fernandes de Lima (IEAv)	METROLOGIA DE VÁCUO (2 h)
1150				(50 mln)	
14:50 15:00				A Section Control Cont	
15:10				Palestra	
15:20				Desaflos Estruturais e Tecnológicos da Indústria	
45.00			Apresentações orais (60 min)	de Óleo e Gás na Era da Transição Energética	
15:30					COFFEE BREAK (20 min)
15:40				Luiz Adolfo Hegele Jr (UDESC/CESFI) (50 mln)	COFFEE BREAK (20 IIIII)
10.40				(30 min)	
15:50			COFFEE BREAK (20 min)	COFFEE BREAK (20 min)	Dalestro
16:00			22.122.222.222		Palestra
16:10			Palactes		SIRIUS's Beamline Vacuum Review and ORION's
1000000			Palestra		Challenges for UHV Applications
16:20			Histórico da tecnologia de plasma na UFSC:		Gustavo L. M. P. Rodrigues (LNLS)
			cases de sucesso e desenvolvimento de		(50 min)
16:30			novas alternativas de processamentos assistidos por plasma	Apresentações orais (60 min)	,
16:40			assistitus pui piasitia		
10.40			Aloísio Nelmo Klein (UFSC)		
16:50			(50 min)		Assembléia da SBV
17:00					Desprised a
17:10					Premiação
17:20			Sessão de Posters (1 h)	Consider de Deutsen (20 min)	Encerramento do CBrAVIC
17:30 17:40			2	Sessão de Posters (50 min)	Section 1997 Control of the Control
17:50					
18:00					
19:00		Cerimônia de			
20:00		Abertura e coquetel		Joseph de cont. I company	
		COGGETET		Jantar de confraternização	





# MINICURSOS

XLV Congresso Brasileiro de Aplicações de Vácuo na Indústria e na Ciência

> Balneário Camboriú - SC 11 a 13 de Novembro de 2024





#### INTRODUCÃO À CIÊNCIA E TECNOLOGIA DO VÁCUO

Idioma: Português.

**Data:** 9/11/2024 (sábado)

Horário: 8:30 h às 12:30 h e 13:30 h às 15:30 h.

Carga Horária: 6 horas.

Público-alvo: Participantes do evento.

**Objetivo:** Apresentar e discutir os princípios básicos da ciência e da tecnologia do vácuo para a aplicação tanto em arranjos experimentais científicos como nos arranjos produtivos dos setores industrial e de serviço.

Forma do Evento: Presencial.

Instrutores: Prof. Dr. Francisco Tadeu Degasperi - Fatec-SP - CEETEPS e Dr. Marcelo Juni

Ferreira - European Spallation Source (ERIC-Suécia).

Vagas: 40. Conteúdo:

- Comportamento dos gases e vapores.
- Teoria cinética dos gases.
- Transporte de gases rarefeitos.
- Condutância e velocidade de bombeamento com cálculos.
- Processo de bombeamento e fontes de gases em vácuo.
- Bombas de vácuo.
- Medidores, calibração e metrologia de vácuo.
- Materiais, processos de limpeza e condicionamento.
- Componentes auxiliares e sistemas de vácuo.
- Especificação de sistemas de vácuo e uso de catálogos.
- Análise de gases residuais e medição de pressão parcial.
- Injeção controlada de gases e vapores.
- Detecção de vazamentos e estanqueidade.
- Estudos de caso em tecnologia do vácuo.
- Discussão de casos de estudo apresentados pelos participantes



#### INTRODUÇÃO À METROLOGIA DO VÁCUO COM CÁLCULO DE INCERTEZAS

Idioma: Português.

**Data:** 9/11/2024 (sábado) **Horário:** 16:00 h às 19:00 h. **Carga Horária:** 3 horas.

Público-alvo: Participantes do evento.

Objetivo: Apresentar e discutir os princípios básicos da ciência e tecnologia da metrologia com

cálculos de incertezas para aplicação em situações da pesquisa da indústria.

Forma do Evento: Presencial.

Instrutores: Dr. Luciano do Nascimento Batista - LAPRE-INMETRO e Prof. Dr. Francisco Tadeu

Degasperi - Fatec-SP - CEETEPS

Vagas: 40. Conteúdo:

· As bases da metrologia de vácuo.

- · Definição das grandezas básicas da ciência e tecnologia do vácuo.
- · Aplicações e importância da metrologia do vácuo.
- · Arranjos metrológicos para baixa pressão.
- · Arranjos metrológicos para a determinação de transferência de gases.
- · Empresas brasileiras que calibram medidores de vácuo.
- · Projeto do padrão brasileiro de vácuo.
- · A metrologia de vácuo aplicada a melhoria dos sistemas de vácuo.
- Atividades da metrologia do vácuo realizadas no laboratório de pressão INMETRO e no laboratório de tecnologia do vácuo – ITV da Fatec-SP – CEETEP



# INTRODUÇÃO À DINÂMICA DOS GASES RAREFEITOS: TEORIA E APLICAÇÕES AOS SISTEMAS DE VÁCUO

Idioma: Português.

**Data:** 10/11/2024 (domingo). **Horário:** 8:30 h às 12:00 h. **Carga Horária:** 3,5 horas.

Público-alvo: Participantes do evento.

Objetivo: Apresentar e discutir os princípios básicos da dinâmica dos gases rarefeitos e sua

aplicação na tecnologia do vácuo.

Forma do Evento: Presencial.

Instrutor: Prof. Dr. Felix Sharipov - Universidade Federal do Paraná - UFPR.

Vagas: 40. Conteúdo:

- Fundamentos da teoria cinética.
- Problemas típicos.
- Regimes de escoamento.
- Potenciais de interação intermolecular.
- Livre caminho equivalente.
- Função de distribuição de velocidade.
- Equação de Boltzmann.
- Equações modelo.
- Deslizamento de velocidade.
- Salto de temperatura.
- Viscosidade e conductividade térmica.
- Simulação direta de Monte Carlo.
- Colisões intermoleculares.
- Potencial de esferas rigidas vs. potencial *ab initio*.
- Fluxo através de orificio.
- Fluxo através de tubos a canais.
- Modelagem de bombas e sensores de vácuo.
- 3D escoamentos.
- Escoamentos não estacionários.
- Interação gás-superfície
- Forma geral de interação gás-superfície.
- Coeficientes de acomodação.
- Modelo difuso-especular.
- Modelo Cercignani-Lampis.
- Resultados baseados no modelo CL.



#### MODELAGEM E CÁLCULO DE SISTEMAS DE VÁCUO

Idioma: Português.

**Data:** 10/11/2024 (domingo). **Horário:** 13:00 h às 16:00 h **Carga horária:** 3 horas.

Público-alvo: Participantes do evento.

**Objetivo:** Apresentar e discutir a construção de modelos de sistemas de vácuo – vácuo grosseiro, vácuo médio, alto vácuo e ultra alto vácuo. Cálculo de sistemas de vácuo usados na ciência e na indústria.

Forma do Evento: Presencial.

Instrutores: Prof. Dr. Nilberto H. Medina – Instituto de Física da USP e Prof. Dr. Francisco Tadeu

Degasperi, FATEC-SP - CEETEPS

Vagas: 40. Conteúdo:

- Comportamento dos gases e vapores.
- Teoria cinética dos gases.
- Transporte de gases rarefeitos.
- Cálculo de condutância.
- Cálculo de velocidade de bombeamento.
- Processo de bombeamento e fontes de gases em vácuo.
- Modelagem de sistemas de vácuo.
- Estudos de caso com modelagem e cálculo da pressão em função do tempo em sistemas de vácuo.



#### TEORIA CINÉTICA DOS GASES E OS COEFICIENTES DE TRANSPORTE

Idioma: Português.

**Data:** 10/11/2024 (domingo). **Horário:** 16:20 h às 19:20 h **Carga Horária:** 3 horas.

Público-alvo: Participantes do evento.

**Objetivo:** Apresentar e discutir os princípios básicos da ciência e tecnologia da metrologia na tecnologia do vácuo. Apresentar a necessidade da metrologia do vácuo para aplicação em situações da pesquisa básica e da indústria.

Forma do Evento: Presencial.

Instrutores: Prof<sup>a</sup>. Dr<sup>a</sup>. Denize Kalempa – Escola de Engenharia de Lorena – USP

Vagas: 40. Conteúdo:

- Introdução: Abordagem termodinâmica e abordagem da teoria cinética dos gases.
- Livre caminho médio.
- Interação entre átomos e moléculas.
- Potenciais nos choques moleculares.
- Regimes de transporte em gases rarefeitos.
- Equações de estado dos gases ideais e reais
- Coeficientes de transporte nos gases rarefeitos.
- Transpiração térmica.
- Transporte de calor por condução em gases rarefeitos.
- Difusão térmica em gases rarefeitos.
- Viscosidade em gases rarefeitos.
- Exemplos de aplicação em sistemas de vácuo.



#### FILMES FINOS E CARACTERIZAÇÃO DE SUPERFÍCIES

Idioma: Português.

**Data:** 9/11/2024 (sábado) e 10/11/2024 (domingo). **Horário:** 8:00 h às 12:00 h e 14:00 h às 18:00 h

Carga Horária: 16 horas.

Público-alvo: Participantes do evento.

Forma do Evento: Presencial.

**Instrutores:** Prof<sup>a</sup>. Dr<sup>a</sup>. Nazir Monteiro dos Santos - Instituto de Estudos Avançados (IEAv); Prof<sup>a</sup>. Dr<sup>a</sup>. Rafael H. Mota Siqueira - Instituto de Estudos Avançados (IEAv) e Prof. Dr. Julio César Sagás

- UDESC/CCT. Vagas: 40. Conteúdo:

- Filmes finos
  - Definição
  - Propriedades: morfologia, microestrutura e composição química
  - Aplicações
- Métodos de deposição de filmes finos
  - Deposição física de vapor (PVD) Evaporação, sputtering
  - Deposição química de vapor (CVD): CVD térmico e CVD assistido por plasma
- Caracterização de superfícies
  - Microscopia eletrônica de varredura
    - Microscopia eletrônica de varredura com emissão por efeito de campo
    - Espectrosocpia de Raios-X por dispersão de energia (EDX/EDS)
    - Princípios e aplicações
    - Morfologia, topografia, imagens, mapeamento e composição elementar
- Microscopia de força atômica (AFM)
  - Funcionamento e tipos de escaneamento
  - Análise da topografia e propriedades mecânicas
- Espectroscopia de fotoelétrons excitados por raios-X (XPS)
- Difração de raios-X (XRD)



#### CIÊNCIA E TECNOLOGIA DE PLASMAS

Idioma: Português.

Data: 10/11/2024 (domingo).

Horário: 8:00 h às 12:00 h e 14:00 h às 18:00 h

Carga Horária: 8 horas.

Público-alvo: Participantes do evento.

Forma do Evento: Presencial.

Instrutores: Prof. Dr. Julio César Sagás e Dra. Júlia Karnopp - UDESC/CCT

Vagas: 40. Conteúdo:

Definição e propriedades de plasmas

• Geração de plasmas em baixa pressão e em pressão atmosférica

Processos colisionais

Técnicas de diagnóstico de plasmas

■ Interação plasma-superfície

Química de plasmas

Aplicações



#### APRENDER CIÊNCIA PODE SER GOSTOSO

Idioma: Português.

**Data:** 12/11/2024 (terça). **Horário:** 9:00 h às 12:00 h **Carga Horária:** 3 horas

Público-alvo: estudantes e professores da rede pública

Forma do Evento: Presencial.

Instrutores: Prof. Dr. Álvaro José Damião (IEAv)





# PALESTRAS TÉCNICAS

XLV Congresso Brasileiro de Aplicações de Vácuo na Indústria e na Ciência

Balneário Camboriú - SC 11 a 13 de Novembro de 2024





#### PALESTRAS TÉCNICAS: Vácuo na Indústria

#### Terça-feira (12/11/2024)

Organização: Francisco Tadeu Degasperi (FATEC-SP) e Luciana Sgarbi Rossini (FATEC-SO):

- 8:00 h − 8:25 h − *Atividades da tecnologia do vácuo na indústria*. Hélcio Onusic − Instituto de Física da USP.
- 8:25 h − 8:50 h − *Bombas de vácuo secas: aplicações na produção industrial.* Achim Lessel − Busch do Brasil Ltda.
- 8:50 h 9:15 h Detecção de vazamentos em sistemas de vácuo industrias Casos na refrigeração. Fernando Zappelline Ahestest Ltda.
- 9:15 h 9:40 h *Sistemas de vácuo para processos industriais de secagem*. Luis Henrique Bonfim Almeida Edwards Vácuo Ltda.
- 9:40 h − 10:05 h − *Bombas de pré-vácuo secas para processos industriais*. Luciano Camacho − Leybold Vácuo Ltda.
- 10:30 h 10:55 h *Componentes auxiliares para melhorar o desempenho dos sistemas de vácuo industriais*. Rafael Shiguematsu Amaral AVACO Ltda.
- 10:55 h 11:20 h *A definir*. Marcelo Azevedo Agilent Vácuo Ltda.
- 11:20 h 11:45 h A definir. Tiago Cerqueira Ulvac Brasil Vácuo Ltda.
- 11:45 h − 12:10 h − *Fabricação de componentes para sistemas de vácuo industriais*. Fernando Arroyo − FCA Brasil Ltda.
- 12:10 h − 12:25 h − *Avaliação da sessão Vácuo na Indústria e propostas de melhoria*. Francisco Tadeu Degasperi e Luciana Sgarbi Rossini.

#### PALESTRAS TÉCNICAS - METROLOGIA DE VÁCUO

#### **Quarta-feira** (13/11/2024)

**Organização**: Francisco Tadeu Degasperi (FATEC-SP) e Luciano do Nascimento Batista (LAPRE-INMETRO)

- 13:30 h − 13:50 h − *A necessidade da metrologia de vácuo na indústria e na ciência*. Luciano do Nascimento Batista − LAPRE-INMETRO.
- 13:50 h − 14:10 h − *Instrumentação para a determinação de estanqueidade e para a medição de quantidade de gás*. Maurício Oliveira − Empresa TEX Instrumentação Eletrônica.
- 14:10 h 14:30 h *A metrologia de vácuo: pressão e quantidade de gás*. Hugo Alexandre Garrido Aguiar Empresa Centro Tecnológico de Metrologia CTM.
- 14:30 h − 14:50 h − *A metrologia de vácuo para processos industriais e pesquisa*. Luís Henrique Bonfim Almeida − Edwards Vácuo Ltda.
- 14:50 h − 15:10 h − Oficina de Metrologia de Vácuo no Laboratório de Tecnologia do Vácuo − LTV da FATEC-SP. Francisco Tadeu Degasperi − FATEC-SP − CEETEPS e Rodrigo Arakawa − ETEC Professor Horácio Augusto da Silveira − CEETEPS.
- 15:10 h − 15:30 h − *Avaliação da sessão Metrologia de Vácuo e propostas de melhoria*. Francisco Tadeu Degasperi e Luciano do Nascimento Batista.



# PALESTRAS

XLV Congresso Brasileiro de Aplicações de Vácuo na Indústria e na Ciência

> Balneário Camboriú - SC 11 a 13 de Novembro de 2024





#### MAGNETRON SPUTTERING COATINGS TECHNOLOGIES APPLIED FOR HYDROGEN AIRCRAFT AND ELECTROCHROMIC DEVICES

Diao Xungang *Beihang University* 

Hydrogen powered airplane through hydrogen produced electricity or directly combusted jet engines can dramatically reduce carbon emissions and is recognized as the most promising future green aviation transportation. The presentation will give an introduction to the recent development and the history of hydrogen aircraft in different countries over the world and some critical technologies on hydrogen aircraft such as proton exchange membrane fuel cells and hydrogen powered engines, as well as their relevant materials with hydrogen embrittlement and electrochemical corrosion protections. Liquid hydrogen storage is also briefly introduced.

All inorganic thin film elelctrochromic materials and multilayer devices are introduced on their fabrication methods, properties on materials fundamentals and electrochemical cycling, their multifunctional applicable performances on solar energy, infrared and other electromagnetic wave spectra modulations. Typical multilayer electrochromic devices Glass/ITO/WO3/LiTaO3/NiOx/ITO and PI/Al/WO3/LiTaO3/NiOx/ITO have been monolithically fabricated layer by layer on a home-made multitarget magnetron sputtering machine. The maximum transparency and reflectance difference in the visible light spectrum region between coloration and bleaching states reaches as high as 80%. Within infrared range, we also get about 0.4-0.6 emissivity modulations recently.

Some vacuum magnetron sputtering and cathodic arc coating machines have innovatively home designed, optimized and manufactured deliberately for fabricating our multilayer functional electrochromic thin film devices, as well as serving our electrochemical corrosion resistant nitride and carbide protective coatings for metallic bi-polar plates in hydrogen fuel cell and water electrolyzer applications.



# THE UPGRADE OF THE TCABR TOKAMAK AND THE NEED FOR A NEW WALL CONDITIONING SYSTEM

Gustavo Paganini Canal Instituto de Física da Universidade de São Paulo (IFUSP)

For many decades, scientists over the world have been working on establishing the conditions in which controlled thermonuclear fusion can become an economically viable energy source. Among the several magnetic concepts proposed to confine thermonuclear plasmas, the tokamak concept is currently the most promising approach for exploiting nuclear fusion. Brazil has the largest tokamak in the southern hemisphere of the planet - the Tokamak à Chauffage Alfvén Brésilien (TCABR), which is operated by the Plasma Physics Laboratory (LFP) of the Institute of Physics of the University of São Paulo (IFUSP). A significant upgrade of TCABR is being designed to make it capable of creating a well controlled environment where the impact of externally applied magnetic perturbations on violent plasma instabilities, termed edge localized modes (ELMs), can be addressed over a wide range of plasma scenarios. The core of this upgrade corresponds to the installation of an innovative set of 108 high current magnetic coils that will be installed inside the vacuum vessel. In addition, graphite protection tiles will be installed to cover more than 95% of the vacuum vessel inner wall in order to protect the coils from the hot plasma. Flush mounted Langmuir probes will be installed in some tiles and will be paired with ball-pen probes for plasma-wall interaction diagnose. The installation of these new components inside the vacuum vessel is expected to significantly increase degassing. To minimize deuterium inventory inside the vacuum vessel, and uncontrolled impurity influx during experiments due to degassing of the newly installed components, a wall conditioning system will also be installed. This system will be composed of a helium DC glow discharge cleaning (GDC) system and a baking system. The GDC system will be composed of 6 retractile electrodes evenly distributed within the vacuum vessel, polarized positively with respect to the grounded vacuum vessel, all connected to the same DC power supply. The baking system will consist of several localized heating elements installed around the vacuum vessel and independently controlled to keep the vacuum vessel and internal components at temperatures as high as 200 degrees Celsius. In preparation for experimental campaigns, a several-day baking of the vacuum vessel at 200 degrees Celsius will be carried out, while 10 minutes of in-between-shots helium GDC are planned. Due to the machine baking, all the internal components, such as the 108 magnetic coils, wall-mounted diagnostics, electrical cables, connections etc., will have to withstand temperatures of about 200 degrees Celsius while still being compatible with ultra-low vacuum. This work will focus on the current status of these developments and future plans.



#### IFMIF/DONES VACUUM SYSTEM DESIGN

# Marcelo Juni Ferreira *Lund University*

The International Fusion Materials Irradiation Facility - DEMO Oriented Neutron Source (IFMIF/DONES) is a critical project within the European Union's fusion roadmap. Its primary goal is to test and qualify materials together ITER for use in future fusion reactors, by exposing them to intense neutron irradiation conditions similar to those such as DEMO. The facility features a linear accelerator delivering high-intensity deuterons to an in vacuum hot liquid lithium loop, generating neutrons that produce material damage equivalent to that expected in a fusion reactor.

The vacuum system must maintain high vacuum conditions with high reliability. A comprehensive study and implementation of the vacuum system for the accelerator have been conducted, including vacuum simulations to estimate the expected pressure profile, and the creation of the IFMIF/DONES Vacuum Handbook to standardize the vacuum requirements and hardware for the facility. Valuable insights have been gained from the IFMIF/Engineering Design and Engineering Validation Activities (EVEDA) prototype installation.

Additionally, two vacuum prototypes are being assembled: the Multipurpose Vacuum Accident Scenarios (MUVACAS) to study air inrush scenarios in the accelerator, and the Quick Disconnecting System (QDS) prototype to evaluate the feasibility of remote handling of the interface on the lithium source. The design of the accelerator's vacuum system and future challenges will also be presented.

#### Acknowledgements

This work has been carried out within the framework of the EUROfusion Consortium, funded by the European Union via the Euratom Research and Training Programme (Grant Agreement No 101052200 — EUROfusion). Views and opinions expressed are however those of the author(s) only and do not necessarily reflect those of the European Union or the European Commission. Neither the European Union nor the European Commission can be held responsible for them.



#### THE CHALLENGES OF HYDROGEN IN MODERN METALLURGY

# Matheus Tunes *University of Leoben*

Hydrogen's integration into modern energy systems brings both significant advantages and critical challenges, particularly for metallurgy. With its high energy density, hydrogen is increasingly vital for sustainable energy and the next energy transition, but the susceptibility of metallic materials to hydrogeninduced degradation remains a major hurdle for both metallurgy and the functional materials that will compose the hydrogen energy infrastructure. The phenomenon of hydrogen embrittlement completes 150 years as it was firstly discovered and reported by the British metallurgist William H. Johnson in 1875 [1]. When hydrogen gas contacts the surface of metals and alloys, it undergoes physisorption-driven dissociative reactions, producing monoatomic hydrogen atoms that can then be chemisorbed into the material. When diffusing within the microstructure of materials, hydrogen interacts with site-specific dependencies and such interactions are reported to be the major cause of hydrogen embrittlement. Over the course of history, a series of theoretical mechanisms have been proposed to explain hydrogen embrittlement, but so far this phenomenon remains poorly understood, particularly considering the persisting limitations in detecting the dynamic action of hydrogen at the microstructural level [2,3]. This plenary talk will introduce the current theoretical mechanisms of hydrogen embrittlement under intense debate by the scientific community and it will show how a better experimental-theoretical understanding remains to be yet performed. The modern challenges that metallurgy is facing towards the development of hydrogen-resistant materials will be also discussed considering the state-of-the-art on the mitigation strategies against hydrogen embrittlement. It will be shown that hydrogen-materials interactions brings materials complexity into a new level where synergistic aspects of plasticity and fracture of materials must be taken into consideration [2]. Despite many advancements over 150 years of history, research gaps persist in establishing effective, longterm solutions for hydrogen-resilient materials. Overcoming these challenges and gaps is essential for the successful and safe deployment of the next green energy transition.

#### **References:**

- [1] W.H. Johnson, On some remarkable changes produced in iron and steel by the action of hydrogen and acids, Nature 11 (1875) 393.
- [2] M.B. Djukic, G.M. Bakic, V. Sijacki Zeravcic, A. Sedmak, B. Rajicic, The synergistic action and interplay of hydrogen embrittlement mechanisms in steels and iron: Localized plasticity and decohesion, Eng Fract Mech 216 (2019) 106528.
- [3] M.A. Tunes, P.J. Uggowitzer, P. Dumitraschkewitz, P. Willenshofer, S. Samberger, F.C. da Silva, C.G. Schön, T.M. Kremmer, H. Antrekowitsch, M.B. Djukic, S. Pogatscher, Limitations of Hydrogen Detection After 150 Years of Research on Hydrogen Embrittlement, Adv Eng Mater (2024) 2400776.



#### HISTÓRICO DA TECNOLOGIA DE PLASMA NA UFSC: CASES DE SUCESSO E DESENVOLVIMENTO DE NOVAS ALTERNATIVAS DE PROCESSAMENTOS ASSISTIDOS POR PLASMA

Aloísio Nelmo Klein Universidade Federal de Santa Catarina (UFSC)

Será apresentado um histórico do desenvolvimento da linha de pesquisa em tecnologia de plasma aplicada a materiais, especialmente a materiais sinterizados e os equipamentos desenvolvidos e em desenvolvimento, bem como, os recursos humanos formados com especialização na área de plasma. Serão também apresentados os principais *cases* de sucesso no desenvolvimento de projetos em parceria com empresas, envolvendo tecnologia de plasma. Será ainda discutida a possibilidade da utilização do ambiente reativo obtido em reator híbrido a plasma para gerar novas soluções na área de engenharia de superfície (tanto para aumentar a resistência ao desgaste de componentes mecânicos quanto para obtenção de camadas de baixo coeficiente de atrito), possibilidades em desenvolvimento para obtenção de pós especiais na forma de partículas compósitas e novos materiais metálicos e compósitos particulados sinterizados via sinterização assistida por plasma.



#### HEAT-TREATMENTS OF A LOW CARBON STEEL IN LASER BEAM WELDING

#### Milton Sergio Fernandes de Lima<sup>1</sup>\*

<sup>1</sup>Photonics Division, Institute for Advanced Studies, Trevo Coronel Aviador José Alberto Albano do Amarante, 1, Putim, 12.228-001São José dos Campos, SP, Brazil.

#### 1. Introduction

In the industrial practice it is common to preheat the steel sheets before laser welding, although the implications of such induced heat on the microstructure and mechanical properties are unknown [1]. The present contribution aims to understand the effect of pre- or pos-heating on the microstructure and hardness of a typical low carbon steel.

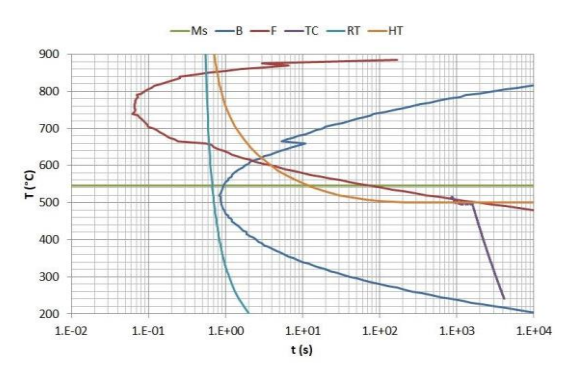
#### 2. Experimental

The materials used in this work were low carbon steel sheets (Fe-0.03%C-0.13%Mn-0,014%P-0,014%S-0,040%Al) with 1.4 mm thickness and galvanized by a 45 g/m² Zn coat. The sheets were welded in a fiber laser workstation comprised a 2 kW YLR2000 laser, a CNC table, an induction furnace and protective shielding gases. In the current setup the steel sheets were welded using an 1000W laser power, a 50 mm/s speed and the focal position on the surface. The sheets were welded in room temperature (RT, 20°C), in high temperature (HT, 500°C), or post-heat treated at 500°C (PWHT). For the current study conventional metallography methods, X-ray diffratometry and Vicker's microhardness testing were employed. The temperature fields were estimated using finite element methods (FEM, SysWeld® software).

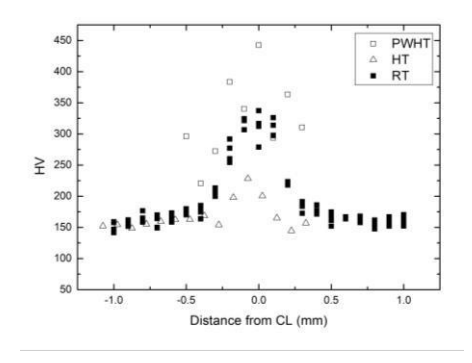
#### 3. Results and Discussions

Fig. 1 presents the FEM calculations together with the current study temperature estimations. As can be seen, the room temperature (RT) welds produce ferrite with possibly some martensite and the high-temperature (HT) welds might produce ferrite plus bainite. As can be seen in Fig. 2, HT greatly reduced the hardness around the weld center line, from approximately 330 HV (RT) to 220 HV (HT). The same effect could not be perceived when the RT weld is annealed in a furnace for 500°C during 10 min, since the PWHT HV values varied from 350 to 450 HV.

The metallography examination of the welds indicated the HT procedure reduced the presence of residual austenite within the grains which will eventually transforms to martensite in RT welds. The same result was not achieved when the RT welds were subjected to PWHT since part of the martensite was tempered and some carbides nucleated, explaining the wide variation in HV values. Therefore, for further steel processing such as coiling or stamping, the pre-heating of the laser weld joint at 500°C (called HT here) is preferable.



**Fig. 1.** Calculated time-temperature-transformation for the current steel together with estimated profiles: Ms: martensite start temperature. B: bainite. F: ferrite. TC: thermocouple measurement. RT: room temperature. HT: high temperature.



**Fig. 2.** Vickers Hardness (HV) profile as a function of the distance of the weld center line (CL). RT: room temperature. HT: high temperature. PWHT: annealed at 500°C after weld.

#### 4. Reference

[1]- A. Jahn, et al. (2008, October). Induction assisted laser beam welding of HSLA steel sheets. In Proceedings of the International Scientific Colloquium on Modelling for Electromagnetics (pp. 195-200).

#### Acknowledgments

This study was financed in part by the Coordenação de Aperfeiçoamento de Pessoal de Nível Superior - Brasil (CAPES) - Finance Code 001.

<sup>\*</sup>Corresponding author: miltonmsfl@fab.mil.br



## SIRIUS'S BEAMLINE VACUUM REVIEW AND ORION'S CHALLENGES FOR UHV APPLICATIONS.

Rodrigues, Gustavo L. M. P. 1\*

Brazilian Synchrotron Light Laboratory

#### 1. Introduction

Sirius and the Orion project are currently the largest and most complex scientific infrastructure projects built or under construction in Brazil. This work will review ultra-high vacuum (UHV) use in the Sirius accelerator and beamlines and explore its challenges in the Orion project, maximum biological containment facilities (BSL-4).

#### 2. Experimental

The use of a vacuum in synchrotron radiation facilities is widespread, ranging from low vacuum (LV) to extreme high vacuum (XHV) in some cases. The XHV use in the storage rings is usual, and some experimental stations are necessary, too. This requirement is essential to prevent the degradation of the X-ray quality, the X-ray optics contamination, and the sample quality.

In the initial phases of all beamline projects, one of the requirements for high quality is the vacuum environment; more than an integration process of commercial pumps, the correct evaluation of the necessities can reduce costs and increase the quality of experimental results. In this work, we will present the choices and results of vacuum quality in the Sirius machine and beamline and future challenges in the Orion Project.

#### 3. Results and Discussions

Figure 1 shows the XHV chamber for storage ring sections; from day 1 to now, the storage ring has worked under XHV pressures, and the philosophy used was a distributed pumping system. In the regime of UHV to XHV, the front-end of the beamlines and optical elements of the beamlines (figure 3), the chamber was manufactured by a Brazilian company with a rectangular CF flange. In Figure 4, a differential pump system conducts the vacuum of the beamline from low vacuum pressures to the UHV vacuum regime.

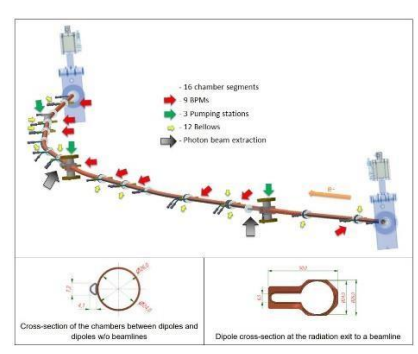


Figure 1: Storage ring section NEG coated vacuum chambers for XHV vacuum level.

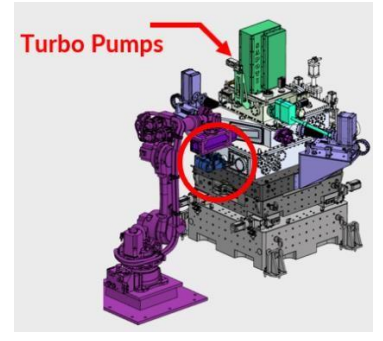


Figure 2: Experimental Station SAPOTI, integrated cryogenic sample chamber, UHV vacuum level with integrated sample cryogenic transfer system



Figure 3: Mirror system working in UHV regime and partial pressure of oxygen to reduce the carbon contamination.



Figure 4: Sape beamline differential pressure system for gas filter and ionization chamber.

#### Acknowledgments

The authors thank the Brazilian Ministry of Science, Technology, and Innovation for funding and the LNLS and CNPEM teams for the collaboration.

<sup>\*</sup>gustavo.rodrigues@lnls.br



# APRESENTAÇÕES ORAIS

XLV Congresso Brasileiro de Aplicações de Vácuo na Indústria e na Ciência

Balneário Camboriú - SC 11 a 13 de Novembro de 2024





#### PLASMA-ASSISTED PRODUCTION OF A FeTi MMNC POWDER

Deivison Daros Paim<sup>1\*</sup>, Antônio Rogerio de Souza<sup>1</sup>, Aloisio Nelmo Klein<sup>1</sup>, and Rodrigo Perito Cardoso<sup>1</sup>, *Materials Laboratory LABMAT - Federal University of Santa Catarina - UFSC* 

#### 1. Introduction

The *in-situ* process is a manufacturing route of metal matrix nanocomposites (MMNC) [1], in which it is possible to obtain a homogeneous dispersion of a fine reinforcement phase, and a strong bond at the interface with the matrix [2], improving the mechanical properties of MMNC [3]. In that context, this contribution deals with developing plasma-assisted processing of metal powders to produce MMNC reinforced with nitrides by the *in situ* technique. In this study, FeTi powders were nitrided in an  $H_2+N_2$  plasma nitriding atmosphere to produce titanium nitride nano-reinforcements in the particles.

#### 2. Experimental

The Plasma-assisted reactor has a rotary drum in which FeTi powder samples ( $d_{90}\sim9\mu m$ ) are placed in their inner, stirred, and exposed to an  $H_2+N_2$  plasma nitriding atmosphere. The plasma was generated in a plane-parallel hollow cathode by a DC power source located inside the rotary drum. The FeTi powder samples were treated in the anode (drum). Two different sets of samples were plasma nitrided at 550°C with a time of 4h ( $S_4_550$ ) and 16h ( $S_16_550$ ). Initially, the substrate was degassed for 1h at 100°C, followed by cleaning with pure hydrogen plasma for 0.5 h at 300°C. The gas flow, plasma pressure, and voltage were kept constant at 10sccm of  $H_2$  and 20sccm of  $N_2$ , 1.5 Torr, and 650V, respectively.

#### 3. Results and Discussions

Figure 1 shows the appearance of the FeTi particles observed in the scanning electron microscope (SEM). The particles, which initially exhibited faceted morphology due to the milling process (Fig.1 a), displayed a morphology with increased circularity after the nitriding treatment (Fig.1 b-c). Additionally, small rounded precipitates were observed on the surface of the particles (indicated by arrows). The change in particle morphology is accompanied to the appearance of the  $\alpha$ Fe and  $\gamma$ Fe phases, as indicated by the X-ray diffraction results (Fig. 2). Regarding the formation of nitrides in the particulate substrates, the development of the Titanium nitride phase is favored because it has the lowest Gibbs free energy of formation compared to iron nitride [4]. In this case, nitrogen chemically bonds with the Titanium present in the substrate to form Ti<sub>2</sub>N, resulting in the release of Fe into the matrix. Since this is predominantly a diffusion-controlled process, both temperature and treatment time influence the quantity and size of the precipitates [5].

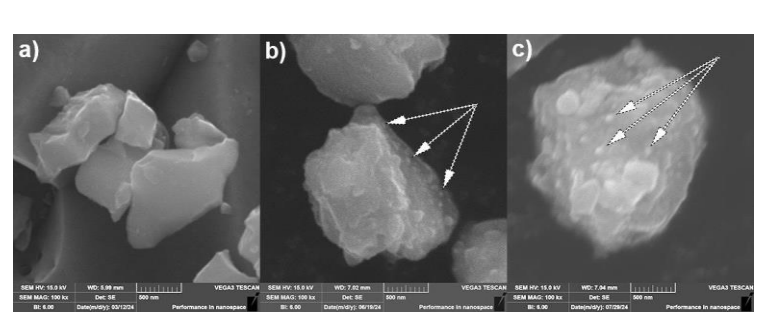


**Fig. 1.** Scanning electron microscope of samples a)FeTi, b)S\_4\_550, and c S 16 550

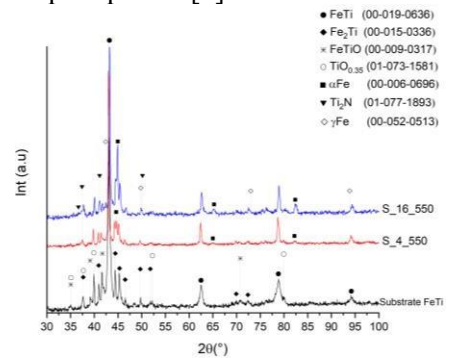


Fig. 2. X-ray diffraction of samples

#### 4. References

- [1] C. Suryanarayana., A. Nasser. "Mechanically alloyed nanocomposites". Progress in Materials Science, **58**, 4<sup>nd</sup> edition, 383-502, (2013).
- [2] L. Zhong., X. et al. "In situ fabrication of titanium carbide particulates-reinforced iron matrix composites". Materials and Design, **32**, 3790-3795, (2011).
- [3] M. Massoud et al. "Advanced metal matrix nanocomposites". Metals, 9, 1-39, (2019).
- [4] G. JR. et al. "Thermochemistry of the rare earth carbides, nitrides, and sulfides for steelmaking". Lowa State Univ. of Science and Technology, Rare-Earth Information Center, Ames, (1971).
- [5] E, J Mittemeijer. "Fundamentals of Nitriding and Nitrocarburizing". ASM Handbook. 619-646, (2013).

#### Acknowledgments

The Federal University of Santa Catarina for the financial support and CNPQ for the scholarship awarded.

<sup>\*</sup>deivison.d.p@labmat.ufsc.br



## INFLUENCE OF Nb DOPING ON THE ELECTRICAL AND OPTICAL PROPERTIES OF TiO<sub>2</sub> THIN FILMS

F. Alfaro<sup>1,2</sup>\*, R. G. Delatorre<sup>1</sup>, J. C. Sagás<sup>3</sup> and D. A. Duarte<sup>1</sup>

<sup>1</sup>Universidade Federal de Santa Catarina, Laboratory of Surface Treatments.

<sup>2</sup> BIOPARK Educação, Laboratory for Biomaterials and Bioengineering.

<sup>3</sup>Universidade do Estado de Santa Catarina, Laboratory of Plasmas, Films and Surfaces.

#### 1. Introduction

Transparent conductive oxides (TCOs) such as ITO and FTO have been widely used in photovoltaic (PV) technology for their excellent optical and electrical properties [1]. Typically, ITO shows a resistivity around  $10^{-4} \,\Omega \cdot \text{cm}$  [2]. Nb-doped TiO<sub>2</sub> (TNO) emerges as a promising alternative, offering high transmittance and low sheet resistance [3]. These properties are crucial for TCO applications, which require a balance between optical transparency and electrical conductivity. Plasma-assisted techniques like magnetron sputtering provide precise control over material properties at the atomic level, enabling the optimization of such characteristics.

#### 2. Experimental

TNO films were deposited on glass substrates using grid-assisted magnetron sputtering with a 4-inch target composed of Ti and four Nb inserts positioned along the target erosion zone. The substrate was maintained at floating potential, and depositions were conducted at room temperature and 300°C. Target current, DC power, target-to-substrate distance, working gas, and deposition thickness were kept constant: 2.00 A, 1.0 kW, 6 cm, 0.80 Pa, and 100 nm, respectively. Ar and O<sub>2</sub> flow rates were 1.5 and 4.4 sccm. The films were evaluated using spectrophotometry, mechanical profilometry (to confirm thickness), four-point probes, X-ray diffraction (XRD), and X-ray photoelectron spectroscopy (XPS).

#### 3. Results and Discussions

Fig. 1 shows the transmittance of Nb-doped TiO<sub>2</sub> samples deposited at 300°C with four Nb inserts. The average transmittance in the visible range was 73%, while in the infrared range it was 63%. Vacuum annealing was found to decrease the average transmittance. The XRD results (Fig. 2) show a shift to lower angles, indicating an increase in the crystal lattice, which is attributed to the incorporation of Nb into the TiO<sub>2</sub> matrix. XPS analysis revealed that Nb doping increases the surface defects, particularly oxygen vacancies. However, vacuum annealing reduces these defects and enhances Nb incorporation. Samples produced with vacuum annealing presented a higher Nb concentration. The resistivity of Nb-doped TiO<sub>2</sub> films was around  $10^{-2} \Omega$ ·cm when deposited at 300°C, significantly lower than undoped TiO<sub>2</sub>, demonstrating the potential of Nb doping to reduce electrical resistivity while maintaining suitable optical transmittance.

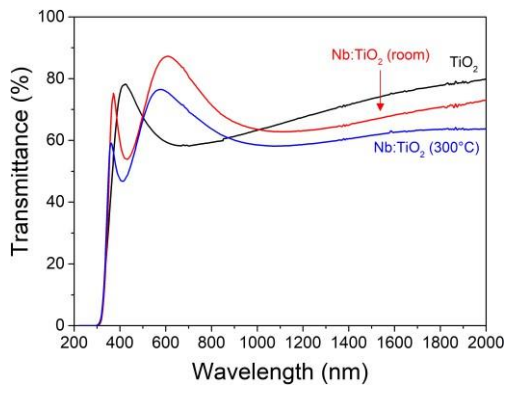


**Fig. 1.** Transmittance spectra of  $TiO_2$  and Nb-doped  $TiO_2$  thin films deposited at room temperature and  $300^{\circ}C$  with 4 Nb inserts.

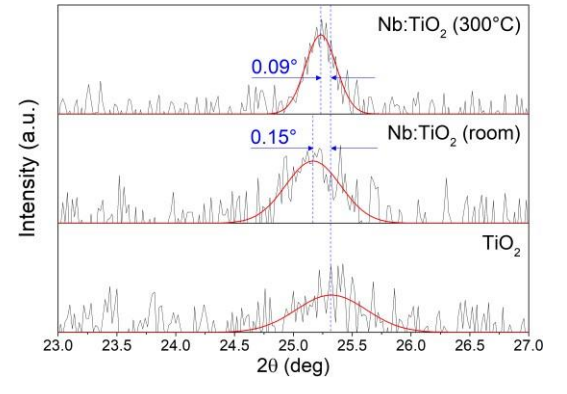


**Fig. 2.** X-ray diffraction (XRD) patterns of TiO<sub>2</sub> and Nb-doped TiO<sub>2</sub> thin films deposited at room temperature and 300°C with 4 Nb inserts.

#### 4. References

- [1] P. Basumatary, P. Agarwal. Materials Research Bulletin, 149 (2022) 111700.
- [2] M.S. Farhan, et al. International Journal of Precision Engineering and Manufacturing. 14 (2013) 1465.
- [3] Y. Furubayashi, et al. Applied Physics Letters, 86 (2005) 252101.

#### Acknowledgments

The authors thank FAPESC (PAP-UDESC) and CNPq (grants 307408/2021-3 and 406376/2022-0).

# COMPARATIVE ANALYSIS OF GRAPHENE OXIDATION VIA PLASMA TREATMENT AND CHEMICAL METHODS

Amanda Valcanaia<sup>1\*</sup>, Bruna Segat<sup>1</sup>, Daniela Becker<sup>1</sup>

<sup>1</sup>Laboratory of Plasmas, Films and Surfaces, Santa Catarina State University (UDESC), Joinville, Brazil.

#### 1. Introduction

With the advancement of nanotechnology, interest in using carbon nanoparticles, such as graphene, has increased due to their remarkable mechanical, thermal, and electrical properties [1]. Graphene is often used in its oxidized form, as introducing oxygen-containing groups enhances its stability in aqueous suspensions, broadening its applications to include electronic components, energy storage, and biomedicine [2]. However, due to polluting chemicals, traditional wet chemical oxidation methods have environmental impacts. Consequently, plasma oxidation emerges as a sustainable, clean technology that generates no waste or environmental harm. Thus, the present study compares graphene oxidation using wet chemical and plasma techniques to determine the more efficient methodology.

#### 2. Experimental

Graphene oxidation via chemical route (GO) was performed using the method proposed by Kathi et al. [3], where graphene was dispersed in sulfuric acid (H<sub>2</sub>SO<sub>4</sub>) and phosphoric acid (H<sub>3</sub>PO<sub>4</sub>) solution in a 3:1 (v/v) ratio under magnetic stirring at room temperature for 18 hours, followed by filtration and washing. For plasma oxidation (GO\_plasma), Dielectric Barrier Discharge plasma was employed, generated by a radiofrequency source (Fig. 1). The discharge was conducted at 20 W for 10 minutes using a gas mixture composed of 20% oxygen and 80% argon at a pressure of 1 Torr. XPS and FTIR characterized the oxidized graphene to verify the introduction of oxygen-containing groups in the samples. Additionally, aqueous graphene oxide suspensions were prepared at 1 mg/mL and homogenized using a probe sonicator. They were subsequently characterized by zeta potential to assess stability.

#### 3. Results and Discussions

In Figure 2, subtle bands characteristic of graphene oxide appeared with oxidation. Both oxidized samples presented a subtle band around 1260 cm<sup>-1</sup> that can be attributed to the C-O-C stretching; the GO sample presented another band around 1720 cm<sup>-1</sup> that corresponds to the C=O stretching, and the GO\_plasma sample presented a band around 1100 cm<sup>-1</sup> characteristic of C-O stretching vibrations [4]. XPS analysis indicated that the pristine graphene (G) sample had around 3.8% oxygen, increasing to 4.8% for the GO and 5.4% for GO\_plasma sample. This increase in oxygen was sufficient to obtain stable aqueous suspensions, with a potential zeta above 30 mV for both oxidized samples, while the pristine G did not disperse in water. Thus, it can be concluded that plasma oxidation is a promising approach to replace wet chemical oxidation, standing out for being a simple, sustainable and effective method.

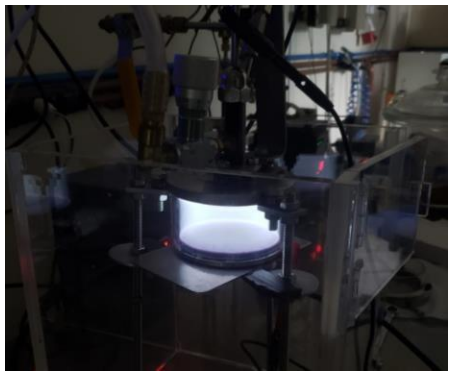
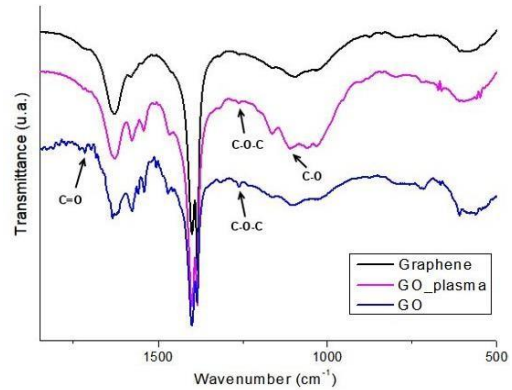


Fig. 1. Plasma oxidation.



**Fig. 2.** *FTIR analysis.* 

#### 4. References

- [1] Z. Sun, S. Fang and Y. H. Hu, Chem. Rev., 120, 10336–10453, (2020).
- [2] A. Nag, A. Mitra and S. C. Mukhopadhyay. Sensors and Actuators A: Physical, 270, 177–194, (2018).
- [3] J. Kathi, K. Rhee and J. H. Lee, Composites Part A: Applied Science and manufacturing, 40, 800-809, (2009).
- [4] K. Krishnamoorthy, M. Veerapandian, K. Yun and S. Kim, Carbon, 53, 38–49, (2013).

#### Acknowledgments

CNPQ, CAPES (code 001) and PAP-FAPESC (2023TR000258), FAPESC (2023TR001350).

<sup>\*</sup>Corresponding author: amandavalcanaia@outlook.com



#### SUBLIMATION AND DEPOSITION OF ARGON IN A GAS MIXTURE

Denize Kalempa<sup>1\*</sup>, Irina Graur<sup>2</sup>, and Felix Sharipov<sup>3</sup>
<sup>1</sup>Escola de Engenharia de Lorena, Universidade de São Paulo, Lorena, 12602-810, Brazil
<sup>2</sup>Aix Marseille Université, CNRS, IUSTI UMR 7343, Marseille, 13453, France
<sup>3</sup>Departamento de Física, Universidade Federal do Paraná, Curitiba, 81531-990, Brazil

#### 1. Introduction

Problems concerning non-equilibrium gas flows due to phase change are of great scientific interest and practical relevance for the development and improvement of technologies such as heat exchangers, chemical reactors, thin films, etc. For instance, the heat and mass transfer caused by sublimation of solid particles are important for the development of new technologies which rely on chemical vapor deposition. In kinetic theory of gases, evaporation and condensation phenomena, analogous to sublimation and deposition, have been intensively studied based on either the Boltzmann equation [1] or the Direct Simulation Monte Carlo method [2]. However, most of the papers available in the literature consider a non-realistic situation with hypothetical molecular masses and the rigid-spheres model of intermolecular interaction. In the present work, a solid sphere of argon in the presence of its vapor and helium as a background is considered. The temperature of the mixture is chosen so that argon can sublimate or deposit, while helium is just reflected from the solid surface.

#### 2. Theory

It is assumed the slow phase change so that the model proposed by McCormack [3] for the linearized Boltzmann equation is used to model the non-equilibrium gas flow. In this model, the quantities dependent on the interatomic interaction are calculated by using the rigid-spheres model as well as data obtained from ab initio calculations available in the literature for the gas species. The complete sublimation/deposition of vapor on the spherical surface is assumed as the boundary condition for argon, while helium just reflects diffusely from the surface. Far from the sphere, the Maxwell distribution function corresponding to thermodynamic equilibrium is used as the asymptotic solution of the problem. The discrete velocity method is used to solve the problem numerically in a wide range of the gas rarefaction parameter. It is worth noting that, in the problem considered, the smaller the pressure of the gas mixture the smaller the gas rarefaction parameter. Thus, in vacuum conditions the gas flow is either in the so called free molecular or in the transitional regime.

#### 3. Results and Discussions

The mass and energy flow rates are calculated as functions of the temperature of the mixture, molar concentration of helium and rarefaction parameter, which allows to classify the gas flow as free molecular, transitional or continuous. To analyze the influence of the interatomic interaction potential on the solution, the rigid-spheres model and ab initio potential are employed. According to the results, the magnitude of the mass flow rate increases as the rarefaction parameter decreases, i.e. in vacuum conditions. Moreover, it decreases as the molar concentration of helium increases. It is noted that the direction of the heat flux depends on the molar fraction of helium and the phenomenon of inverted temperature appears. Concerning the influence of the interatomic potential, the results obtained from the rigid-spheres model and ab initio potential show a significant difference.

#### 4. References

- [1]- C. Cercignani. "The Boltzmann Equation and its Application", Springer (1988).
- [2]- G. A. Bird. "Molecular Gas Dynamics and the Direct Simulation of Gas Flows", Oxford University Press (1994).
- [3]- F. J. McCormack. Construction of linearized kinetic models for gaseous mixture and molecular masses. Phys. Fluids, **16**, 2095-2105 (1973).

#### Acknowledgments

D. Kalempa and I. Graur acknowledge Fundação de Amparo à Pesquisa do Estado de São Paulo (FAPESP) grant 2022/10476-1, for support of the research.

<sup>\*</sup>Corresponding author: kalempa@usp.br



# DEPOSITION OF Al<sub>2</sub>O<sub>3</sub> USING ATOMIC LAYER DEPOSITION WITH PLASMA ACTIVATED WATER

Júlia Karnopp<sup>1\*</sup>, Thais M. Vieira<sup>2</sup>, Helen C. de Souza Barros<sup>2</sup>, Julio C. Sagás<sup>1</sup>, Rodrigo S. Pessoa<sup>2</sup>

<sup>1</sup>Universiade do Estado de Santa Catarina - Joinville

<sup>2</sup>Instituto Tecnológico de Aeronáutica – São José dos Campos

#### 1. Introduction

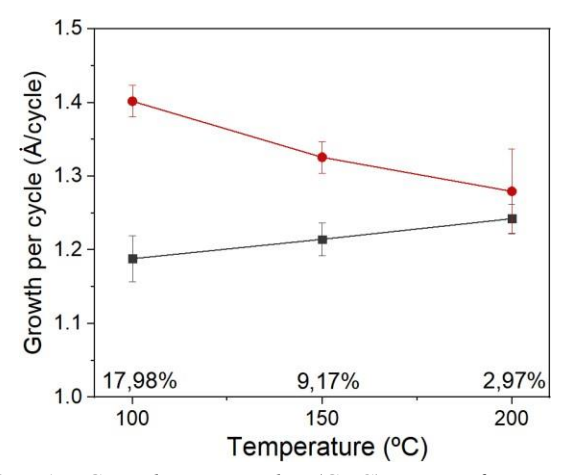
Thin films are used to modify the surface properties of materials. Among the vapor phase deposition methods is atomic layer deposition (ALD). Recently, a variation of this technique has been proposed in which the oxidizing precursor is changed from water to plasma-activated water (PAW) [1]. In this work, plasma-activated water-assisted atomic layer deposition (PAW-ALD) was studied both experimentally and theoretically to understand the effects of the reactive oxygen and nitrogen species produced in PAW on the growth mechanisms of Al<sub>2</sub>O<sub>3</sub> films deposited by PAW-ALD technique.

#### 2. Methodology

Alumina thin films were deposited using as oxidizing precursors water, PAW and aqueous solutions of the main species found in PAW, O<sub>3</sub>, H<sub>2</sub>O<sub>2</sub>, NO<sub>3</sub><sup>-</sup>, and a composite solution with these three species, were produced at the same concentrations in which they were identified and characterized. Depositions were made at 100°C, 150°C, and 200°C for 250, 500, and 1000 cycles. Theoretically, a zero-dimensional surface kinetic model was applied to simulate the chemical mechanisms occurring during the deposition of Al<sub>2</sub>O<sub>3</sub> films using trimethylaluminum (TMA) and H<sub>2</sub>O, H<sub>2</sub>O<sub>2</sub> and O<sub>3</sub> as oxidant precursors to model the mechanisms occurring in PAW-ALD.

#### 3. Results and Discussions

The results showed that the increase in temperature causes a slight increase in thickness for conventional ALD due to increased surface reaction rates, which is observed through simulation results. For PAW-ALD, the thickness decreases as the substrate temperature increases. At all three temperatures, the thickness is greater when using PAW, indicating that it is a better oxidant compared to water (Fig. 1).



140 H<sub>2</sub>O H<sub>2</sub>O H<sub>2</sub>O<sub>2</sub>

• H<sub>2</sub>O + H<sub>2</sub>O<sub>2</sub>

• H<sub>2</sub>O + NO<sub>3</sub>
• H<sub>2</sub>O + NO<sub>3</sub>
• H<sub>2</sub>O + NO<sub>3</sub>
• H<sub>2</sub>O + O<sub>3</sub> + H<sub>2</sub>O<sub>2</sub> + NO<sub>3</sub>
• PAW

20
200 300 400 500 600 700 800 900 1000

ALD cycles

**Fig. 1.** Growth per cycle (GPC) as a function of temperature for the depositions using  $H_2O$  and PAW.

**Fig. 2.** Film thickness at 150°C for different oxidant precursors as function of ALD cycles.

When using aqueous solutions in depositions at 150°C, the solutions containing NO<sub>3</sub><sup>-</sup> where the only ones that increased the film thickness, though still below what was observed using PAW (Fig. 2). These solutions also had physicochemical parameters closest to those of PAW. It was possible to conclude that H<sub>2</sub>O<sub>2</sub> and O<sub>3</sub>, being in low concentration in PAW, are not capable of significantly altering the deposition. The same was observed on simulations results. NO<sub>3</sub><sup>-</sup> plays an important role in the deposition; however, it was observed that there are more species or phenomena associated with PAW that need to be identified.

#### 4. References

[1]- Chaves, J. P. et al. *Nanomaterials*, *13*(24), 3110, (2023).

#### Acknowledgments

Júlia Karnopp thanks CAPES (Finance Code 001) and CNPq for the PhD and PDJ scholarships, respectively.

<sup>\*</sup>Corresponding author: julia\_karnopp@outlook.com



## OBTAINING LEAK-PROOF NBTI/NB/CU-OFHC BILLETS FOR MECHANICAL PROCESSING OF SUPERCONDUCTOR MONOFILAMENTS

Bruna Costa<sup>1\*</sup>, Tales Ferreira<sup>1</sup>, Daniel Kakizaki<sup>1</sup>, Rogério Ribeiro<sup>1</sup>, Daniel Doretto<sup>1</sup>, Danilo Silva<sup>1</sup>, Rafael Defavari<sup>1</sup>, Thiago Mendes da Rocha<sup>1</sup>, Rafael Seraphim<sup>1</sup>, Osmar Bagnato<sup>1</sup>, Maysa Terada<sup>1</sup>, Lucas Otani<sup>2</sup>

<sup>1</sup>Brazilian Center for Research in Energy and Materials (CNPEM), Campinas, SP, Brazil

<sup>2</sup>Department of Mechanical Engineering, Federal University of São Carlos, São Carlos, SP, Brazil

#### 1. Introduction

NbTi superconducting multifilament wires are widely used in MRI systems and particle accelerators. Each monofilament is obtained from mechanical processing of larger billets that may be described by a NbTi superconducting core surrounded by Cu-OHFC caps and, sometimes, a diffusion barrier of pure Nb. These billets must be leak-proof, since any signs of impurities or oxidation at interfaces will influence negatively the later mechanical processing. Differences on mechanical properties, mainly hardness, between the billets' components are also critical [1,2]. Usually, electron beam is used to seal billets with no significant impacts on mechanical properties, however, this is an expensive method. Thus, an adequate method to seal Cu-OFHC caps around NbTi/Nb cores, with viable cost-benefit, without strong decreasing on Cu mechanical properties, namely hardness, should be found.

#### 2. Experimental

Two different methods to seal NbTi/Nb/Cu-OFHC billets for later mechanical processing of leak-proof superconducting monofilaments were investigated: brazing and gas tungsten arc welding (GTAW). Brazing was performed in vacuum furnace at 800 °C, using CuSil® (72% Ag and 28% Cu) filler. GTAW was performed using a robotic arm, current of 160 A, frequency of 6 Hz, helium gas flow rate of 10 L/min and a 1.6 mm of diameter tungsten electrode, separated from the pieces to be joined from 1 mm. Leak tests were performed (Leak Detector G8601-60000, Agilent Technologies), billets were evacuated and sealed. Then, Vickers' microhardness measurements were also performed (Leco 100 AT, using 0.2 kgf).

#### 3. Results and Discussions

Both tested methods were effective in sealing the billets, since they were approved in the leak tests. No signs of oxidation were found in the billets' internal components for both methods, which may be observed in Fig. 1, in detail, for the brazed billet. Vickers' microhardness measurements, however, point to a significant decrease (50%) for Cu-OFHC cap of billet sealed from brazing. Better results were observed for billets sealed from GTAW, which presented specifically localized decreasing on Vickers' microhardness values, only in the lid area and no significant decrease on this parameter along the Cu-OFHC cap length. Since hardness at the lid area is not critical for the billets' mechanical processing, GTAW was an effective method on obtaining leak-proof billets of NbTi/Nb/Cu-OFHC billets for mechanical processing of superconducting monofilaments.

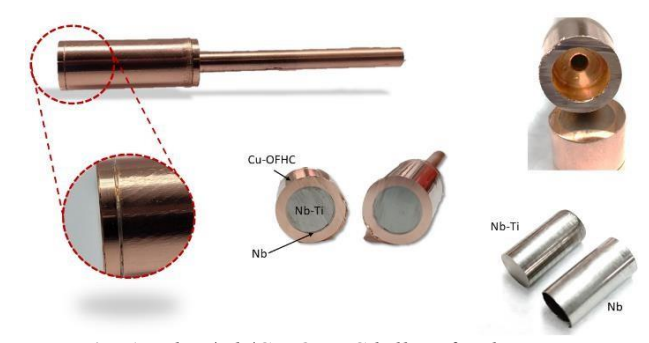


**Fig. 1.** *NbTi/Nb/Cu-OFHC billet after brazing.* 

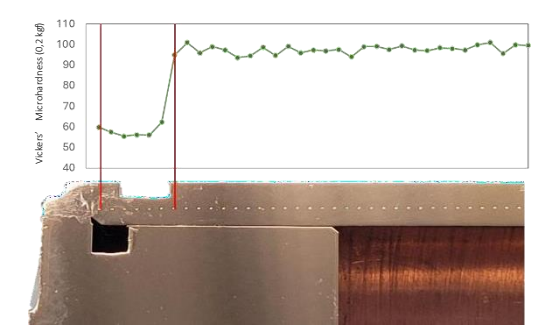


**Fig. 2.** Vickers' microhardness profile along the Cu-OFHC length.

#### 4. References

- [1]- H. Kumakura, Jpn. J. Appl. Phys. **51**, 010003 (2012).
- [2]- R. W. Heussner, P. J. Lee, D.C. Larbalestier, IEEE Trans. Appl. Supercond., 3, 757–760 (1993).

#### Acknowledgments

Authors acknowledge The National Council for Scientific and Technological Development (408917/2022-9 and 383360/2023-4) for the financial support and scholarship.

<sup>\*</sup>Corresponding author: Bruna Costa (bruna.costa@cnpem.br)



# CONTROL OF NITROGEN CONCENTRATION ON EXPANDED AUSTENITE BY GAS PULSES IN LOW-TEMPERATURE PLASMA NITRIDING

Andrey Matheus Vianna<sup>1</sup>, Euclides Alexandre Bernardelli<sup>1</sup>, Julio Cesar Klein das Neves<sup>1</sup> and Márcio Mafra<sup>1</sup>\*

<sup>1</sup>Universidade Tecnológica Federal do Paraná – Campus Curitiba

#### 1. Introduction

The low-temperature plasma nitriding of stainless steel has recently been extensively studied. Despite a large amount of research focused on describing the improvement in mechanical properties of nitrided stainless steel, results can be found reporting a brittle behavior of the expanded austenite. In some cases, as sintered austenitic stainless steel, nitriding results in a hardened, however cracked, surface [1]. The present work shows a way to control the toughness of the nitrided surface of nitrided stainless steel by pulsing nitrogen flow during the plasma nitriding. As a result of the interruption of nitrogen supply, as nitriding temperature is kept, the interstitial diffusion continues, leading to a decrease in nitrogen concentration in the S-phase layer. By controlling the duty cycle of nitrogen flow, it is possible to control the nitrogen concentration of nitrided stainless steel.

#### 2. Experimental

The experimental setup can be found in a previous work [2]. ISO 5832-1 SS samples were nitrided in a pulsed nitrogen flow for 2 and 8h with 50% and 10% duty cycles and compared with a sample nitrided in a continuous nitrogen flow. Samples were characterized by metallographic examination, XRD measurements, and nanoscale hardness.

#### 3. Results and Discussions

The cross-sections of nitrided samples are presented side-by-side in Figure 1. As can be seen, pulsed gas nitriding results in thinner expanded austenite layers, and this effect is more intense at lower duty cycles. A brittle aspect of the sample surface nitrided in continuous nitrogen flow can also be observed. The influence of the nitrogen-pulsed flow on the hardness is shown in Figure 2. As the offer of nitrogen decreases, lower hardness is found. However, for the samples nitrided with a duty cycle of 10%, a surface hardness of 12.8GPa (8P10) and 11.6GPa (2P10) were measured, a 3,5 factor from the untreated material, and 90% of the sample nitrided in continuous nitrogen flow.

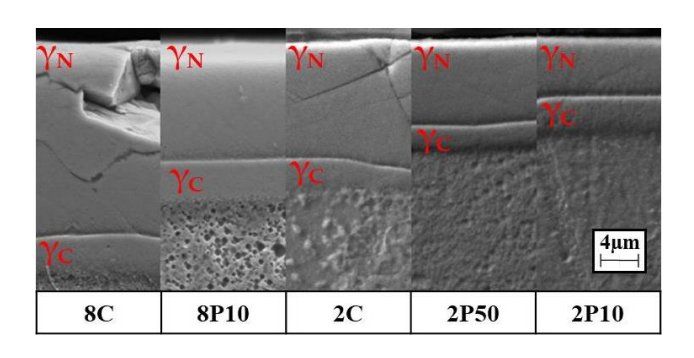


**Fig. 1.** Comparison between treated samples with continuous (8C and 2C) and pulsed (8P10, 2P50, and 2P10) nitrogen flow.

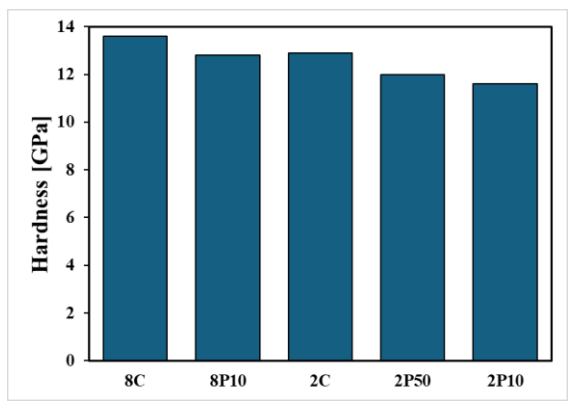


**Fig. 2.** Maximum surface hardness of samples nitrided with continuous (8C and 2C) and pulsed (8P10, 2P50, and 2P10) nitrogen flow.

#### 4. References

- [1]- A. F. Mendes, et al., Mat. Res., 17, 100-109, (2014).
- [2]- A. M. Vianna, et al., Mat Res. **23**, e20200249, (2020).

#### Acknowledgments

The authors would like to thank CAPES and FUNTEF for financial support. To the Multi-User Center for Materials Characterization - CMCM of UTFPR-CT and the Nanomechanical Properties Laboratory of UFPR.

<sup>\*</sup>Corresponding author: mafra@utfpr.edu.br



#### COMPARISON OF CNT-CVD AND CNT-PECVD INGESTION BY EARTHWORMS

Vitória P. Candido<sup>1</sup>, Alana M. Corá<sup>1\*</sup>, Larissa S. Almeida<sup>2</sup>, Gabriel A. C. Gonçalves<sup>3</sup>, Luciana S. Rossino<sup>1,2</sup>, Idalina V. Aoki<sup>3</sup>, Silvia P. Irazusta<sup>1,4</sup>.

<sup>1</sup>FATEC Sorocaba; <sup>2</sup>UFSCar Sorocaba; <sup>3</sup>Departamento de Engenharia Química da USP; <sup>4</sup> Programa de Mestrado Profissional em Gestão e Tecnologia em Sistemas Produtivos

#### 1. Introduction

The Plasma Enhanced Chemical Vapor Deposition (PECVD) is a film synthesis technique that derivates from Chemical Vapor Deposition (CVD) which uses plasma to transform gas into nanostructures in shorter treatment time [1]. This study aim is to compare the ingestion by earthworms for both Carbon Nanotubes (CNT).

#### 2. Experimental

The subjects were exposed to CVD and PECVD CNT's for 14 days, removed and then the clitellum cut and preserved in paraformaldehyde to posterior histological sections. Once the slides were obtained, they were analyzed by 2D Raman Spectroscopy to assess the presence of CNT at the earthworms, for both techniques, such as the CNT spectrum.

#### 3. Results and Discussions

The Fig. 1 shows the histological section analyzed for Carbon Nanotubes. In the Fig. 2 is observed that both CNTs present the characteristic spectrum of these nanoparticles, with bands D and G, as described in the literature. It can be observed, however, that the CNT-PECVD does not present the Radial Breathing Mode band, which can be observed in the CNT-CVD around 2550 cm<sup>-1</sup>. In general, the most intense peak present in both spectra is the peak around 1350 cm<sup>-1</sup>, which is the peak adopted for the application of the Filter function in the Large Area Scan (LAS) analyses. When comparing Figure 3 with Figure 4, it can be observed that the intensity of the green color in the CNT-CVD (Fig. 4) samples is more intense and occurs in greater quantity than in the samples exposed to the CNT-PECDV (Fig. 3). It is worth noting that, in the case of the CNT-CVD, the intense green coloration was observed even at lower concentrations, while the CNT-PECDV presented an intense green coloration only at the highest concentrations. These data demonstrate that the CNT-PECVD is possibly a cleaner process than CNT-CVD, once that there is less impact at the earthworms.

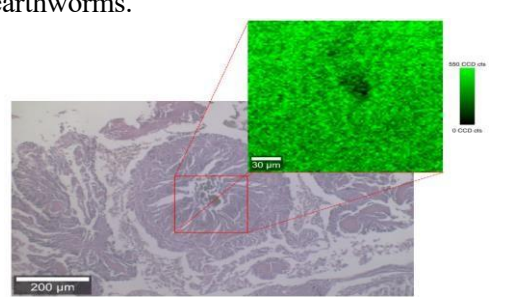


**Fig. 1.** *CNT spectrum of histological section obtained.* 

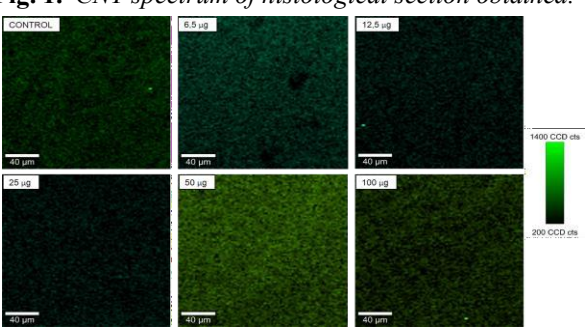


**Fig. 3.** Raman of the histological sections for different concentrations of CNT-PECVD.

Fig. 2. Raman spectrum for both CNT.

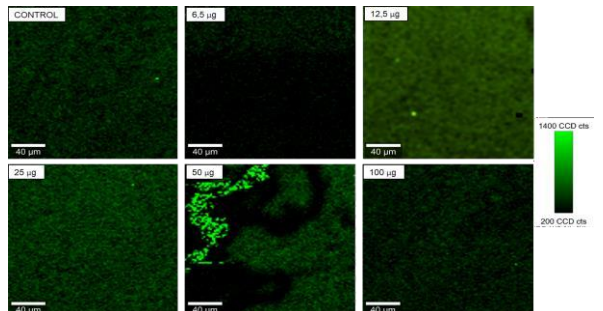


**Fig. 4.** Raman of the histological sections for different concentrations of CNT-CVD.

#### 4. References

[1] M. Cristaldo-Oliveira. Revista Brasileira de Ensino de Física, v. 42, e20200297, 2020.

#### Acknowledgments

To Instituto de Patologia e Citologia de Sorocaba for made the histological slides.

<sup>\*</sup>Corresponding author: alana.cora@fatec.sp.gov.br



#### SUBSTRATE FLOATING POTENTIAL IN A CATHODIC CAGE SYSTEM

Gabriel Corteletti Camargo, Luis Guilherme da Silva Rosa, Julio César Sagás\*

Laboratory of Plasmas, Films, and Surfaces, Universidade do Estado de Santa Catarina, JoinvilleSC. Brazil

#### 1. Introduction

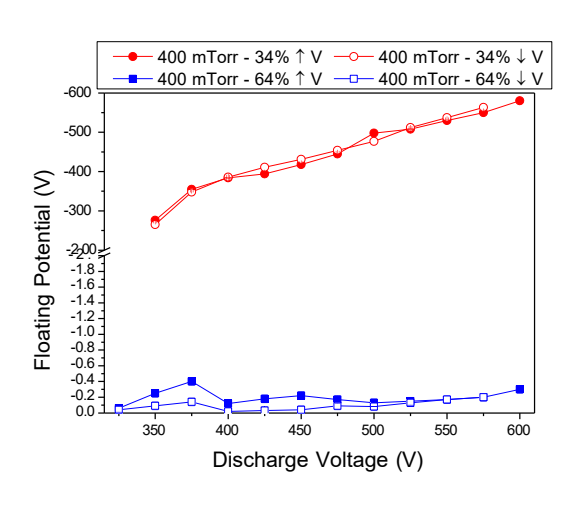
Cathodic cage plasma systems have been studied for different surface treatments, including nitriding, polymerization [1], and polymer surface modification [2]. For the last one, the main advantage is the possibility of maintaining the plasma outside the cage, avoiding excessive sample heating. On the other hand, the plasma can form inside the cage creating a hollow cathode discharge. The spatial distribution of the plasma depends on the cage geometry and working pressure. In this work, we measured the floating potential of a substrate holder inside the cathodic cage as a function of discharge voltage for different meshes and pressures. Plasma simulations of a cathodic cage system were also performed to compare qualitatively with the experimental results.

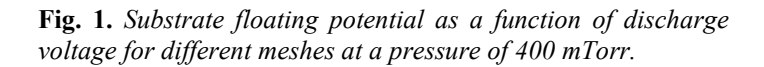
#### 2. Experimental

The cathodic cage is composed of a mesh of austenitic stainless steel. Two different meshes were used, one with 64% of open area and another one with 34%. We measured the substrate floating potential for discharge voltages between -350 V to -600 V using a Pinnacle Plus DC Power Supply. The working pressures varied between 300 mTorr and 500 mTorr using argon as the plasma forming gas. The simulations were conducted using the Plasma module of COMSOL Multiphysics.

#### 3. Results and Discussions

The plasma is generated inside the cage for the mesh with 64% of open area in all conditions tested. The contact of the plasma with the substrate causes the substrate floating potential to maintain values above – 0.6 V (Fig. 1). On the other hand, for 34% of open area the plasma is kept outside the cage, and the substrate floating potential is close to the discharge voltage (Fig. 1). The same qualitative behavior is observed in the simulations, where the increase of open area leads to the formation of plasma inside the cage (Fig. 2).





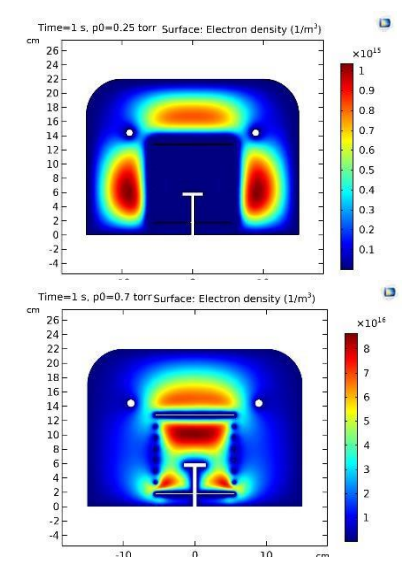


**Fig. 2.** Simulated plasma density distribution for different meshes.

#### 4. References

[1] Guinter, E.; Fontana, L. C.; Becker, D. (2019). Maleic anhydride film deposition through an active screen plasma system. Bulletin of Materials Science, v. 42. 23.

[2] Alonso, J.G.; Dalmolin, C.; Nahorny, J.; Recco, A. A.C.; Fontana, L.C.; Becker, D. (2018) Active screen plasma system applied to polymer surface modification: poly(lactic acid) surface activation before polyaniline graft polymerization in aqueous medium. J Polym Eng 38(8), 795-802.

#### Acknowledgments

Thanks to FAPESC (grant 2024TR000258) and CNPq (grant 304053/2021-0 and PIBIC).

<sup>\*</sup>corresponding author: julio.sagas@udesc.br



# EXPLORING THE THERAPEUTIC POTENTIAL OF SURFACE DBD PLASMA IN B16F10 CELLS TREATMENT: A COMPARATIVE STUDY OF DIRECT AND INDIRECT APPROACHES

Luan Gonçalves de Lima<sup>1</sup>, Michaela Shiotani Marcondes<sup>1</sup>, Rafaela Campos Queiroz<sup>2</sup>, Dayane Batista Tada<sup>2</sup>, Clodomiro Alves Júnior<sup>3</sup>, Rodrigo Sávio Pessoa<sup>1</sup>

<sup>1</sup>Aeronautics Institute of Technology (ITA), São José dos Campos-SP, Brazil <sup>2</sup>Federal University of São Paulo (UNIFESP), São José dos Campos-SP, Brazil <sup>3</sup>Federal Rural University of the Semi-Arid (UFERSA), Mossoró-RN, Brazil

### 1. Introduction

The growing interest in utilizing cold atmospheric pressure plasma (CAP) for cancer therapy has recently garnered attention [1-4]. CAP has emerged as a highly promising therapeutic option for tumor treatment due to its selective ability to induce cancer cell death [3,4]. Moreover, recent findings demonstrate that plasma not only directly affects cells but also exerts an influence through indirect treatment using previously prepared plasma-activated medium (PAM) [2,3]. Therefore, this study investigates the application and characterization of surface Dielectric Barrier Discharge (DBD) plasma as a potential treatment for B16F10 cells, a widely used cell model for melanoma studies. The experiment encompasses both direct and indirect treatment approaches.

### 2. Experimental

A surface DBD plasma was applied onto a 24-well plate containing B16F10 cells in RPMI culture medium, with a concentration of 6.10<sup>4</sup> cells/mL per well. In the direct treatment, DBD plasma was directly administered to the cell culture medium containing B16F10 cells for different exposure times: 1, 2 and 3 minutes. In contrast to direct application, indirect plasma treatment involves irradiating the cell culture medium, which was subsequently transferred to a culture plate containing cells. The generated DBD plasma was characterized for its physicochemical properties, including the composition of reactive species via OES and electrical characterization. The PAM was characterized using UV-Vis spectrophotometry. The effects of DBD plasma treatment on cell viability were assessed in both application methods using the MTT assay after 24 h and 48 h of activation.

### 3. Results and Discussion

For the different activation times, the time in which the best results were achieved was exposing the cells in 3 minutes, resulting in a 29% decrease in cell viability for the direct method, and 51% for the indirect method. This difference in results between direct and indirect methods can be explained because, in the direct method, at least three factors can be related: short-lived reactive species (O<sub>3</sub><sup>-</sup> and OH), long-lived species (H<sub>2</sub>O<sub>2</sub>, NO<sub>2</sub><sup>-</sup>, NO<sub>3</sub><sup>-</sup> and HNO<sub>2</sub>) and physical factors (UV radiation). On the other hand, in the indirect method only long-lived species should be considered.

### 4. References

- [1] Adachi, T., Tanaka, H., Nonomura, S., Hara, H., Kondo, S. I., & Hori, M. Free Radical Biology and Medicine, 79, 28–44 (2015).
- [2] Yan, D., Sherman, J. H., & Keidar, M. In Oncotarget Vol. 8, Issue 9 (2017).
- [3] Malyavko, A., Yan, D., Wang, Q., Klein, A. L., Patel, K. C., Sherman, J. H., & Keidar, M. In Materials Advances (Vol. 1, Issue 6, pp. 1494–1505). Royal Society of Chemistry (2020).
- [4] Saadati, F., Mahdikia, H., Abbaszadeh, H. A., Abdollahifar, M. A., Khoramgah, M. S., & Shokri, B.. Scientific Reports, 8(1) (2018)

### Acknowledgments

CNPq Universal grant 420775/2023-4.

<sup>\*</sup>Corresponding author: luangoncalveslima@gmail.com



# SESSÃO DE PÔSTER 1

Segunda-feira (11/11/2024)

XLV Congresso Brasileiro de Aplicações de Vácuo na Indústria e na Ciência

Balneário Camboriú - SC 11 a 13 de Novembro de 2024





# ANALYSIS OF THE BIOACTIVITY OF BIOSILICATE FUNCTIONALIZED WITH MALEIC ANHYDRIDE BY PLASMA

Davi J. Espíndola<sup>1\*</sup>, Camila T. Mamani<sup>1</sup>, Teresa T. Steffen<sup>1</sup>, Luis G. S. Rosa<sup>1</sup>, Bruna Segat<sup>1</sup>, Daniel A. L. V. da Cunha<sup>2</sup>, Lidiane C. Costa<sup>2</sup>, Luiz A. Pessan<sup>2</sup>, Daniela Becker<sup>1</sup>.

<sup>1</sup>Laboratory of Plasmas, Films and Surfaces, Santa Catarina State University (UDESC), Joinville, Brazil <sup>2</sup>Department of Materials Engineering (DEMa), Federal University of São Carlos

### 1. Introduction

Polylactic acid (PLA), known for its biodegradability and biocompatibility, is a promising *scaffold* material when aiming for repair of injured tissues, however, it lacks osteoinductive properties [1]. Biosilicate® (BIO) can serve as an osteoinductive agent in the polymeric matrix [2], yet, causing polymer chain cleavage during the processing, resulting in early degradation of the PLA. In order to prevent PLA degradation by BIO, this particle can be surface modified. This study evaluates the effect of functionalizing BIO with maleic anhydride (MA) on the hydroxyapatite formation through the bioactivity test.

### 2. Experimental

Three samples, as shown in the Table 1, were made with 90% BIO and 10% MA, then treated in a homemade Capacitive Coupled Plasma (CCP) reactor using an Asymmetric Bipolar Plasma Power Supply (ABiPPS). Argon gas was used, starting at a base pressure of  $2.5 \times 10^{-1}$  Torr and adjusted to  $7.0 \times 10^{-1}$  Torr.

Tab1. Samples characteristics.

Sample name	Treated	Power	Pulse	Voltage	Pulse	Pulse
	time (h)	(W)	type	(V)	width (μs)	Duration (μs)
BIO_MA_1h_ABIPPS_6 μs	1	200	Bipolar	400	6	1
BIO_MA_1h_ABIPPS_10μs	1	200	Bipolar	400	10	1
BIO_MA_2h_ABIPPS_10μs	2	200	Bipolar	400	10	1

For the bioactivity test, a simulated body fluid basis (SBF) was prepared as per ISO 23317:2014, and 100 ml of SBF was mixed with 150 mg of each sample and shaken at 37 °C for 4h, 8h, 24h, 48h, and 72h, based on Anthony et al [3]. Later the solution was filtered, and the materials were stored in a desiccator. The compounds were then analyzed using a Scanning Electron Microscope (SEM) Neo Scope, model JCM-7000.

### 3. Results and Discussions

Fig 1 and Fig. 2 present the micrography after 72h in the SBF solution of pure BIO and BIO\_MA\_1h\_ABiPPS\_6µs, respectively. Despite MA functionalization, the BIO still had hydroxyapatite on its surface, concluding that the particle bioactivity did not have significant changes.

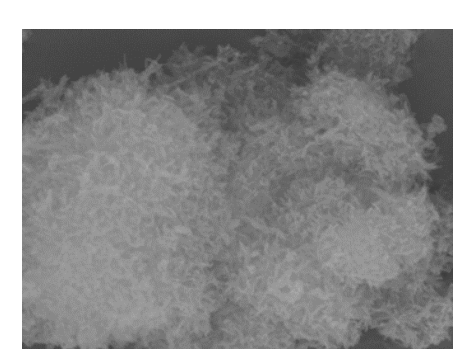
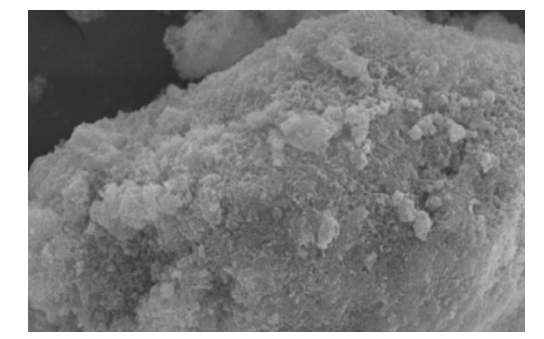


Fig. 1. Pure Biosilicate® 72 hours shaken.



**Fig. 2.** BIO\_MA\_1h\_ABiPPS\_6µs 72 hours shaken.

### 4. References

- [1]- L. A. Klok, funcionalização de nanopartículas de óxido de zinco por plasma utilizando compostos orgânicos. Joinville, 2022.
- [2]- R. L. Siqueira e E. D. Zanotto, Quim. Nova, 34, 1234-1240, (2011).
- [3]- ANTHONY L. B. et al., J Mater Sci: Mater Med, 26, 115, (2015).

### Acknowledgments

The authors are grateful for the support given by CNPq through scholarship and projects [306823/2021-7,404401/2023-6], FAPESC [2020TR1450, PAP-FAPESC 2023TR000258] and FAPESP [2019/27415-2].

<sup>\*</sup>Corresponding author: davijoao123@hotmail.com



# OPTIMIZING E. COLI INHIBITION WITH COLD ATMOSPHERIC PLASMA JET DELIVERY PROTOCOL

Diego Morais da Silva<sup>1,2\*</sup>, Augusto Stancampiano<sup>1</sup>, Sébastien Dozias<sup>1</sup>, Pablo Escot Bocanegra<sup>1</sup>, Konstantin Georgiev Kostov<sup>2</sup>, Cristiane Yumi Koga-Ito<sup>2</sup>, Eric Robert<sup>1</sup>

<sup>1</sup>GREMI-CNRS/Université d'Orléans, France

<sup>2</sup>São Paulo State University (UNESP), Brazil.

### 1. Introduction

Cold atmospheric plasma jets (CAPJ) have been studied as a tool for microbial decontamination in different fields, such as the food industry and the medical environment. CAPJ produce oxygen and nitrogen reactive species (RONS) that interact with the microorganism structure, leading to inhibition. Its efficacy is correlated to the plasma parameters [1]. In this work, we studied the influence of the number of discharges, i.e. plasma pulses, on *Escherichia coli* inhibition.

### 2. Experimental

The inhibition halo test was performed using the E. coli CIP 54 117 strain. The inoculum containing  $1.10^6$  CFU/mL was standardized using a spectrophotometer (OD = 0.068,  $\lambda = 600$  nm). Then, 3 mL of the inoculum was transferred to a Luria-Bertani (LB) agar plate distributed all over the surface. After 15 min of contact, the suspension was removed, and the plates were kept inside a laminar flow until completely dried (15 min). The plasma reactor used was described elsewhere [2]. The distance between the plasma reactor output and the agar surface was 5 mm. The helium gas flow of 1.5 SLM was set to the treatment. Ten or one hundred plasma pulses were delivered as burst at 10 or 20 kHz, with various duty cycles and treatment times, as summarized in Table 1. The used parameters are described in Table 1. The voltage was set to 10 kV for all the experiments. All the experiments were performed in triplicate (n = 9).

**Table 1.** CAPJ parameters were used for the inhibition halo test.

Parameter	No of Pulses/second	Internal frequency (kHz)	Nº of Pulses	Time off (ms)	Duty cycle (%)
Base	500	10	10	19	5%
10x	5000	10	100	10	50%
20x	10000	20	100	5	50%

### 3. Results and Discussions

After 300s treatment, the Base parameter resulted in an area of  $0.59 \pm 0.06$  cm<sup>2</sup> of inhibition (Fig 1). Using parameter 10x, it delivered the same n° of pulses as the Base parameter in a shorter time (30s), showing an inhibition zone of  $0.6 \pm 0.04$  cm<sup>2</sup>. Duty cycle modulation is thus a convenient way to achieve the same inhibition but with a much shorter treatment time, which could be an essential protocol for medical applications. Similar behavior was observed during the second test, with more pulses delivered. Ten times more pulses were delivered compared to the previous test. The treatment of 300s using the parameter 10x resulted in an area of  $2.76 \pm 0.1$  cm<sup>2</sup>, and using the parameter 20x for 150s, the inhibition of  $2.17 \pm 0.04$  cm<sup>2</sup> was observed. Discharge frequency is a second way to improve inhibition performance with again reduced treatment time. Work is ongoing to assess the role of short- and long-living RONS in decontamination for these various plasma delivery parameters. In conclusion, a strong correlation was observed between the number of pulses and even shorter treatment times.

### 4. References

- [1] Do Nascimento, Fellype, et al. IEEE Trans Radiat Plasma Med Sci. 8 (3), 307–322 (2024)
- [2] Omran, A.V., et al. Plasma Sources Sci Technol. 29 (10), (2020)

### Acknowledgments

This work was supported by FAPESP (grant no. 2023/02432-2, 2021/02680-5, 2019/05856-7).

<sup>\*</sup>Corresponding author: diego.m.silva@unesp.br



# INFLUENCE OF TEMPERATURE ON THE MELTING OF A FILM DEVELOPED FROM MACROALGAE

Daniela Pravato Vieira<sup>1\*</sup>, Fábio de Farias Neves<sup>2</sup> and Daniela Becker<sup>1</sup>

<sup>1</sup>Santa Catarina State University (UDESC), Joinville, SC, Brazil

<sup>2</sup> Santa Catarina State University (UDESC), Laguna, SC, Brazil

### 1. Introduction

The extraction of biofertilizers from the macroalgae *Kappaphycus alvarezii* in Santa Catarina generates biomass [1], the application in polymeric films emerges as a solution to value this waste, transforming it into a biopolymer that can be used in packaging and single-use products [2].

### 2. Experimental

The biomass is dried in an oven at 40°C for 24 hours, after drying it is passed through a high-energy mill. A water/glycerin/macroalgae mixture is made in a 48/32/20 ratio, then it is passed through a Haake rheometer. The sample is dried again in an oven at 40°C for 24 hours and placed in a press (1 TON) for the production of the film at three different temperatures (110°C, 130°C and 150°C).

### 3. Results and Discussions

As this material is being developed, the temperature used in the press was tested to check the material's melting under an optical microscope. Fig. 1 shows the film obtained without magnification. Figs. 2, 3, and 4 show the difference in the fusion of the material as the temperature of the press increased. Fig. 4 shows the most homogeneous film, concluding that a temperature of over 150°C is needed for the material to fuse completely.



Fig. 1. Biofilm without magnification.



Fig. 2. Micrograph 110°C.

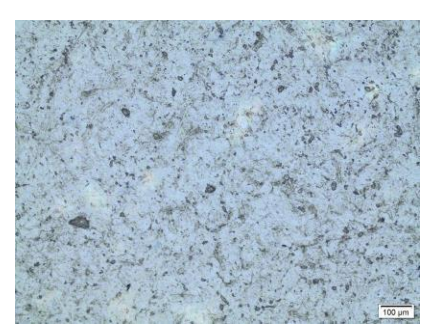


Fig. 3. Micrograph 130°C.

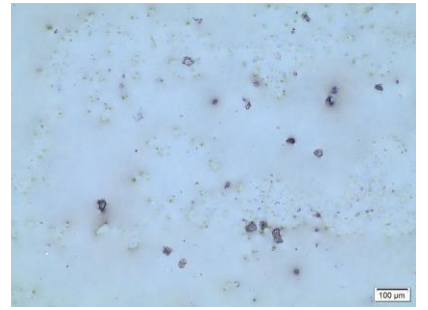


Fig. 4. Micrograph 150°C.

### 4. References

[1]- EPAGRI. Macroalgas: Epagri cria novo mercado para maricultores catarinenses. Epagri, 18 jul. 2023. Disponível em: https://www.epagri.sc.gov.br/index.php/2023/07/18/macroalgas-epagri-cria-novo-mercado-para-maricultores-catarinenses/. Acesso em: 25 jun. 2024.

[2]- SCHMIDTCHEN, Ludwig et al. Processing technologies for solid and flexible packaging materials from macroalgae. **Algal Research**, v. 61, p. 102300, 2022.

### Acknowledgments

This research was supported by CNPQ, CAPES (code 001), and PAP-FAPESC (2023TR000258)

<sup>\*</sup>Corresponding author: daniela.vieira@edu.udesc.br

# DESIGN AND CONSTRUCTION OF A SYSTEM OF MAGNETIC FIELD INDUCED BY COILS IN A VACUUM CHAMBER

### FOR EXPERIMENTS WITH PLASMA PHYSICS

João Gabriel B. Aquino<sup>1\*</sup>, José Leonardo Ferreira<sup>1</sup>, and Rodrigo Andrés Miranda<sup>1</sup> *Universidade de Brasília*, *Brasília*, *DF*, *Brasil*.

### 1. Introduction

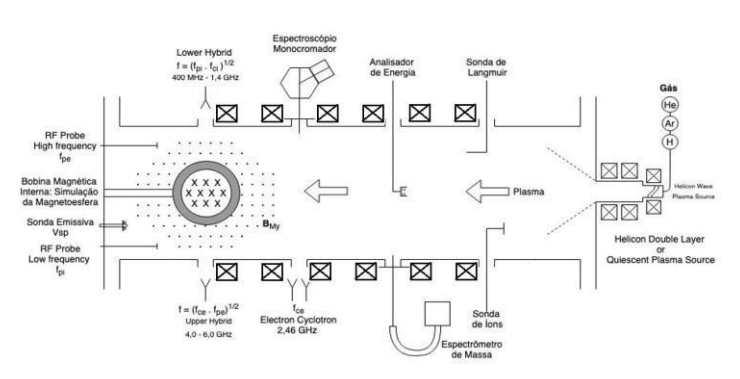
This work aims to present the planning and development of an apparatus for the generation of a uniform magnetic field in a vacuum chamber for plasma experiments, related to space weather, at the Plasma Physics Laboratory of the University of Brasília (*LFP-UnB*). This work aims to build a device that can produce plasmas confined by magnetic fields in different configurations. The purpose is to experimentally simulate the conditions found in space plasmas near Earth, and to study waves and turbulence that occur in the Earth's magnetospheric plasma, wave-particle interactions, plasma dynamics, and magnetic confinement phenomena. These experiments require a uniform magnetic field to represent the interplanetary magnetic field (*IMF*). A system of coils to generate the magnetic field was developed. This magnetic field has an axial configuration, aligned with the main axis of the cylindrical vacuum chamber, and is generated by six coils. This work was divided into the following stages: creation of a computer-assisted design (*CAD*) representing the *LFP-UnB* vacuum chamber, analysis of the coil system theory, analysis of positioning, sizing, and distribution of the coil system, simulation in the Finite Element Method Magnetics (FEMM) software, structure development, and comparison of results.

### 2. Experimental Scheme

The vacuum chamber of the LFP-UnB has 0.5 m in diameter and 2.0 m in length. This vacuum chamber is already installed and fully operational, being mainly employed for testing plasma thrusters. The central component of this apparatus is the cylindrical vacuum chamber, made of stainless steel, capable of reaching a pressure corresponding to  $10^{-7}$  Torr. This chamber is equipped with a total of four vacuum pumps for suction. The first is a mechanical pump with a capacity of up to  $10^{-3}$  Torr and has a flow rate of 35 m³/h. The other three are diffusion pumps with a total average flow rate of 10,800 m³/h. The characterization of the plasma parameters inside the chamber - such as electron density and temperature, plasma potential, and instabilities - is carried out using Langmuir probes. Ion acceleration is determined by energy sensors, while ion dynamics in the acceleration channel is measured based on ion temperature, using the plasma spectroscopy technique. Recently, we finished the installation of 6 coils with 250 turns each using AWG 7 copper wire.

### 3. Results and Discussion

The results obtained from numerical simulations with the FEMM software demonstrated that an approximately uniform magnetic field in 70% of the vacuum chamber can be obtained using the installed 6 coils. This result is of great importance since the chamber cannot support more coils due to structural symmetry issues. The magnitude



of the resulting magnetic field will be enough for the confinement of electrons at the center of the vacuum chamber. The comparison between the computational simulation data and those obtained experimentally is also addressed in this work.

**Fig. 1.** Schematics of the vacuum chamber, showing the position of the six coils providing an uniform magnetic field.

### 4. References

[1]- Yur, G. et al. Laboratory facility for magnetospheric simulation., v. 100, n. A12, p. 23727–23736, dez. (1995).

[2]- SHAIKHISLAMOV, I. F. et al. Laboratory

model of magnetosphere created by strong plasma perturbation with frozen-in magnetic field. Plasma Physics and Controlled Fusion, IOP Publishing, v. 56, n. 12, p. 125007, (2014).<sup>2</sup>

[3]- MINAMI, S.; TAKEYA, Y. Flow of artificial plasma in a simulated magnetosphere: Evidence of direct interplanetary magnetic field control of the magnetosphere. Journal of Geophysical Research: Space Physics, v. 90, n. A10, p. 9503–9518, (1985).

.

<sup>1</sup> joaogabriel2256@hotmail.com

Universidade do Estado de Santa Catarina - UDESC, November 11-13, 2024
[4]- BAUM, P. J.; BRATENAHL, A. The laboratory magnetosphere. Geophysical Research Letters, v. 9, n. 4, p. 435– 438, (1982).



# EVALUATING ANTIMICROBIAL EFFECTS OF PLASMA-ACTIVATED LIQUIDS USING SURFACE-WAVE MICROWAVE PLASMA JET: A COMPARATIVE ANALYSIS OF DEIONIZED WATER AND SALINE SOLUTION

Michaela Shiotani Marcondes<sup>1</sup>, Luan Gonçalves de Lima<sup>1</sup>, Lady Daiane Pereira Leite<sup>2</sup>, Victória Kelly Fonseca Tavares<sup>2</sup>, Clodomiro Alves Júnior<sup>3</sup>, Felipe de Souza Miranda<sup>1,2</sup>, Cristiane Yumi Koga-Ito<sup>2</sup>, Rodrigo Sávio Pessoa<sup>1</sup>

<sup>1</sup>Aeronautics Institute of Technology (ITA), São José dos Campos-SP, Brazil <sup>2</sup>Paulista State University (UNESP), São José dos Campos-SP, Brazil <sup>3</sup>Federal Rural University of the Semi-Arid (UFERSA), Mossoró-RN, Brazil

### 1. Introduction

The use of non-thermal plasma for liquid activation results in plasma-activated liquids (PAL), a substance that has garnered significant attention in various sectors, including agriculture, environmental studies, sterilization, and healthcare [1,2]. Notably, in the medical and dental fields, PAL acts as an effective antimicrobial agent [2]. This research aims to conduct a microbiological evaluation of two plasma-activated liquids: deionized water and 0.9% saline solution. The PALs were produced using a surface wave microwave plasma jet, targeting inactivation of *S. aureus*, *E. coli* and *C. albicans*.

### 2. Experimental

The study used a surface-wave microwave plasma jet operating at 2.45 GHz with continuous argon gas flow. The microwave power up to 200 W was supplied by a solid-state source (Sairem), with experiments conducted at 70 W. Deionized water (DI) and 0.9% saline solution (SS) were activated in volumes of 40 mL at 10- and 30-min intervals. The antimicrobial efficacy was evaluated in groups: DI (control), SS (control), DI activated for 10 min, DI activated for 30 min, SS activated for 10 min, and SS activated for 30 min. A standardized microbial suspension (750  $\mu$ L) containing 10<sup>6</sup> cells/mL was meticulously prepared in sterile saline solution (0.9% NaCl) using a spectrophotometer (AJX1600, Micronal, São Paulo, SP, Brazil) to ensure uniformity. Subsequently, the prepared microbial suspension was mixed with 1250  $\mu$ L of PAL and incubated for 10- and 30-min. Serial dilutions were made in sterile saline and 100  $\mu$ L aliquots were spread on the appropriate culture media. The same procedure was repeated for SS. The plates were then incubated aerobically at 37°C for 24 hours, after which CFU/mL were determined based on colony counts.

### 3. Results and Discussion

Microbiological tests demonstrated a significant reduction in the bacteria *E. coli* and *S. aureus* with plasma-activated deionized water (DI), particularly evident at the 40-minute mark. However, this effect was less pronounced with the plasma-activated 0.9% saline solution. The research suggests that the low pH of the samples is a critical factor in their antimicrobial activity [2]. Consequently, activated DI proves to be an effective, low-cost method for bacterial inactivation, though it does not exhibit the same efficacy against fungi under the current conditions. In contrast, the 0.9% saline solution did not display comparable effectiveness against bacteria and showed a smaller pH reduction than activated DI.

### 4. References

[1] S. Kim, C. Kim. Biomedicines, 9(11), 1700. (2021).

[2] N. Milhan. W. Chiappim. A. Sampaio, M. Vegian. R. Pesoa. C. Koga-Ito, Int. J. Mol. Sci., 23(8), 4131. (2022)

### **Acknowledgments**

FAPESP grants 2019/05856-7 and 2022/13141-0, and CNPq Universal grant 420775/2023-4.

<sup>\*</sup>Corresponding author: marcondes.micaela5@gmail.com



# DEVELOPMENT OF COATINGS USING ASYMMETRIC BIPOLAR PULSED PLASMA IN A CATHODIC CAGE: AN EXPLORATORY

Amanda Gabrielly de Matia<sup>1</sup>, Guilherme de Oliveira Silva<sup>1</sup>, Gustavo Serenini<sup>1</sup>, Igor Simon Santos<sup>1</sup>, Maria Eduarda Baittinger<sup>1</sup>, Paola Egert Ortiz<sup>2</sup>, Joel Stryhalski<sup>1\*</sup>, Alexandre Galiotto<sup>1</sup>, Fernando Henrique Gruber Colaço<sup>1</sup>, Luis César Fontana<sup>3</sup>

<sup>1</sup>Instituto Federal de Santa Catarina <sup>2</sup>Universidade do Vale do Itajaí <sup>3</sup>Universidade do Vale do Itajaí

### 1. Introduction

In this study, the technique of plasma discharge with an asymmetric pulsed bipolar source [1], [2], [3] in a cathodic cage [4], [5], [6], [7], [8] was employed to deposit titanium nitride films. A comparison was made of the effect on the morphological, electrical, and optical properties of the films deposited on glass and monocrystalline silicon substrates using two titanium cages with lids of different open area percentages. To characterize the films, X-ray diffraction and EDX analyses were performed to obtain the composition of the coatings. Thickness measurements by profilometry and atomic force microscopy were done to obtain the thickness and morphology of the films. Electrical and optical properties were obtained by Hall effect, in the Van-der Pauw configuration, and UV-Vis spectrophotometer.

### 2. Results and Discussions

Thickness measurements indicated variation in the deposition rate as a function of the open area of the screen, and the roughness of the films also increased with the use of the cage with a more open mesh. The film deposited in an atmosphere of 100 sccm of nitrogen and 50 sccm of hydrogen, at a pressure of 1 torr, showed low transmittance in the red and near-infrared regions, suggesting its viability as a candidate for an infrared filter

### 3. References

- [1] C. M. Valdez, R. A. Barnes, C. C. Roth, E. K. Moen, G. A. Throckmorton, and B. L. Ibey, Sci Rep, vol. 7, no. 1, 2017
- [2] P. Fin, A. A. C. Recco, J. S. Scholtz, and L. C. Fontana, Materials Research, vol. 25, 2022,
- [3] J. S. Scholtz, L. C. Fontana, and M. Mezaroba, IEEE Transactions on Plasma Science, vol. 46, no. 8, 2018
- [4] R. R. M. de Sousa, P. S. Sato, B. C. Viana, C. Alves, A. Nishimoto, and P. A. P. Nascente, Journal of Vacuum Science & Technology A: Vacuum, Surfaces, and Films, vol. 33, no. 4, 2015
- [5] R. R. M. De Sousa et al., Materials Research, vol. 18, no. 2, 2015,
- [6] R. R. M. De Sousa, Y. J. L. Moura, P. A. O. De Sousa, J. Q. M. Neto, T. H. De Carvalho Costa, and C. A. Junior, Materials Research, vol. 17, no. 3, 2014,
- [7] R. M. Sousa et al, Matéria (Rio de Janeiro), vol. 13, no. 1, 2008,
- [8] S. S. Da Silva, C. D. L. R. Bottoni, L. C. Gontijo, and S. O. Ferreira, Revista Materia, vol. 22, no. 3, 2017



# THE IMPACT OF REPLACING MACOR WITH SHAPAL IN RF CATHODES FOR HALL THRUSTERS

Hudson M. Costa<sup>1\*</sup>, Jhonatha W. S. Paula<sup>2</sup>, José L. Ferreira<sup>3</sup>, Rodrigo A. Miranda<sup>4</sup> and CH Llanos Quintero<sup>5</sup>

<sup>1</sup>Faculty of Technology and Institute of Physics, University of Brasília (UnB)

<sup>2</sup>Dept. of Aeroespace Engineering and Institute of Physics, University of Brasília (UnB)

<sup>3</sup>Institute of Physics, University of Brasília (UnB)

<sup>4</sup>Dept. of Aeroespace Engineering and Institute of Physics, University of Brasília (UnB)

<sup>5</sup>Faculty of Technology, University of Brasília (UnB)

### 1. Introduction

Historically, hollow cathodes have served as the primary electron source in Hall thrusters. However, these devices require heating to elevated temperatures for electron emission, are costly to produce, and necessitate a complex power supply. Recently, there has been considerable interest in exploring alternative electron sources for use in plasma thrusters. Among the most promising is the radiofrequency (RF) cathode, notable for its straightforward design, ease of manufacture, and cost-effectiveness. The RF cathode primarily consists of Macor, stainless steel, and copper. Therefore, studying the thermal effects associated with the RF cathode is crucial to ensure that there is no risk of demagnetizing the permanent magnets within the electric thrusters when integrated into electric propulsion systems. Consequently, a thermal simulation is proposed to replace the ceramic material of the RF cathode. The concept of the RF cathode was derived from previous studies [1, 2, 3].

### 2. Experimental

The thermal simulation was conducted using ANSYS software, focusing solely on heat transfer through radiation and conduction. The basic operation of the RF cathode relies on the ionization of argon gas within the Macor chamber. Consequently, the ionized gas was treated as the heat source, with a thermal power of 30 W. To prevent the demagnetization of the magnets in a Hall-type thruster, thermal simulations were performed using alternative ceramic materials to assess whether there is a reduction in the temperature gradient.

### 3. Results and Discussions

Figure 1 depicts the RF cathode in operation at the Plasma Physics Laboratory (LFP) at the University of Brasilia (UnB), while Figures 2 and 3 present the thermal simulations for the RF cathode using Macor and Shapal ceramics, respectively. Upon analyzing these figures, a reduction in temperatures and a more uniform distribution of the temperature gradient can be observed. This improvement is attributable to the fact that the thermal conductivity of Shapal is approximately 36 times greater than that of Macor.

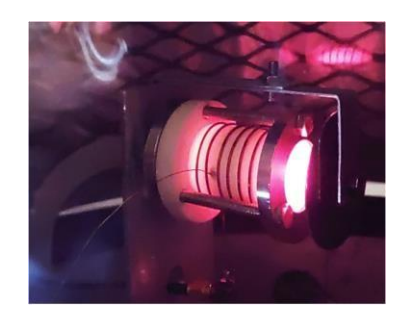


**Fig. 1.** *RF* cathode of the *LFP/UnB* in operation.

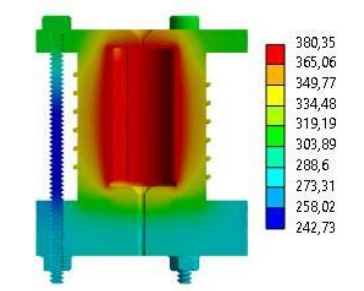


**Fig. 2.** Internal view of Macor RF cathode thermal simulation.

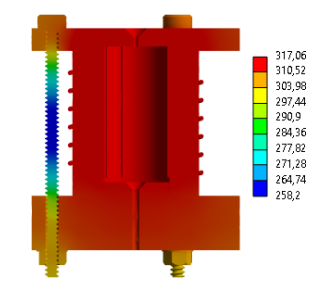


**Fig. 3.** Internal view of Shapal RF cathode thermal simulation.

### 4. References

- [1]- Celik, Murat, and Huseyin Kurt. "Ferromagnetic enhanced inductively coupled plasma cathode for thruster ion neutralization." *AIP Conference Proceedings*. Vol. 2011. No. 1. AIP Publishing, 2018.
- [2]- Hatakeyama, Tomoyuki, et al. "Preliminary study on radio frequency neutralizer for ion engine." *30th International Electric Propulsion Conference, Florence, Italy.* 2007.
- [3]- Jahanbakhsh, Sina, and Murat Celik. "Experimental investigation of operational parameters of a prototype radio frequency plasma cathode." 2015 7th International Conference on Recent Advances in Space Technologies (RAST). IEEE, 2015.

<sup>\*</sup>Corresponding author: hudson\_m.costa@outlook.com



# COMPARATIVE ANALYSIS ON THE GENERATION OF REACTIVE SPECIES (RONS) IN LIQUIDS WITH PLASMA EQUIPMENTS FOR CANCER THERAPY.

Diego V. Neves<sup>1</sup>, Kaique G. Hergesel<sup>2</sup>, Joelen O. Silva<sup>4</sup>, Amanda D. R. Lima<sup>3</sup>, Fernando Pradela<sup>3</sup>, Leonilda M. B. Santos<sup>3</sup>, Elidiane C. Range, Elaine C. Oliveira<sup>2,3</sup>, Nilson C. Cruz<sup>1</sup>, <sup>1</sup>UNESP – Paulist State University, <sup>2</sup>ImunnoCell Laboratory – FATEC, CEETEPS-SP; <sup>3</sup>University of Campinas – UNICAMP; <sup>4</sup>University Federal de São Carlos - UFSCar

### 1. Introduction

Atmospheric Pressure Plasma (APP) can be generated by applying high voltages in a gas at ambient pressure. This process generates short- and long-lived reactive nitrogen and oxygen species (RONS)[1]. Therapies using RONS stand out due to their versatility and effectiveness in different types of cancers [2]. One advantage of using plasmas in such a context is that the generated reactive species may vary according to the electrical configurations and the gases used to establish the discharge. In this work, lactated Ringer (Rilac) and NaCl solutions have been exposed to plasmas generated in two different systems and analyzed using spectrophotometric techniques and biological assays.

### 2. Experimental

Rilac and NaCl have been treated in two different systems: a commercial kINPen Ind. and a homemade generator. The solutions were exposed to the plasmas for 2, 5, and 10 minutes and subsequently characterized by UV-vis absorbance, pH analysis, and conductivity. Biological assays have been performed through the MTT oxidation technique, flow cytometry for cell death, and morphology to identify cell structural changes.

### 3. Results and Discussions

Figure 1 presents absorbance curves of NaCl and Rilac solutions exposed to plasmas for 30, 45, and 60 minutes. The shapes of the peaks are different, indicating that modifying the exposure time also affects the proportions of the species incorporated in the liquid.

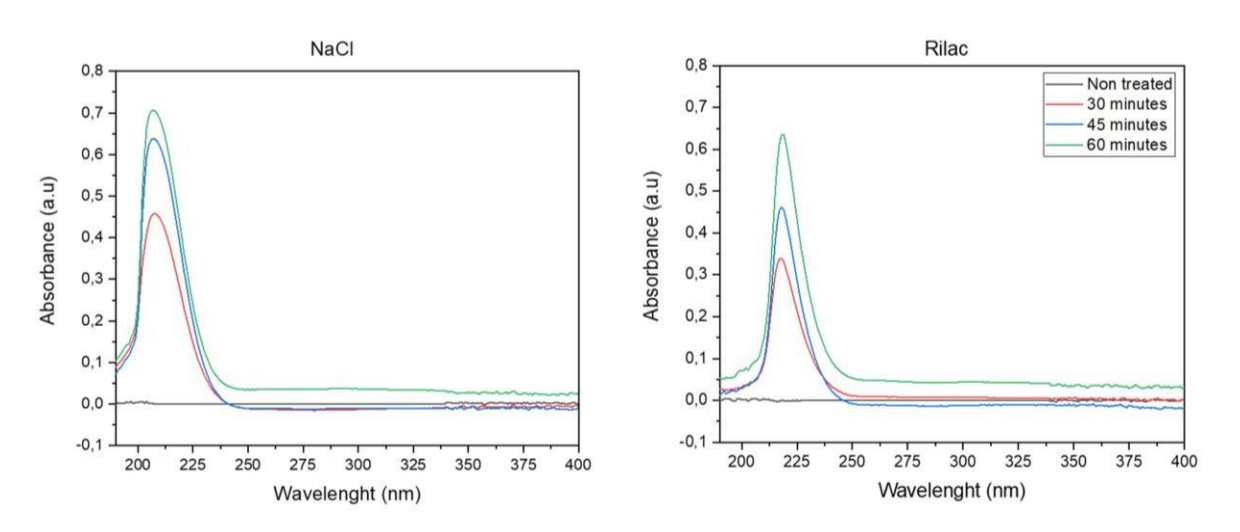


**Figure 1:** Absorbance spectra of Nacl and Rilac solution exposed to app treatment for 30, 45, and 60 minutes.

### 4. References

[1] Rahimpour, M., Taghvaei, H., Zafarnak, S., Rahimpour, M. R., & Raeissi, S. (2019). Post-discharge DBD plasma treatment for degradation of organic dye in water: A comparison with different plasma operation methods. Journal of Environmental Chemical Engineering, 7(4).

[2] Freund, E., Liedtke, K. R., Gebbe, R., Heidecke, A. K., Partecke, L. I., & Bekeschus, S. (2019). *In vitro* anticancer efficacy of six clinically approved liquids exposed to physical *plasma*. IEEE Transactions on Radiation and Plasma Medical Sciences, 3(5), 588–596.

### Acknowledgments

The authors acknowledge UNESP, CNPq, and Fapesp for the financial support.

<sup>\*</sup>Corresponding author: diegoverduino@hotmail.com



# TESTING A MACHINE LEARNING ALGORITHM TO DISCOVER THE GOVERNING EQUATIONS OF ELECTRICAL CIRCUITS

Marcelo Francisco Krol, Julio César Sagás\*

Laboratory of Plasmas, Films, and Surfaces, Universidade do Estado de Santa Catarina, Joinville-SC, Brazil

### 1. Introduction

Machine learning tools have been progressively used to analyze and control plasma systems, including the discovery of the governing equations from experimental data [1] through algorithms like the Sparse Identification of Nonlinear Dynamics (SINDy) [2]. The challenges to performing this include the data treatment to remove noise and the evaluation of the system to acquire the necessary quantities. In this context, we aim to develop a data-driven mathematical model for a plasma jet using SINDy. However, before trying to accomplish this task, it is necessary to benchmark the algorithm and data treatment. Thus, in this work, we present the results of the analysis with SINDy of synthetic and experimental data for a RLC circuit to evaluate the suitability of the algorithm to analyze plasma systems with unknown dynamics.

### 2. Theory

The experimental data were obtained by measuring the voltage across the resistor and the capacitor (minimum data to characterize the system). The values of resistance, inductance, and capacitance were  $68~\Omega$ , 1.3~mH, and 47~nF. The excitation signal was a sinusoidal waveform with an amplitude of 2.0~V and frequency of 21.98~kHz. To obtain the synthetic data, we solve numerically the system of ordinary differential equations (ODEs) obtained from Kirchoff's laws using the same parameters of the experiment. The simulated models (simulations with the equations discovered using SINDy) were made with the package PySindy. We considered the possibility of linear terms in the ODEs as well as sinusoidal terms due to the forcing added to the circuit by the voltage source.

### 3. Results and Discussions

The governing equations obtained were solved to compare the results with the synthetic and experimental data (Figures 1 and 2). The simulated models reproduce the circuit dynamics, however, the governing equations obtained differ from those obtained from Kirchoff's laws, including more terms in the ODEs. It indicates that PySindy successfully discovers the system's dynamics but encounters difficulty in implementing sparsity. From this, it is evident the necessity to implement physical constraints to guarantee that the model obtained has physical sense.

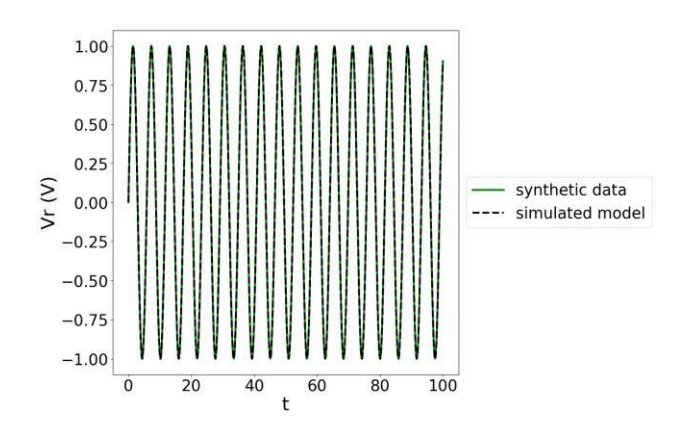


**Fig. 1.** Comparison of synthetic data and simulated model for the voltage across the resistor.

**Fig. 2.** Comparison of experimental data and simulated model for the voltage across the resistor.

### 4. References

- [1] Thakur, B., Sen, A., & Chaubey, N. (2022). Data driven discovery of a model equation for anode-glow oscillations in a low pressure plasma discharge. Physics of Plasmas, 29 (4): 042112.
- [2] Brunton, S. L., Proctor, J. L., & Kutz, J. N. (2016). Discovering governing equations from data by sparse identification of nonlinear dynamical systems. Proceedings of the National Academy of Sciences, 113(15), 3932-3937.
- [3] de Silva, B. M. et al. (2020). PySindy: a Python package for the sparse identification of nonlinear dynamics from data. Journal of Open Source Software, 5(49), 2104.

### Acknowledgments

Thanks to FAPESC (grant 2024TR000258) and CNPq (grant 304053/2021-0 and PIBIC).

<sup>\*</sup>Corresponding author: julio.sagas@udesc.br



# ANALYSIS OF CHANGES IN THE PHYSICAL-CHEMICAL PROPERTIES OF N95/PFF2 RESPIRATOR FABRICS AFTER TREATMENT WITH LOW PRESSURE PLASMA

Batista, M. C. S. <sup>1</sup>, Rangel, E. C. <sup>1</sup>

<sup>1</sup>Universidade Estadual Paulista (UNESP), Instituto de Ĉiência e Tecnologia de Sorocaba (ICTS) – Avenida Três de Março, 511 - Alto da Boa Vista - Sorocaba/SP - CEP 18087-180

### 1. Introduction

Excessive disposal of Personal Protective Equipment (PPE) causes significant environmental impact. Concern for health and the environment has driven new technologies to treat these materials [1]. In this work it is evaluated if physical-chemical structure of n95/pff2 fabric respirators are preserved after exposure to low pressure plasma treatment with different proportions of oxygen (O<sub>2</sub>) and argon (Ar).

### 2. Experimental

Samples of 1.0 cm x 2.0 cm of blue (polyester) and white (polypropylene) fabrics from N95/PFF2 respirators were treated with low-pressure plasma in a capacitively coupled system. The samples were attached on the grounded upper electrode and on the driven lower electrode was excited by radiofrequency (150W, 13.56 MHz). The treatment lasted 10 minutes in an atmosphere with oxygen (O<sub>2</sub>) and argon (Ar), with a base pressure of 2.7 Pa and a working pressure of 9.3 Pa. Changes in the physical-chemical properties of the fabric were analyzed by infrared spectroscopy, scanning electron microscopy and energy dispersive spectroscopy.

### 3. Results and discussions

The analyzes showed that the treatments did not significantly alter the structural characteristics of the mask samples. The infrared spectra were compatible with polyester and polypropylene. The surface morphology revealed that even with the variation in gas proportions, the mask fibers remained similar to the control samples, as well as in the analysis of the elemental composition, the samples maintained carbon and oxygen percentages close to the control.

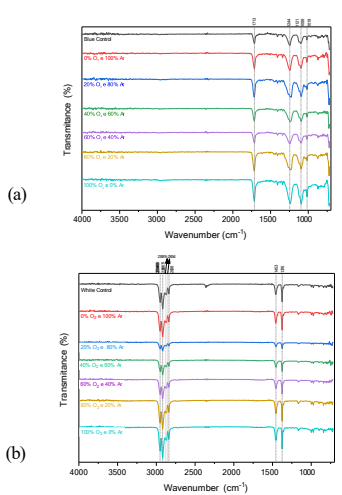


**Figure 1:**Infrared spectra obtained by Attenuated Total Reflectance Analysis (ATR) for samples of (a) blue fabric and (b) white fabric treated with different proportions of oxygen (O<sub>2</sub>) and argon (Ar) gases.

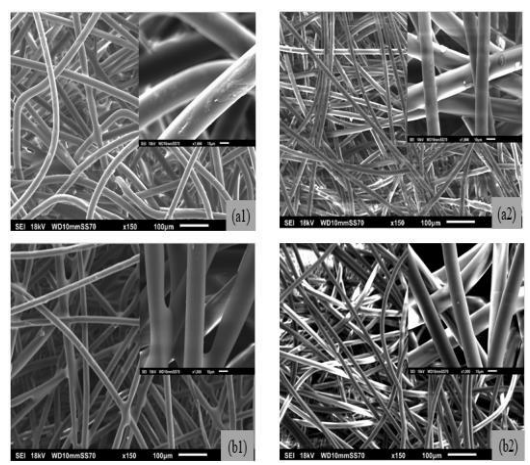


**Figure 2:**Micrographs of samples (a1) blue control and (b1) treated with  $40\%O_2$  60%Ar - blue fabric; and (a2) white control and (b2) treated with  $40\%O_2$  60%Ar - white fabric at magnifications of 150x and 1000x.

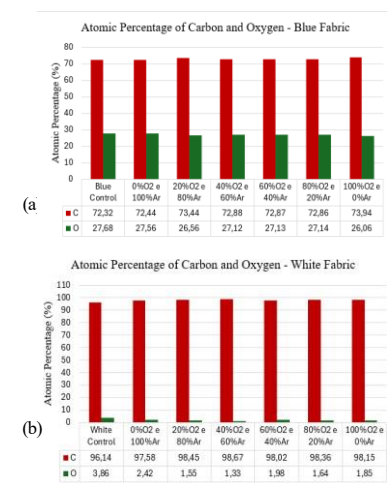


**Figure 3:**Elemental composition of samples of (a) blue fabric and (b) white fabric treated with different proportions of oxygen (O<sub>2</sub>) and argon (Ar) gases.

### 4. References

[1] - MT Khan et al., "Personal protective equipment (PPE) disposal during COVID-19: An emerging source of microplastic and microfiber pollution in the environment," **Science of the Total Environment**, vol. 860. Elsevier BV, Feb. 20, 2023. doi:10.1016/j.scitotenv.2022.160322

### Acknowledgments

The authors would like to thank the Laboratório de Plasmas Tecnológicos (LaPTec) of UNESP - ICTS of Sorocaba and the Conselho Nacional de Desenvolvimento Científico e Tecnológico (CNPq) - process (131439/2024-3)

<sup>\*</sup>Corresponding author: mariaclaudiasilvabatista@gmail.com



# DEVELOPMENT OF METAL-FILLED PASTE FOR ROBOCASTING WITH PADS: A NOVEL APPROACH FOR SUSTAINABLE METAL 3D PRINTING

Augusto Adami Vidal<sup>1</sup>, Bruno Hotza<sup>1</sup>, Millene Abreu Pauli<sup>1</sup>, Felipe Gonçalvez Jedyn<sup>1</sup>, Fernando Irto Zanetti<sup>1</sup>, Rodrigo Perito Cardoso<sup>1</sup>

<sup>1</sup>Federal University of Santa Catarina – Materials Laboratory (LabMat)

### 1. Introduction

In this paper, we present part of the development of a novel indirect additive manufacturing technique for producing metal components. The technique, called Robocasting [1, 2], utilizes a slurry containing metal powder and a polymer, i.e., a metal-filled paste enabling a feedstock with low content of organic binder [3] and eliminating the chemical debinding step [4], which typically involves the use of toxic solvents such as hexane. To achieve the final material properties debinding and sintering of the component is essential. On this work a PADS (Plasma Assisted Debinding and Sintering) reactor was applied for this purpose [5]. Preliminary results have demonstrated the feasibility of the technique, with the production of a metal component without the need for chemical debinding. Therefore, test specimens, such as those presented in this work, were manufactured for preliminary analysis of manufacturing parameters and plasma assisted sintering parameters.

### 2. Experimental

In the initial phase of this research, cubic test specimens (fig. 1) were produced using a volumetric ratios of ethanol and polyvinyl butyral (PVB) in the binder paste of 90/10. Through a series of tests, key manufacturing parameters were established, including head displacement speed, material flow rate, layer height, and bed temperature. Additionally, the dimensions and characteristics of the test specimens, such as wall thickness, were defined during the optimization process. For the sintering stage, the baseline parameters were identical to those currently used for test specimens produced PIM at LabMat (UFSC's Materials Laboratory) [4]. However, modifications to the heating ramps are underway to optimize the thermal removal of the PVB binder. It is important to note that all other sintering parameters, including gas mixture, gas mixture flow rate, pressure, DC plasma source settings, and sintering time and temperature, will be maintained as established in the conventional metal injection moulding process [4]. Optical microscopy (OM) of sintered samples was taken to porosity and printing defects analysis.

### 3. Results and Discussions

Results show that a 10% PVB content in the binder system is sufficient to maintain the shape during the printing, handling and sintering processes, as illustrated in Figure 1 (a) green/as-printed and b) PADS sintered). Dimensional shrinkage was measured at 10.5% in the x and y directions and 12.5% in the z (height) direction. As expected, the samples experienced a weight loss of approximately 2% due to thermal debinding. Figure 2 presents a porous structure comparable to metal injection molded sintered parts, confirming PADS' effectiveness in achieving densification not only for metal injection moulding but also for robocasting additive manufacturing without the need for chemical debinding.

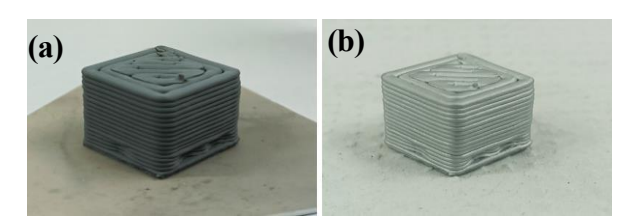


**Fig. 1.** Figure's Printed sample containing 10% PVB in the binder system before (a, green part) and after sintering under PADS (b).

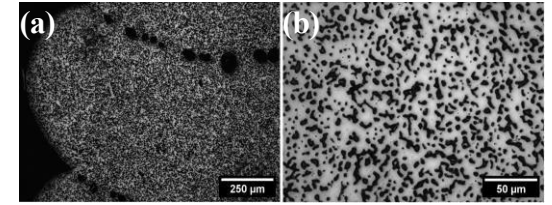


**Fig. 2.** Cross-sectional view, by OM, of the sintered sample at 100x (a) and 500x (b) magnification.

### 4. References (bold face Times New Roman 11 pt)

- [1]- S. Lamnini et al. 2022. Heliyon (8), e10651 (2022)
- [2]- A. I. Nurhudan et al. 2021. *Journal of Manufacturing Processes* (66), 228-237 (2021).
- [3]- J. Gonzalez-Gutierrez et al. 2018. Materials (11), 840 (2018).
- [4]- A. A. Vidal et al. 2023. 27<sup>th</sup> International Congress of Mechanical Engineering. Proceedings, 2023.



### MINIMUM CONDITIONS FOR GENERATION OF A REMOTE PLASMA JET

Lais Bastos da Silva Lima<sup>1</sup>, Marcelo Francisco Krol<sup>1</sup>, Matheus Henrique Lemos de Oliveira<sup>1</sup>, Anderson de Carvalho Fernandes<sup>1,2</sup>, Daniela Becker<sup>1</sup>, Julio César Sagás<sup>1\*</sup>

<sup>1</sup>Laboratory of Plasmas, Films, and Surfaces, Universidade do Estado de Santa Catarina, Joinville-SC.

Brazil

<sup>2</sup>Centro Univeristário SENAI, Joinville-SC, Brazil

### 1. Introduction

Atmospheric pressure remote plasma jets [1] are a useful tool for surface treatments that require a continuous movement of the plasma jet, as in the case of in situ plasma treatment during 3D printing. In this work, we performed an electrical characterization of a remote argon plasma jet focusing on the determination of the minimum conditions for the generation of the jet. This mapping will be useful to the design of a 3D printing system coupled with a remote plasma jet for in situ surface treatment of polymers.

### 2. Experimental

A remote plasma jet system is composed of two parts: a primary plasma, in this case, generated through a dielectric barrier discharge (DBD) in argon (Fig. 1) and the remote plasma jet itself. The primary plasma is generated between the high-voltage electrode (covered by an insulator) and the tip of a floating metallic wire. This wire is inserted in a plastic tube where the working gas flows. The other end of the tube (and of the wire) is placed near the surface to be treated. Thus, the remote plasma jet is formed between the wire tip and a dielectric surface that covers the ground electrode. The discharge was generated by an Inergiae Alternis power supply with variable frequency from 2 kHz to 20 kHz. For frequencies below 10 kHz, the voltage waveform consists of near-sinusoidal pulses and, above 10 kHz, the voltage waveform is sinusoidal. The voltage and current waveforms were measured with a TDS2024B Tektronix oscilloscope using a voltage divider and a shunt resistor, respectively.

### 3. Results and Discussions

The primary plasma can be generated at any frequency for nominal peak voltages above 5 kV. However, the remote plasma jet is generated only at higher voltages, as can be seen in Figure 2, where green corresponds to the plasma jet formation. Except for 2 kHz, the driven frequency has a minor role in the determination of minimum voltage. No significant differences were observed in the voltage and current waveforms in the cases with and without the remote plasma jet. It shows the need for proper diagnostics of the plasma jet to establish mechanisms besides the visual that allow to verify the occurrence of the remote plasma jet.

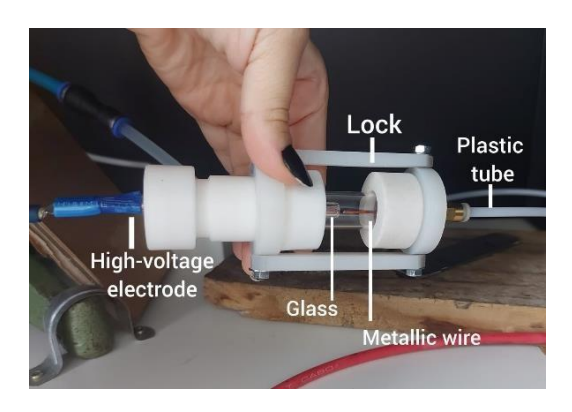


**Fig. 1.** *DBD reactor for generation of the primary plasma* 

**Fig. 2.** Map of minimum conditions to generate the remote plasma jet.

### 4. References

[1] Kostov, Konstantin G. et al. Transfer of a cold atmospheric pressure plasma jet through a long flexible plastic tube. Plasma Sources Science and Technology, v. 24, 025038, 2015.

### Acknowledgments

Thanks to FAPESC (grant 2024TR000258) and CNPq (grant 304053/2021-0 and PIBIC).

<sup>\*</sup>Corresponding author: julio.sagas@udesc.br



# ENHANCED PLASMA-ACTIVATED SALINE PRODUCTION USING SERIALLY COMBINED DIELECTRIC BARRIER DISCHARGE AND GLIDING ARC SYSTEMS

N. F. Azevedo Neto<sup>1</sup>, F. S. Miranda<sup>1,2</sup>, P. W. P. Moreira Junior<sup>1</sup>, M. P. Gomes<sup>1</sup>, C. Alves-Junior<sup>1</sup>, C. Y. Koga-Ito<sup>2</sup>, R. S. Pessoa<sup>1</sup>

<sup>1</sup>Plasmas and Process Laboratory, Department of Physics, Aeronautics Institute Technology, São José dos Campos, 12228-900, Brazil.

<sup>2</sup>Department of Environment Engineering, Institute of Science and Technology, São Paulo State University, São José dos Campos, 12247-016, Brazil.

### 1. Introduction

Plasma-activated saline (PAS) has shown potential in various applications, including antimicrobial activity, anti-inflammatory effects, and cancer therapy [1]. The production of PAS typically involves cold atmospheric plasmas (CAPs) that generate reactive oxygen and nitrogen species (RONS) in aqueous solutions [2]. However, the presence of chloride ions (Cl $^-$ ) in saline can inhibit the formation of key RONS like nitrite (NO $_2$  $^-$ ) [3]. This study introduces a novel hybrid plasma discharge (HPD) system combining dielectric barrier discharge (DBD) and gliding arc plasma jet (GAPJ) in a serial configuration to enhance the production of RONS in saline.

### 2. Experimental

The HPD system involves a two-stage plasma process: DBD generates the primary plasma discharge, and the effluent is further ionized by GAPJ. This combination enhances the production of RONS in saline water. Electrical characterization of the DBD and GAPJ systems, plasma diagnostics using optical emission spectroscopy, and chemical analyses (UV-Vis spectroscopy, Raman spectroscopy) were conducted to evaluate the impact of plasma treatment on the physicochemical properties of the saline water

### 3. Results and Discussions

The serial configuration of DBD and GAPJ effectively increased the concentrations of RONS such as hydrogen peroxide (H<sub>2</sub>O<sub>2</sub>), ozone (O<sub>3</sub>), nitrite (NO<sub>2</sub><sup>-</sup>), and nitrate (NO<sub>3</sub><sup>-</sup>). Significant reductions in pH and increases in oxidation-reduction potential (ORP) and total dissolved solids (TDS) were observed. UV-Vis and Raman spectroscopy confirmed the presence of RONS and their impact on the molecular structure of the saline, including a weakening of the hydrogen-bonding network. This enhanced production of RONS demonstrates the potential of the HPD system for producing PAS with improved reactivity and stability for therapeutic applications.

### 4. References

- [1]- C.Y. Koga-Ito, K.G. Kostov, F.S. Miranda, et al. (2023). Cold Atmospheric Plasma as a Therapeutic Tool in Medicine and Dentistry. Plasma Chem. Plasma Process.
- [2]- Kutasi K, Bencs L, Tóth Z, et al. (2023). The role of metals in the deposition of long-lived reactive oxygen and nitrogen species into the plasma-activated liquids. Plasma Process. Polym., 20.
- [3]- Chiappim W, Sampaio A da G, et al. (2021). Antimicrobial effect of plasma-activated tap water on Staphylococcus aureus, Escherichia coli, and Candida albicans. Water (Switzerland), 13, 1-16.

### Acknowledgments

This research was funded by FAPESP under grant numbers 2023/02268-2, 2021/14181-3, and 2019/05856-7, and by CNPq under grant numbers 313482/2021-7 and 405637/2022-5.

<sup>\*</sup>Corresponding author: place the e-mail of the corresponding author here (bookman old style 9 pt)



### PLASMA SURFACE TREATMENT ON HIPS BY PECVD

Michel F. R. da Rosa<sup>1\*</sup>, Larissa S. Almeida<sup>2</sup>, Alana M. Corá<sup>1</sup>, Marcos D. Manfrinato<sup>1</sup>, Luciana S. Rossino<sup>1, 2</sup> *Faculdade de Tecnologia de Sorocaba*, <sup>2</sup>UFSCar Campus Sorocaba

### 1. Introduction

Plasma surface treatment can modify the superficial behavior of the material and increase the properties such as hardness, corrosion, and wear resistance [1]. The objective of this work is to deposit DLC (diamond like-carbon) film by PCVD (plasma enhanced chemical vapor deposition) using a DC-pulsed source supply on high impact polystyrene (HIPS) and determine the effect of the thin film on wear resistance of the studied material.

### 2. Experimental

The samples of HIPS with 12x12x2mm dimension were treated by PECVD. The treatment began with ablation process using 20% H<sub>2</sub> and 80% Ar for 15 minutes at 100°C. After that, an organosilicon interlayer was deposited using 70% HMDSO and 30% Ar for 20 minutes. Then, the DLC film was deposited with 90% CH<sub>4</sub> and 10% Ar for 120 minutes at 75°C. The treated and untreated material was characterized by Fourier transform infrared spectroscopy (FTIR), scanning electron microscope (SEM) and wear test, that was carried out with a load of 1 N and 150 RPM with different testing time.

### 3. Results and Discussions

The FTIR result (Fig. 1) demonstrates chemical bonds related to the DLC film formation, in that the peaks in the 3100 to 2700 cm<sup>-1</sup> region are particularly interesting. Specifically, for DLC films, the characteristic peaks are 2850 cm<sup>-1</sup>, related to the CH<sub>2</sub> (sp<sup>3</sup>) bond, 2920 cm<sup>-1</sup>, also associated with the CH<sub>2</sub> (sp<sup>3</sup>) bond, 2970 cm<sup>-1</sup>, corresponding to the CH<sub>3</sub> (sp<sup>3</sup>) bond, and 3000 cm<sup>-1</sup>, which corresponds to the CH (sp<sup>2</sup>) bond [2]. The Carbon-Hydrogen bond is the most observed, but some peaks can be associated with silicon-carbon and silicon-oxygen interaction. The peak related to the CO bond is observed due to the interaction between the film and the atmosphere. The maximum wear volume for the treated sample was 0,13mm<sup>2</sup> while the minimum wear volume for the sample without treatment was 0,10mm<sup>2</sup> reaching 0,43mm<sup>2</sup>. The wear resistance is higher for the treated sample than the sample without treatment due to the film formation. The energy dispersive x-ray spectrometry (EDS) data (Tab. 1) of the surface sample show the presence of carbon, oxygen, and silicon after the plasma treatment over the sample, evidencing the presence of the DLC film on the HIPS, observed in the SEM analysis (Fig. 3) with thickness of 6μm.

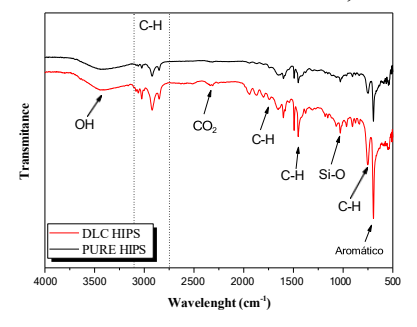


**Fig. 1.** FTIR analyses of the sample with and without DLC film deposition.

Sampla	at (%)				
Sample	С	О	Si		
without treatment	94,13	5,72	0,02		
with DLC	68,5	24,5	7,5		

**Tab. 1.** EDS analyses of samples with and without the film deposition.

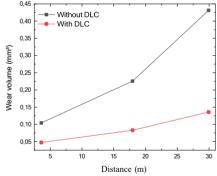


**Fig. 2.** Wear volume of HIPS with and without DLC film deposition

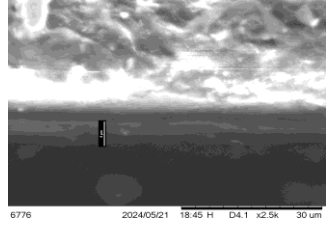


**Fig. 3.** SEM analysis of a HIPS showing the film formation deposited on the HIPS.

### 4. References

- [1] Miklós Berczeli and Zoltán Weltsch. Polymers, 13, 1-13, (2021).
- [2] L. S. Almeida, et al. Rev. Bras. Apl. Vac., 39, 42-55, (2020).

<sup>\*</sup>Corresponding author: michel.felipe.18@hotmail.com

# MODIFICATION OF THE WATER AFFINITY OF THE SEED SURFACE OF 'CARRIZO' CITRANGE BY PLASMA

Aline R. Almeida<sup>1\*</sup>, Luis Guilherme Silva Rosa<sup>1</sup>, Luana Aparecida Castilho Maro<sup>2</sup>, Luis César Fontana<sup>1</sup> and Daniela Becker<sup>1</sup>

<sup>1</sup>Laboratory of Plasmas, Films, and Surfaces, Santa Catarina State University (UDESC), Joinville, SC, Brazil

### 1. Introduction

The use of high-quality seeds with good genetic, physical, physiological and sanitary performance is essential for successful cultivation, as they ensure the germination and growth of vigorous plants. Chemical treatment with fungicides and hormones is widely used to improve seeds, but these methods are expensive, laborious and can cause soil pollution. In view of this, seed treatment with plasma has been gaining attention as a sustainable alternative. This technique modifies the surface of the seed, increasing germination, suppressing diseases and increasing productivity with less environmental impact [1].

### 2. Experimental

The plasma coating deposition technique was Dielectric Barrier Discharge (DBDs), using N2 as treatment gas at 33.4 sccm flow at 2.5<sup>-1</sup>mBar pressure with pre-vacuum of two hours and temperature of 25±2°C. After the treatment, the contact angle of the samples was measured and compared with the control (without treatment).

### 3. Results and Discussions

Seeds from the 'Carrizo' citrange [Poncirus trifoliata (L.) Raf. x Citrus sinensis (L.) Osbeck] were used. After treatment, the contact angle of the seeds decreased significantly, which confirms the modification of the substrate surface (Table 1). This same trend can be observed in the micrograph. Another important parameter is the loss of water from the sample, confirmed by the difference in weight, which was probably caused by the pre-vacuum [2].

Sample	Micrografia (50x)	Weight (g)	Contact angle	Contact angle (°)
In natura	kera	0.30±0.03ª		75.8±5.0 <sup>a</sup>
Vácuo		0.23±0.02 <sup>b</sup>	all's.	78.4±4.7ª
Plasm 20w		0.24±0.04 <sup>b</sup>		35.9±4.1 <sup>b</sup>

**Tab.1** Results of plasma treatment on seeds

### 4. References

[1]- A. Meier et al., Gravitational and Space Research, 9, 133–158, (2021).

[2]- ARM da Silva et al., Colloids and Surfaces B: Biointerfaces, 157,280-285, (2017).

### Acknowledgments

The authors are thankful for the Multi-User Facility infrastructure from Santa Catarina State University's, EPAGRI and FAPESC.

<sup>&</sup>lt;sup>2</sup>Agricultural Research and Rural Extension Company of Santa Catarina (EPAGRI), Itajaí, SC, Brazil.

<sup>\*</sup>Corresponding author: alinerosaufpr@gmail.com

### Universidade do Estado de Santa Catarina - UDESC, November 11-13, 2024

# SILICON-BASED FILMS DEPOSITED BY PLASMA ENHANCED ATOMIC LAYER DEPOSITION FOR CORROSION PROTECTION

### 1. Introduction

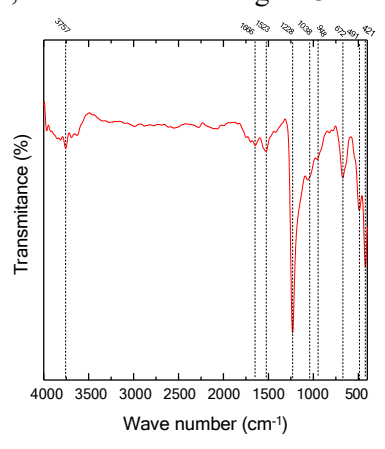
Due to its good mechanical properties and low cost, carbon steel is widely used in a wide range of sectors, such as the oil and gas, transportation and aircraft [1]. However, even the presence of small amount of water and corrosive gases, can cause degradation of steel. One solution to this type of problem can be the use of corrosion inhibitors. Regarding corrosion inhibitors, the most used are generally organics molecules rich in oxygen, nitrogen, and sulfur heteroatoms [2]. This work aims to evaluate the corrosion resistance of carbon steel coated with silicon-based films containing nitrogen and carbon heteroatoms which were deposited from plasma-assisted atomic deposition (PEALD). Plasma deposition allows the deposited film to be uniform, without the presence of pores, making it difficult for the corrosive medium to infiltrate on the substrate.

### 2. Experimental

PEALD of Oxford Instruments – OpAL was utilized with Trisdimethylaminosilane and O<sub>2</sub> as an oxidizing agent. Process temperature was 150°C. The films were deposited on rectangular 1020 carbon steel substrates (10 mm x 20 mm), which were polished to 1200 grit, cleaned in an ultrasonic bath with ethanol and dried using a thermal dryer. Fourier transform infrared spectroscopy (FTIR) was used for chemical structure determination and Electrochemical impedance spectroscopy in 3,5% NaCl medium was utilized for analysis of films corrosion protection.

### 3. Results and Discussions

Figure 1 shows the FTIR spectrum of the samples. It is possible to observe the characteristic bands of the Si-O-Si groups in 1038, 948, 490 and 421 cm<sup>-1</sup>. The contribution related to Si-CH<sub>3</sub> group also appears at the peak of 1228 cm<sup>-1</sup> and 670 cm<sup>-1</sup> [3]. It also can be observed contributions of O-H group in 3757 and 1523 cm<sup>-1</sup> and contribution of N-H group in 1666 cm<sup>-1</sup>. Figure 2 presents the Nyquist representations for the carbon steel samples without deposited film and with film. This diagrams indicated an increase in the resistance to polarization with the film deposition [1]. The film deposited via PEALD presented important characteristics of SiO<sub>2</sub> and SiC<sub>x</sub> deposition, and the presence of impurities could also be observed. The EIS results indicated possible protection of carbon steel. If compared with literature data [2], the polarization value found are three orders of magnitude bigger than organic commercial inhibitors. This fact indicates that the silicon carbide film deposition process via PEALD is a good alternative to common inhibitors. This protection can be achieved by the fact that deposition via PEALD produces an extremely smooth and compact film, without the presence of pores, as can be seen in Figure 3.



3,0x10<sup>6</sup>
2,5x10<sup>6</sup>
2,5x10<sup>6</sup>
3,0x10<sup>6</sup>
2,5x10<sup>6</sup>
3,0x10<sup>6</sup>
3,0x10



b

**Fig. 1.** FTIR spectra of film deposited by PEALD

**Fig. 2.** (a) EIS diagram of  $SiC_x$  films deposited on carbon steel; (b) diagram of carbon steel.

Fig 3. MEV of carbon steel (a) without film; (b) with deposited film

### 4. References

- [1] Delimi, A., et ali, RSC Adv., 2022, 12, 15601
- [2] Raja, P.B. and Sethuraman, M.G., Materials Letters, 62, (2008), 113-116.
- [3] Spigarollo, D. C. F. S., et ali, Coatings, 2023, 13, 1730.



# INCREASING PLA WETTABILITY BY REMOTE PLASMA JET TREATMENT DURING 3D PRINTING

Anderson de Carvalho Fernandes<sup>1</sup>,<sup>2\*</sup>, Marcelo Francisco Krol<sup>2</sup>, Julio César Sagás<sup>2</sup>, Daniela Becker<sup>2</sup>

"Centro Universitário SENAI/SC Campus Joinville"

<sup>2</sup>Laboratório de Plasmas, Filmes e Superfícies, Centro de Ciências Tecnológicas, Universidade do Estado de Santa Catarina - UDESC

### 1. Introduction

Tissue engineering, aiming to repair damaged tissues, uses scaffolds to guide cell growth. Additive Manufacturing (AM) has been highlighted in the production of customized scaffolds with optimized properties for biomedical applications [1]. On the other hand, atmospheric plasma treatment can modify surface properties like wettability and cell adhesion. In this study, we aim to evaluate the influence of varying the excitation frequency of a remote plasma jet [2] on the *in situ* surface modification of PLA parts manufactured by AM, aiming to optimize the production of scaffolds for tissue engineering.

### 2. Experimental

For the experiments, test specimens (TS) with dimensions of 60 x 10 mm and a thickness of 1.5 mm were fabricated from PLA filament using a hybrid 3D printing equipment with a remote plasma jet system (Fig. 1). The plasma was generated through a high voltage Inergiae Alternis power supply. The TS were exposed to an argon plasma generated at a nominal peak voltage of 18 kV, with the frequency varying between 8 kHz and 20 kHz. The distance between the electrode and the surface of the TS was kept constant at 1 mm. The surface wettability was evaluated by measuring the contact angle with water.

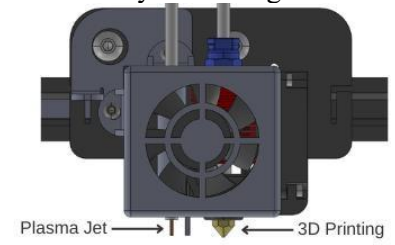


Fig. 1. Hybrid 3D printing equipment with a remote plasma jet system

### 3. Results and Discussions

After each printing process, the surface wettability of the specimens was measured with a goniometer to evaluate the contact angle, checking for possible surface changes. The experimental sequence was as follows: one specimen without plasma treatment, while the others were subjected to frequencies varying between 8 kHz and 20 kHz. The values obtained are presented in Table 1.

	Without	8 kHz	10 kHz	12 kHz	14 kHz	16 kHz	18 kHz	20 kHz
Mean	78,1	68,9	56,3	53,2	54,4	54,5	63,8	67,5
Standard Deviation	2,0	3,4	1,8	1,1	2,5	2,5	0,6	3,1

Table 1. Mean contact angles

The analysis of the contact angles of the TS showed that the variation of the excitation frequency directly impacts the PLA surface. Without treatment, presented the highest contact angle (78.1°), indicating lowest hydrophilicity. With the treatment, there was a significant reduction of the contact angle, especially between 10 kHz and 16 kHz, with 12 kHz presenting the lowest value (53.2°). From 16 kHz onwards, the contact angle starts to increase, suggesting that higher frequencies may decrease plasma efficiency.

### 4. References

[1] Wang, C., Huang, W., Zhou, Y., He, L., He, Z., Chen, Z., He, X., Tian, S., Liao, J., Lu, B., Wei, Y., Wang, M. 3D printing of bone tissue engineering scaffolds. Bioactive Materials, Volume 5, Issue 1, 2020, Pages 82-91.

[2] Kostov, Konstantin G. *et al.* Transfer of a cold atmospheric pressure plasma jet through a long flexible plastic tube. Plasma Sources Science and Technology, v. 24, 025038, 2015.

### Acknowledgments

The authors would like to thank the funding agencies FAPESC (2024TR000258) and CNPq (304053/2021-0, 404401/2023-6 and 306823/2021-7) for the financial support provided for this research.

<sup>\*</sup>Corresponding author: andersoncafer@gmail.com



### AUTOMATION OF A TENSIOMETER USING VACUUM TRANSDUCER VIA MEMS PIEZO-RESISTANT BRIDGE FOR APPLICATION IN IRRIGATION SYSTEMS

Pedro Luis Calheiros da Silva<sup>1</sup>, João Roberto Moro<sup>1</sup>

<sup>1</sup> Instituto Federal de Educação, Ciência e Tecnologia de São Paulo Campus Bragança Paulista

### 1. Introduction

Modern ICT (Information and Communication Technology) technologies such as the Internet of Things, GPS (Global Positioning Systems) and sensors are used to identify farmers needs and select suitable solutions for their problems. These innovations increase the precision and timeliness of decisions made and improve crop productivity. Several multilateral organizations and developing countries around the world have proposed smart agricultural technologies to increase agricultural production [1].

A tensiometer measures the moisture potential on the basis of the suction force exerted on water by soil. The instrument consists of an airtight water filled hollow tube with a permeable ceramic cup attached to the tube. The instrument is inserted into the soil, and a vacuum gauge is attached to the upper end. The porous ceramic cup is connected to the manometer, which can be buried at the soil depth where the moisture content is to be measured. The system is filled with water and sealed. Changes in the capillary tension in the soil are accompanied by a movement of water through the soil pores until the capillary tension inside the ceramic cup is equal to the tension outside it. The manometer measures the capillary tension. The water flow is determined by the change in volume required to produce the new reading of the manometer [2].

### 2. Experimental

The automation project intended at this stage of development is part of a predecessor project for irrigation control in agricultural greenhouses using IoT technologies to monitor and control environmental variables. Low accuracy in reading commercial soil moisture sensors was observed. Therefore, the automation project for a tensiometer was discussed and proposed to incorporate its reading data into the LoRaWAN network and display on a dedicated platform.

The method focuses on replacing the analog vacuum pressure gauge installed in most tensiometers with a battery-based sensing device, with a vacuum transducer via piezo-resistive bridge MEMS (Micro-Electro-Mechanical System), LoRa connectivity and sufficient processing power to acquire, process, package and transmit the necessary data to monitor the soil matrix potential.

The laboratory validation of automation aims to explore two methods: first, to compare data acquired by the automated device with analog devices allocated in the same periods and positions and second, to compare the soil matrix potential with moisture approximation experiments using the process of drying a portion of the soil

Both validation processes will provide statistical data, such as R<sup>2</sup> and p-value, for subsequent analysis of reliability, accuracy and resolution.

### 3. Results and Discussions

According to the results obtained by Abdelmoneim et al. [3], the accuracy obtained through correlation (R<sup>2</sup>) is 0.99, meaning the differences between the automated model and the analog model are almost imperceptible. Therefore, although the development method and materials are not the same as those used in the aforementioned study, it is expected to observe the replicability of the results and obtain equal or greater metrics for sensor reliability.

Another expected result is the complete and lossless transmission of data. Only in this way can the soil matrix potential and humidity be approximated and, consequently, the data can be used in a feedback soil irrigation system.

### 4. References

- [1] R. K. Goel et al., Smart agriculture Urgent need of the day in developing countries. Sustainable Computing: Informatics and Systems, v. 30, p. 100512, (2021).
- [2] P. Dobriyal et al. A review of the methods available for estimating soil moisture and its implications for water resource management. Journal of Hydrology, v. 458-459, p. 110–117, (2012).
- [3] A. A. Abdelmoneim et al., Internet of Things (IoT) for Soil Moisture Tensiometer Automation. Micromachines, v. 14, n. 2, p. 263–263, (2023).

### Acknowledgments

We gratefully acknowledge the Campus Bragança Paulista of the Instituto Federal de Educação, Ciência e Tecnologia de São Paulo for their support.

<sup>\*</sup>Corresponding author: place the e-mail of the corresponding author here (bookman old style 9 pt)



# PRESSURE SENSOR FOR OPERATION IN THE ROUGH VACUUM REGION OBTAINED BY 3D PRINTING

Marcelo Bariatto Andrade Fontes<sup>1</sup>, Henrique Chaves Gulino<sup>2</sup>, Eduardo Acedo Barbosa<sup>3</sup> and Francisco Tadeu Degasperi<sup>4</sup>

Laboratório de Processos e Dispositivos – LPD – Faculdade de Tecnologia de São Paulo – CEETEPS
 Laboratório de Sistemas Integráveis – LSI – Escola Politécnica da Universidade de São Paulo – EPUSP
 Laboratório de Óptica Aplicada – LTO – Faculdade de Tecnologia de São Paulo – CEETEPS
 Laboratório de Tecnologia do Vácuo – LTV – Faculdade de Tecnologia de São Paulo – CEETEPS and Programa de Pós-Graduação – Mestrado Profissional – CEETEPS

### 1. Introduction

Pressure sensors have a wide range of applications in various fields, ranging from the automotive industry and production processes to medical equipments. [1]. It is well known that additive synthesis facilitates prototyping and is now a standard process in scientific and industrial development laboratories. Although the use of 3D printing to obtain vacuum components presents difficulties regarding the outgassing and permeability of the parts, on the other hand, the low cost and great flexibility can be attractive [2]. In this work we explore a 3D capacitive pressure sensor as a mass production and low-cost fabrication.

### 2. Experimental

The pressure sensor was produced in the KF-25 pattern of PLA using FFF type 3D printing. Several geometries have been explored, such as circular and square shape. Typical sensor dimensions include a 1,5mm frame within a 0,1mm central membrane. The capacitive measurements were possible providing an evaporated aluminum conductive layer on the sensor's surface and using a vacuum chuck for ground terminal and an 'O'ring spacer. It was also verified the profile of the deflected membrane using oblique projection of structured light technique.

### 3. Results and Discussions

As expected, the measured sensor capacitance showed values inversely proportional to the evaluated pressure during pumping, from 50pF for atmospheric pressure and 350pF for 100mbar, figure 1(a), which promoted the maximum deflection of 2,2mm in the membrane central area, figure 1(b). These preliminary results showed the viability of using additive prototyping for mass production and low-cost pressure sensor fabrication.

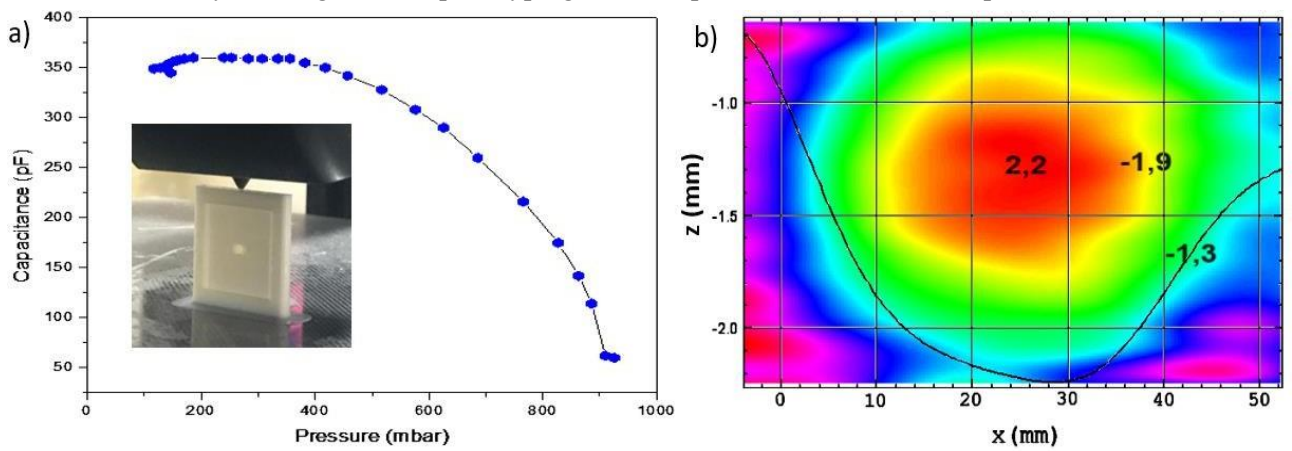


Fig.1 a) analysis of the maximum deflection of the sensor membrane through oblique projection of structured light and b) capacitance as a function of pressure and the 3D pressure sensor fabrication (inset).

### 4. References

- [1] Madou, M; Fundamentals of Microfabrication and Nanotechnology, CRC Press, 3<sup>rd</sup> Ed., 2012.
- [2] T. Chaneliere. Vacuum compatibility of ABS plastics 3D-printed objects. [Research Report] CNRS, Laboratoire Aimé Cotton, 2017.

### Acknowledgments

We would like to acknowledge Dr. Luis da Silva Zambom for the sensor metallization, CNPq and CAPES for the scholarship and TEX Equipamentos Eletrônicos Company for the financial support.

<sup>\*</sup>Corresponding author: bariatto@fatecsp.br



# POSSIBLE INDUSTRIAL APPLICATIONS OF A ROUTE DEVIATION SYSTEM USING SENSING TECHNOLOGY

Alicia Caldeira da Silva<sup>1\*</sup>, Walter Jonas de Sousa Viana<sup>2</sup>, Carlos Alberto Oliveira de Freitas<sup>3</sup>

<sup>1</sup>Federal University of Amazonas (ICET-UFAM), PIBIC Program, Itacoatiara, AM, Brazil.

<sup>2</sup>Federal University of Amazonas (ICET-UFAM), PIBIC Program, Itacoatiara, AM, Brazil.

<sup>3</sup>Federal University of Amazonas (ICET-UFAM), PIBIC Program, Itacoatiara, AM, Brazil.

### 1. Introduction

The use of manipulator robots in industrial environments has grown significantly, due to their efficiency in performing repetitive and potentially dangerous tasks. However, these robots still face challenges in terms of dynamically adapting to changes in their working environment, such as the presence of unforeseen obstacles. Thus, the trajectory deviation aims to avoid collisions during the robot's movement [reference number 1]. When the manipulator approaches an obstacle, the end effector is raised, allowing the robot to pass over the obstacle through a linear trajectory [reference number 2]. This work explores sensing routes and their possible applications in industry, expanding the results obtained in the PIB-E/0139/2022 project. The objective of this study was to identify specific areas where this technology can be implemented to increase the efficiency and safety of industrial processes, in addition to verifying the economic viability of its adoption.

### 2. METHODOLOGY

The project was structured into six main stages, aiming to identify industrial areas that can benefit from the use of a sensing route diversion system. These steps were:

- Step 1: Literature review on manipulator robots and route deviation systems.
- Step 2: Analysis of industrial areas where there is potential application of the technology.
- Step 3: Verification of the potential use of the system in specific industrial contexts.
- Step 4: Development of solutions and simulations to test the effectiveness of the technology.
- Step 5: Evaluation of the solutions developed, focusing on efficiency, safety and economic viability.
- Step 6: Final adjustments and revisions based on simulation results.

### 3. Results and Discussions

The results demonstrated that the sensing route diversion system can be successfully implemented in various industrial sectors, such as assembly, welding, palletizing and collaborative robotics; providing significant improvements in terms of efficiency and safety.

When assembling components, the simulation proved to be effective in automatically adjusting the trajectory of the manipulators to ensure precision and safety, with parts of different sizes and shapes.

During simulation of the welding processes, dynamic adjustments were made to the trajectory of the manipulator, ensuring welding precision, even in situations where the position of the parts varied.

In the palletizing area, the sensing system adjusted the trajectory of the robots in real time, ensuring efficient stacking of goods and avoiding damage to products. The continuity of the project focused on industrial applications, identifying and validating areas where the sensing route deviation system can be applied. Below are images of the palletizing simulations that were carried out.

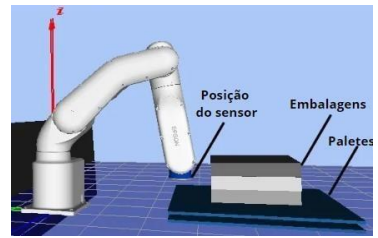


Fig. 1. (Packaging Palletizing)

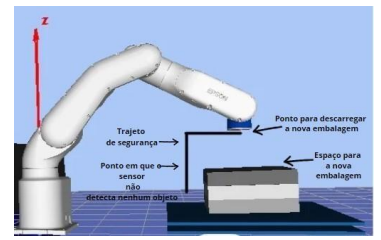


Fig. 2. (Dynamic palletizing)

### 4. References

[1]- Alizadeh, M.; Khooban, M. (2018). Robotic manipulators: control, sensing, vision, and intelligence. John Wiley & Sons.

[2]- Souza, A (2021). Automatic generation of trajectories in collaborative robots.

### Acknowledgments

Thanks to FAPEAM for the Scientific Initiation Support Program – PAIC UFAM 2023-2024 and PROPESP-UFAM.

<sup>\*</sup>Alicia Caldeira da Silva: alicia.silva@ufam.edu.br



# CALCULATION OF DRAG AND LIFT COEFFICIENTS IN A PLATE IMMERSED IN A GAS IN THE FREE MOLECULE REGIME

Juan Felipe Cardoso Elias<sup>1</sup>, Denize Kalempa<sup>1</sup>
<sup>1</sup>Escola de Engenharia de Lorena, Universidade de São Paulo – EEL/USP

### 1. Introduction

The objective of this study is to determine the drag and lift coefficients of a flat plate submerged in a rarefied gas. These coefficients are influenced by various factors such as the Knudsen number, which indicates the rarefaction of the gas, the Mach number, the angle of attack, and the plate temperature. It is assumed that the Knudsen number is very high, indicating a high rarefaction of the gas, rendering the interaction between molecules negligible compared to the interaction with the plate surface (free molecular flow regime). This scenario is common in problems related to spacecraft aerodynamics, satellites, vacuum technologies, microelectronics, aerosol transport in the atmosphere, etc. In such cases, equations from continuum mechanics are not applicable, necessitating the use of kinetic methods like solving the Boltzmann equation [1].

The problem is solved using a relationship between the velocity distribution functions of incident and reflected molecules on the plate [1], and a gas-surface interaction model suitable for analyzing the influence of gas-surface interaction on aerodynamic coefficients [2]. The hypothesis of diffuse scattering of molecules on the solid surface is widely adopted due to its mathematical simplicity. However, in situations demanding greater precision, this hypothesis is not valid, necessitating the use of a more accurate scattering kernel.

### 2. Theory

In the proposed approach, a gas-surface interaction model is used to investigate the influence of this interaction on aerodynamic coefficients. This model, developed by Cercignani and Lampis [2], introduces two accommodation coefficients: one for tangential momentum and another for the energy of molecules at the surface. These accommodation coefficients make the model more suitable and precise in describing the complex physics of this interaction, as they can be experimentally determined to ascertain plate material and gas characteristics. The diffuse kernel corresponds to both accommodation coefficients equal to 1. Drag and lift coefficients are calculated from the forces acting on the plate, dependent on both the accommodation coefficients and the Mach number.

### 3. Results and Discussions

Expressions for the drag and lift coefficients are obtained in terms of the angle of attack, Mach number, and accommodation coefficients that characterize the gas-surface interaction, and these are compared to literature through tables and graphs.

The results show that both aerodynamic coefficients depend significantly on the accommodation coefficients and the Mach number. It is also observed that the tangential momentum accommodation coefficient has a greater influence on the aerodynamic coefficients than the energy accommodation coefficient. Additionally, the larger the Mach number, the larger the deviation between the results for diffuse and non-diffuse scattering of gas molecules on the surface. These findings indicate a significant need for using a more precise scattering kernel for modeling the gas-surface interaction.

### 4. References

[1]- F Sharipov. Rarefied Gas Dynamics. Fundamentals for Research and Practice. Berlin: Wiley-VCH, 2016. [2]- C Cercignani e M Lampis. "Free Molecular Flow Past a Flat Plate in the Presence of a Non-trivial Gas-Surface Interaction". Em: J. Appl. Math. Phys. (ZAMP) 23 (1972), pp. 713-728.

### Acknowledgments

My sincere thanks to my family and advisor for their encouragement and FAPESP - São Paulo State Research Support Foundation (Process no. 2022/10551-3) for the essential financial support to carry out this project.



# EFFECT OF PRESSURE ON SAHA AND BOLTZMANN EQUILIBRIA IN PLASMAS GENERATED IN OPEN HOLLOW CATHODE

Marcelo P. Gomes<sup>1</sup>, <u>Pedro W. Paiva</u><sup>1</sup>, Felipe S. Miranda<sup>1</sup>, Nilton F. A. Neto<sup>1</sup>, Bogos S. Nubar<sup>1</sup>, Homero S. Maciel<sup>1</sup>, Gilberto Petraconi<sup>1</sup>

<sup>1</sup>Departamento de Física, Instituto Tecnológico de Aeronáutica, São José dos Campos, SP, Brasil

### 1. Introduction

Due to the reduction of the dimensions of the devices used to generate plasmas, the term microplasmas emerged in the scientific world. This term is only valid for plasmas with less than 1 mm dimensions. At the beginning of this century, there was a significant increase in works involving microplasmas. A major advantage in generating microplasmas about conventional plasmas is related to the low-cost experimental apparatus. Their applications are mainly bacteriological decontamination [1,2] and thin film deposition. One of the goals of this study was to conduct a more thorough analysis of possible equilibria (Saha, Boltzmann, Maxwell, and Planck Equilibrium) presented by microplasmas through the profiles of the atomic states distribution functions (ASDF) of the neutral atom of argon (Ar I). ASDF which describes how the neutral atoms and ions are distributed about their quantum states, has much information from the plasma where these neutral atoms and ions are inserted.

### 2. Experimental

The configurations of microplasmas generators found in the literature and the materials used in their fabrication are diverse. In the case of this work, the configuration chosen for the study of microplasmas was an open micro hollow cathode (OMHC), which is formed by a capacitor of plane-parallel plates with a dielectric (mica) between them and a hole diameter (diameter chosen:  $250 \mu m$ ,  $500 \mu m$ , and  $1000 \mu m$ ), perforating the center of the plates along with the dielectric. This device was powered by a high-voltage direct current (DC) source. We used copper, molybdenum, and tantalum as electrodes to produce OMHC discharges. About the experimental conditions, our microplasmas were generated in a gas mixture, Ar-H<sub>2</sub>, for a pressure range of 90-800 Torr. We used a high-resolution optical spectrometer with a focal length of 1 m to perform the spectroscopic analysis.

### 3. Results and Discussions

According to Fig. 1, the microplasmas tend to achieve the thermodynamic equilibrium depending on the local increase of the pressure in the reactor. It was also found that the electron density increases with pressure due to the ionization efficiency of the medium. Regarding partial balances, which have the partial local Boltzmann equilibrium, it is presented in all graphs of Fig. 1 belonging to the states at 4p and part of states belonging to the 5p level. Both Saha and Maxwell partial and local equilibrium are present only in graph (d) due to the overlapping tail of experimental ASDF with Saha distribution. Under all experimental conditions, our microplasmas are ionization-type [3]; hence, this implies that particles are transported away from the active region of the plasma, causing this loss of thermodynamic equilibrium.

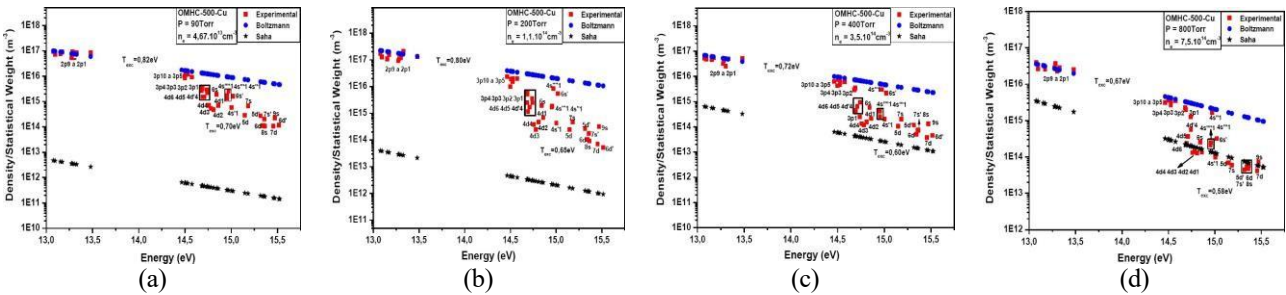


Fig. 1. ASDF of Ar I cupper MHC with a hole diameter of 500µm and pressures of 90, 200, 400, and 800 Torr.

### 4. References

- [1] R. E. J. Sladek, E. Stoffels, "Deactivation of Escherichia coli by the plasma needle." J. Phys. D: Appl. Phys., v. 38, no. 11, p. 1716-1721, May 2005.
- [2] R. Rahul et al. "Optical and RF electrical characteristics of atmospheric pressure open-air hollow slot microplasmas and application to bacterial inactivation." Journal Physics D: Applied Physics, v. 38, no. 11, p. 1750-1759, May 2005.
- [3] J. M. A. Mullen, "Excitation equilibria in plasmas: a classification." Ph.D. dissertation, Fac. Technische Natuurkunde, Technische Universiteit Eindhoven, Eindhoven. 1986.

<sup>\*</sup>Corresponding author: gomesmpfisica@gmail.com



# FORNO DE INDUÇÃO A VÁCUO APLICADO EM DESENVOLVIMENTO DE CERÂMICAS ESPECIAIS

PEREIRA V.F.<sup>1\*</sup>, KAKIZAKI D.Y.<sup>1</sup>, DORETTO D.S.<sup>1</sup>, RIBEIRO R.D.<sup>1</sup>, JANES D.B.<sup>1</sup>, TERADA M.<sup>1</sup>, BAGNATO O. R.<sup>1</sup>, DEFAVARI R.<sup>1</sup>

<sup>1</sup>Centro Nacional de Pesquisa em Energia e Materiais (CNPEM)

### 1. Introdução

O uso de fornos a vácuo é necessário em aplicações nas quais as características iniciais dos materiais não possam sofrer alterações causadas pelos gases da atmosfera em temperaturas elevadas [1]. Além do uso para proteção dos elementos trabalhados sob temperatura, a câmara do forno trabalhando em vácuo permite preservar a integridade de diversos componentes por maior tempo, como escudos de proteção térmica e elementos aquecedores utilizados na composição do forno, que se degradam rapidamente com a presença de oxigênio no interior da câmara, em alta temperatura.

Nesse trabalho é apresentado o processo de construção de um protótipo de forno a vácuo, com o princípio de aquecimento por indução [2]. Devido à principal aplicação ser a sinterização de cerâmicas especiais [3], foi utilizado um susceptor de grafite, cuja finalidade é ser aquecido pelo processo de indução e, consequentemente, aquecer as peças cerâmicas por radiação.

### 2. Experimental

A construção do forno foi feita utilizando uma câmara de vácuo de aço inoxidável com dimensões aproximadas de 400 mm de diâmetro e 350 mm de altura. O sistema de aquecimento é constituído de uma fonte de aquecimento por indução da fabricante Ambrell, de 4,2 kW de potência, uma bobina de cobre com 80 mm de diâmetro e um susceptor de grafite de 20 mm de diâmetro interno. O sistema ainda conta com um conjunto de barreira térmica constituído por multicamadas de folhas de molibdênio polidas e barreiras cerâmicas, para reduzir o aquecimento da parede da câmara do forno, evitando danos nas vedações para vácuo. O controle de temperatura foi feito com um pirômetro óptico Mikron MI-GA140, interligado com um controlador da marca Honeywell, que permite a programação de ciclos térmicos automáticos. O sistema de vácuo foi montado com uma bomba de vácuo modelo Pfeiffer DUO 20 - 24 m3/h e uma bomba difusora modelo VHS6 - 1550 l/s.

### 3. Resultados e Discussões

Durante os testes, foi possível aferir a temperatura do processo somente até 1800 °C devido à temperatura máxima da faixa de leitura do pirômetro óptico utilizado. Essa temperatura foi registrada com o uso de cerca de 80% da potência da fonte de aquecimento por indução.

Em relação à pressão de vácuo, os valores variaram na ordem de 5,0x10<sup>-6</sup> mbar em temperatura ambiente e 10<sup>-5</sup> mbar no patamar de temperatura máxima. A pressão oscilava durante a rampa de aquecimento devido a liberação de gases residuais nas amostras e dos próprios componentes internos da câmara do forno, no entanto a pressão logo se estabilizava quando a temperatura atingia o patamar máximo.

Devido ao desempenho apresentado nos testes iniciais, o equipamento está sendo utilizado com sucesso como ferramenta para o desenvolvimento de cerâmicas especiais e para outras aplicações com amostras de pequenas dimensões. A limite de aferição da temperatura não foi um limitante do equipamento, devido à temperatura de aplicação geralmente não ser superior à 1700 °C.

### 4. Referências

- [1]- Lee, Chin C., David T. Wang, and Won S. Choi. "Design and construction of a compact vacuum furnace for scientific research." Review of Scientific Instruments 77.12 (2006).
- [2]- Park JS, Taniguchi S, Park YJ. Maximum Joule heat by tubular susceptor with critical thickness on induction heating. Journal of Physics D: Applied Physics 2009;42.
- [3] Gizowska M, Perkowski K, Piątek M, Konopka G, Witosławska I, Tymowicz-Grzyb P. Investigation of YAP/YAG powder sintering behavior using advanced thermal techniques: Sintering to transparency. Journal of Thermal Analysis and Calorimetry 2019;138:1987–95.

<sup>\*</sup>Corresponding author: victor.pereira@cnpem.br



### TEMPORAL EVOLUTION OF SPATIAL DISTRIBUTION OF HYDROGEN AT TCABR-UPGRADE

### 1. Introduction

For a long time, the Plasma Physics Study in Brazil had the TCABR, a Tokamak at Plasma Physics Laboratory of the Institute of Physics at the Universidade de São Paulo. In need to elevate Brazil to innovation, the TCABR will upgrade, in direction to improve the plasma study. For this upgrade, it demands simulations and calculations. An important part of this upgrade is the vacuum chamber. Understanding the behavior of the gas in temporal evolution in a vacuum system motivates an analysis of the spatial distribution of hydrogen during the process of plasma synthesis.

### 2. Experimental

The motivation of this project emerges from a need to elaborate the dynamics of the vacuum chamber and its vacuum system of the TCABR – UPGRADE. The principal objective of this research is to develop a theoretical and numerical model to describe the pressure dynamics, to apply it over the upgrade. The main strategy is to deal with a theoretical model and validate it using the MolFlow software (a Monte Carlo simulator for vacuum systems).

### 3. Results and Discussions

This study started with a simpler geometry, to understand the MolFlow functions. The simpler geometry was a rectification of the current Tokamak, and the theoretical model came from the [ref number 1], the simulation is shown at the [fig number 1]. The second step was to complexify the model, inserting the pumps symmetrically. The current part of the project is to develop the theoretical model of Tokamak's torus geometry and simulate it with the MolFlow. All the simulations were made considering a stationary state, the next step of the project is to simulate the theoretical transitory model with the COMSOL software

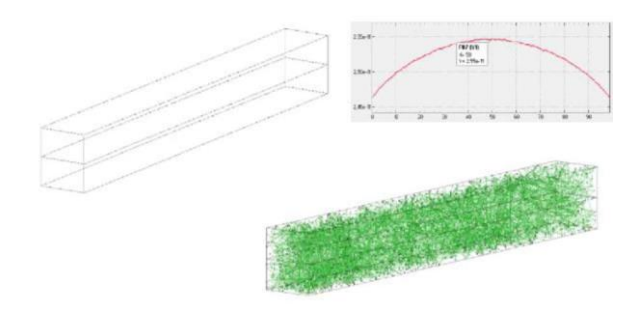


Fig. 1: Simulation of rectified TCABR.

Fig. 2: TCABR geometry for simulation.

### 4. References

- [1]- F. T. Degasperi, Contribuições para Análise, Cálculo e Modelagem de Sistemas de Vácuo, Universidade Estadual de Campinas, Brazil (2006).
- [2]- M. Ady and R. Kersevan, MolFlow+ User Guide, France (2014)
- [3]- A. Roth, Vacuum Technology, 3rd edition, Elsevier Science B.V., Netherlands (1990)



### VACUUM TECHNOLOGY COURSE: AN APPROACH TO THE INDUSTRY

### 1. Introduction

Vacuum Technology is a basic and fundamental tool in several areas of Experimental Physics and in several sectors of Industry. Aiming to contribute this knowledge to Society, since the beginning of the 1970s, the Vacuum Technology course has been offered at the USP Physics Institute. This course is offered to IFUSP undergraduate students, being a pioneering course in Brazil and it is estimated that it has trained around 800 students throughout its existence. The course is recommended for students who are interested in Experimental Physics or even getting a professional start in this technology. Given the significance of this technology, the course has been extended to researchers and technicians outside USP. Originally, the course was available to both IFUSP students and industry participants. However, acknowledging the varying needs and goals of institute students versus industry professionals, it was decided to establish a specialized Vacuum Technology course tailored specifically for professionals working in companies and industries that utilize this technology. The course, which ran until 1985, was attended by approximately 300 professionals from various industries and institutions, covering both theoretical and experimental aspects. It was reintroduced in 2012 under the name "Vacuum Technology for Industry," spans 4 months, and has since been completed by over a hundred professionals in the field [1].

### 2. Vacuum Technology for Industry Course

In the Vacuum Technology for Industry course, the basic concepts of gas kinetic theory necessary for vacuum study are covered, including pumping speed, gas flow in molecular, viscous, and intermediate regimes, as well as calculations and concepts of conductance for vacuum system design. The course includes detailed discussions on vacuum systems, pressure gauges, vacuum pumps, real and virtual leaks, materials, and gas sources with their respective models, such as gas volume, thermal desorption, diffusion, permeation, vaporization, and backstreaming [2-4]. The diameters of molecules relative to leak dimensions and the number of particle collisions as a function of pressure are also calculated. Common issues encountered with pressure gauges and vacuum pumps in industrial settings are discussed. The theoretical classes are complemented by specific experiments that are crucial for the interaction of the participants with vacuum systems and learning about behavior during gas flow in different regimes. Practical activities include experiments for calibrating pressure gauges, both for low and high vacuum conditions, measuring pumping speeds under both conditions, and determining tube conductance [5]. Additional hands-on training covers vacuum deposition techniques and the detection of real and virtual leaks using specialized detectors. Various materials and components used in vacuum systems are also presented.

In summary, this talk will highlight fundamental concepts in vacuum technology based on gas kinetic theory, illustrating their applications and the order of magnitude of different vacuum technology approaches with significant examples.

### 4. References

- [1]-https://portal.if.usp.br/tecvac/pt-br/node/323. Last access 08/08/2024
- [2]- B. Suurmeijer, T. Mulder and J. Verhoeven, *Vacuum Science and Technology*, The High Tech Institute and Settels Savenije Van Amelsvoort, 2016
- [3]- Nagamitsu Yoshimura, Vacuum technology: practice for scientific instruments, Springer, 2008
- [4]- A. Roth Vacuum Technology North-Holland, 1990
- [5]- B.A. Rodrigues Filho, L.M.F. Fagundes and N.H. Medina 2021 *J. Phys.: Conf. Ser.* **1826** 012001 **DOI** 10.1088/1742-6596/1826/1/012001

### Acknowledgments

The authors would like to extend their gratitude to all the professors who have developed and taught this course over the past 50 years: Dirceu Pereira, Ewa Wanda Cybulska, Juan Carlos A. Quadros, Luiz Marcos Ferreira Fagundes, Oscar Sala, Ross Allan Douglas, Salvador Troise, and Sylvio Dyonísio de Souza,



### MODELING WITH EXPERIMENTAL DESIGN OF COMPLEX PRE-VACUUM SYSTEMS

<sup>1</sup>Igor Junior de Lima <sup>2</sup>Francisco Tadeu Desgaperi

### 1. Introduction

Vacuum technology is present today in practically all areas in some way, directly or indirectly. Approximately 70% of vacuum usage occurs in the pre-vacuum region [1]. In this pressure range, gas flow in vacuum systems occurs mainly in the laminar viscous flow regime. Given this, we, from the vacuum technology laboratory, will size and analyze the gas pumping process and its respective conductance in the mentioned region. We propose to analyze the pressure variation as a function of time, considering two types of polyflow tubes with different diameters and lengths.

### 2. Experimental or Theory

We used the conventional method to analyze the pressure variation in the vacuum chamber as a function of time, where we used gauges to collect the pressure data and then plotted a graph. First, we determined the conductance of the pumping line; for this initial determination, we used the calculation of conductance in the laminar viscous regime:

$$C = 136.\frac{d^4}{l}.(\frac{p_1+p_2}{2})(1)$$

 $C=136.\frac{d^4}{l}.\left(\frac{p_1+p_2}{2}\right) (1)$  The techniques for measuring conductance are practically the same as those for measuring pumping speed. All devices remove gases from the systems by evacuating at a rate measured by the pumping speed Sb, which is defined as the volume of gas per unit time  $dV_{gas}/dt$  that the pumping device removes from the system [2]. Thus, the pumping speed at any point in the system can be obtained by knowing the pumping speed at another point and the conductance of the system. In particular, the combination of the pump's pumping speed and the conductance C of the tube gives us the effective pumping speed Sef:  $sef = \frac{Sb.C}{Sb+C} (2)$ 

$$sef = \frac{Sb.C}{Sb+C}(2)$$

### 3. Results and Discussions

Through the graphs, it was possible to observe the modifications made to the diameter and length of both tubes. The difference is much more evident in the smaller diameter tube, demonstrating that the length of the pumping line in this case has a greater influence on the medium's conductance. In contrast, for the larger diameter, the graphs begin to overlap, which was expected since the medium's conductances were previously calculated and showed minor differences for lengths exceeding 10 meters.



CONDUTANCIAS DO TUBO DE 3/16 POLIFLOW

**Fig. 1.** *Pressure versus time graph for the tube of 1/4.* 

Fig. 2. Pressure versus time graph for the tube of 3/16.

### 4. References

- [1] F.T. Degasperi REEF 00 Introduction to vacuum technology. Fatec São Paulo, São Paulo 2020.
- [2] F.T. Degasperi REEF 04 Conductance calculations. Fatec São Paulo, São Paulo 2020.

### Acknowledgments

To the Vacuum Technology Laboratory of Fatec-SP.

<sup>\*</sup>Corresponding author: place the e-mail of the corresponding author here (bookman old style 9 pt)



### MONTE CARLO METHOD APPLIED TO HIGH-VACUUM TUBULAR SYSTEM MODELING

Samuel da Silva Lima<sup>1\*</sup>, Francisco Tadeu Degasperi<sup>2</sup>

<sup>1,2</sup>Laboratório de Tecnologia do Vácuo – LTV, Faculdade de Tecnologia de São Paulo – FATEC-SP

### 1. Introduction

Various important high-vacuum systems feature tubular geometry. These vacuum systems have numerous applications in industry as well as in research. Therefore, it is necessary to determine the pressure field along the entire structure of the vacuum chamber to design effectively [1]. The primary objective of this work is to develop a simulation software capable of determining the pressure field of a high-vacuum tubular system using the Monte Carlo Method for system modeling and to verify its results by comparing them with the results from the Molflow+ simulation software developed by CERN.

### 2. Experimental

The software was developed using the Python programming language, with NumPy for numerical processing and Matplotlib for graph plotting and 3D visualization of the high-vacuum system. The high-vacuum system consists of a cylindrical tube with a length of 200 cm and a diameter of 1.6 cm, with two vacuum pumps connected at its ends. For modeling and simulation, we assumed that the system is stationary and that gas transport occurs in the molecular flow regime. We also determined a degassing rate per unit area of  $10^{-9}$  mbar·l·s<sup>-1</sup>·cm<sup>-2</sup>.

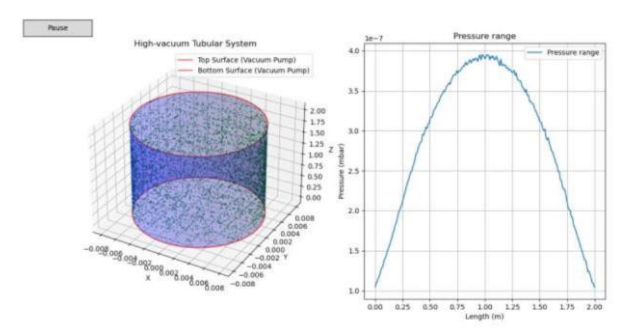
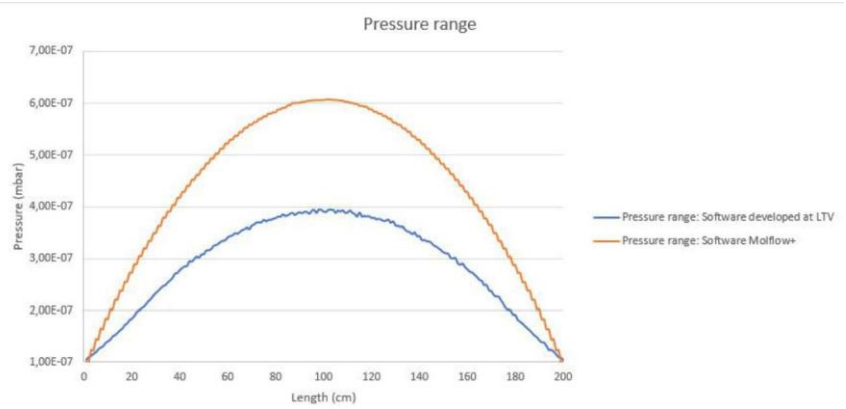


Fig. 1. Interface of the developed software

### 3. Results and Discussions

Based on the simulation conducted with the developed software, we also performed a simulation using Molflow+ to compare and verify the reliability of the values obtained from the developed software. Figure 2 presents a comparison between the pressure field obtained from the developed software and Molflow+. The results were very close, with the difference being imperceptible by pressure gauges. Therefore, it can be concluded that the Monte Carlo method is capable of modeling high-vacuum tubular systems.



**Fig. 2.** Pressure field obtained from the developed software and Molflow+

### 4. References

[1]-F.T. Degasperi, Contributions to the Analysis, Calculation, and Modeling of Vacuum Systems, UNICAMP, Brazil, (2006).

### Acknowledgments

To CNPq for the PIBIC scholarship.

<sup>\*</sup>Samuel Lima: samuellima0919@gmail.com



# EVALUATION OF THE BASE PRESSURE OF A VACUUM CHAMBER FOR DEPOSITIONS BY MAGNETRON SPUTTERING

E. Kressin<sup>1</sup>, E. B. Silva<sup>1</sup>, C. S. Kruger<sup>1, 2</sup>, F. Alfaro<sup>1, 3</sup>\*, J. C. Ságas<sup>4</sup> and D. A. Duarte<sup>3</sup>

<sup>1</sup> Centro Universitário UniSENAI, Jaraguá do Sul, SC.

<sup>2</sup> 4KSolid, Schroeder, SC.

<sup>3</sup> Universidade Federal de Santa Catarina, Laboratório de Tratamentos de Superficie, Joinville, SC <sup>4</sup> Universidade do Estado de Santa Catarina, Laboratório de Plasmas, Filmes e Superficies, Joinville, SC.

### 1. Introduction

Magnetron sputtering is a conventional technique for thin film deposition, notable for its ability to process a wide variety of materials and its extensive use in industrial applications [1]. The technique requires a high vacuum level to ensure efficient and contamination-free processing, which necessitates the use of a vacuum chamber made from materials that guarantee chemical stability and mechanical resistance. Among the available materials, stainless steel is often selected due to its inert surface and its ability to withstand large pressure variations. [2]. Thus, this work explores the details of a vacuum chamber constructed from stainless steel for magnetron sputtering deposition, with a focus on design and material selection.

### 2. Experimental

The cylindrical chamber, with a diameter and height of 400 mm and wall thicknesses of 4.25 mm (side) and 10.00 mm (top and base), was designed in SolidWorks and subjected to an analysis to assess wall deformation under a pressure gradient of 1 atm. After its fabrication, the chamber's airtightness was evaluated by generating a vacuum inside it. The tests were conducted using a set of mechanical vacuum pumps (Pfeiffer Vacuum model Pascal 2021 SD) and a turbopump (Pfeiffer Vacuum model HiCube 300 Eco), with pressure measurements obtained through a full-range sensor (Pfeiffer Vacuum model PKR 360).

### 3. Results and Discussion

Fig. 1 shows that the greatest deformation, although still below the yield limit, was observed at the center of the top plate where the magnetron will be installed, indicating the mechanical stability of the chamber. Fig 2 displays the pressure curves over time for the mechanical pump (solid red line) and the turbopump (dashed black line). The mechanical pump was initially used to reduce the pressure to the medium vacuum range, while the turbomolecular pump was employed to achieve high vacuum pressures. The curves indicate that the mechanical pump takes approximately 25 minutes to reach 1.5 mTorr, whereas the turbopump takes around 2 hours and 30 minutes to achieve just belo w  $3 \cdot 10^{-6}$  Torr. Extrapolation of the data indicates that it is possible to reach  $1 \cdot 10^{-6}$  Torr after just over 7 hours and  $1 \cdot 10^{-7}$  Torr in 13 hours.

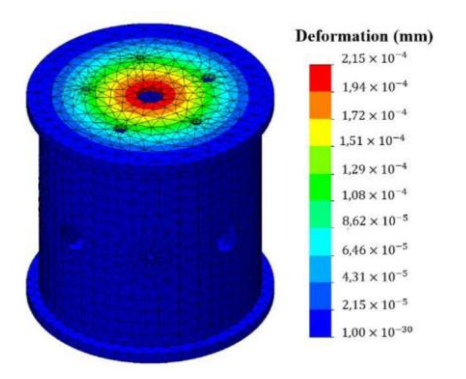


**Fig. 1.** Simulation for chamber wall deformation due to a 1 atm pressure difference.

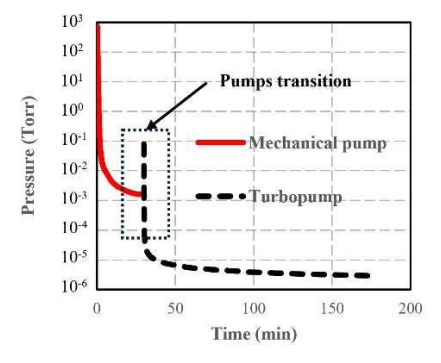


**Fig. 2.** *Pressure curves for the mechanical pump and the turbopump.* 

### 4. References

- [1] J. T. Gudmundsson, D. Lundin, High power impulse magnetron sputtering, Elsevier (2020) 1-48.
- [2] D. M. Mattox, Handbook of physical vapor deposition processing, William Andrew Publishing (2010)

### Acknowledgments

The authors thank CNPq for the financial support (grants 406376/2022-0 and 307408/2021-3).

<sup>\*</sup>Corresponding author: eduardo.kressin@gmail.com



# VACUUM COMPONENTS OBTAINED BY 3D PRINTING FOR HIGH-VACUUM APPLICATIONS

Henrique Chaves Gulino<sup>1</sup>, Francisco Tadeu Degasperi<sup>2</sup>, Ricardo Cardoso Rangel<sup>3</sup>

1.3 LSI/PSI/USP, University of Sao Paulo, Sao Paulo, Brazil
2.3 LTV/DSE/FATEC-SP, Faculty of Technology of Sao Paulo Paulo, Sao Paulo, Brazil

### 1. Introduction

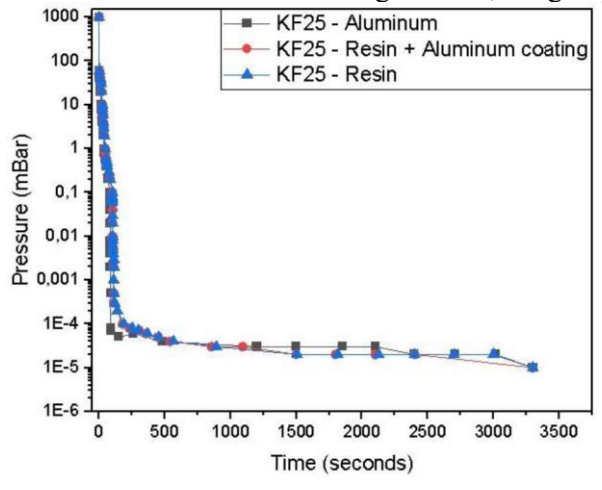
Photopolymer resins (composed of acrylates and/or methacrylates) are widely used in additive manufacturing, especially for parts requiring a high level of detail and tightness, factors that only stereolithography (SLA) can guarantee when compared to the Fused Filament Fabrication (FDM) technique. In addition to the flange made entirely of aluminum, two sets of flanges in the KF25 pattern were produced in this work for high-vacuum system applications.

### 2. Experimental or Theory

In this work, three sets of flanges were tested. The first flange used was made entirely of aluminum; the second was constructed from resin and subsequently subjected to a physical vapor deposition (PVD) process for the application of a thin aluminum film; and finally, the third flange used is made entirely of resin. The flanges were produced in the KF25 pattern using photopolymer resin dedicated to 3D printing based on stereolithography. The flanges were tested by replacing an aluminum flange from an Edwards Auto 306 evaporator at the Laboratory of Integrated Systems (LSI-USP) [1].

### 3. Results and Discussions

The same testing pattern mentioned earlier was replicated for the three cases presented. Two methodologies were used for comparison: In Figure 1, the pumping of the flanges was conducted to determine the final pressure in the available system, and subsequently, in Figure 2, the evolution of pressure after the shutdown of the diffusion pump was observed to compare outgassing. When analyzing Figures 1 and 2, we see that the three curves overlap completely. This indicates that the resin flange has excellent sealing and outgassing characteristics. Additionally, the flanges with and without the thin aluminum film exhibit the same behavior, suggesting that there is no need for external processes to improve the flange's efficiency. Notably, each resin flange constructed cost less than 1 dollar. In conclusion, we can affirm that vacuum components constructed through low-cost 3D printing, which achieve progressively lower pressures, are already possible, as this work demonstrates. Moving forward, the group will continue to dedicate itself to this topic.



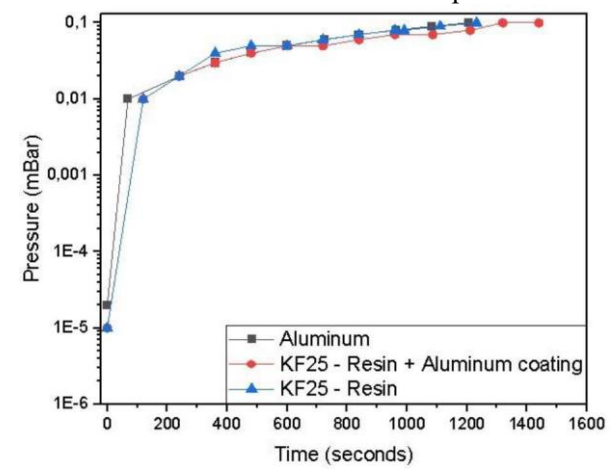


**Fig. 1.** Pressure as a function of time for the different types of flanges obtained.

Fig. 2. Raising pressure as a function of time (outgassing) for the different types of flanges obtained.

### 4. References

[1] - Rangel, R. C., Gulino, H. C., & Degasperi, F. T. (2024). Vacuum components obtained by 3D printing using biodegradable plastic. Rev. Bras. Apl. Vac, 43, e0124.

### Acknowledgments

To CAPES and FINEP for financial support.

<sup>\*</sup>Corresponding author: gulino@usp.br



### EXPERIMENTAL VERSUS THEORETICAL AND NUMERICAL RESULTS OF THE PRESSURE FIELD IN A TUBULAR HIGH VACUUM SYSTEM

Francisco Tadeu Degasperi\*, Regina Maria Ricotta and Vinicius Carvalho de Morais Faculdade de Tecnologia de São Paulo – FATEC-SP – CEETEPS

### 1. Introduction

Tubular high vacuum systems are largely used in arrangements of vacuum technology such as particle accelerators, elementary particle storage rings and electronic microscope. In all cases, the knowledge of the pressure field along the entire structure of the vacuum chamber is essential for the proper performance of its function. This work presents the construction of a cylindrical tubular system designed at the Vacuum Technology Laboratory – LTV of FATEC-SP to enable direct experimental measurements of the pressure field along the structure. To corroborate these experimental results, analytical analysis of the pressure field distribution for the stationary case considering the diffusion of gases under high vacuum of a tubular system of cylindrical geometry. Simulations were also performed using the Monte Carlo method through the Molflow program and COMSOL Multiphysics<sup>TM</sup>, under the Molecular Flow Module [2], which is based on the slope method in the molecular flow module.

### 2. Experimental Analysis, Modeling and Simulation

Figure 1 shows the scheme of the high vacuum system that consists of four cylindrical tubes of length l and diameter D displayed in series, connected on one side to turbomolecular vacuum pump and vacuum gauges along the tubes. The specific conductance and specific outgassing rates were both considered in the calculations. The modeling performed assumes that the transport of gases occurs in the molecular gas transport regime (free particles) and that it can be considered a diffusive phenomenon, with l > 5D. The pressure field along the tube increases parabolically and is maximum at the opposite end of the pump, [1]. The simulation was performed using the Monte Carlo Method with the Molflow and the COMSOL Multiphysics<sup>TM</sup> programs, [2].

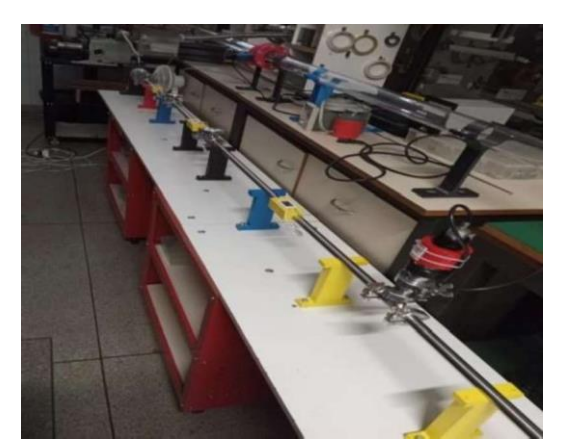


Fig. 1. Image of the high vacuum tubular system with different experimental constructed pressure measurement positions.

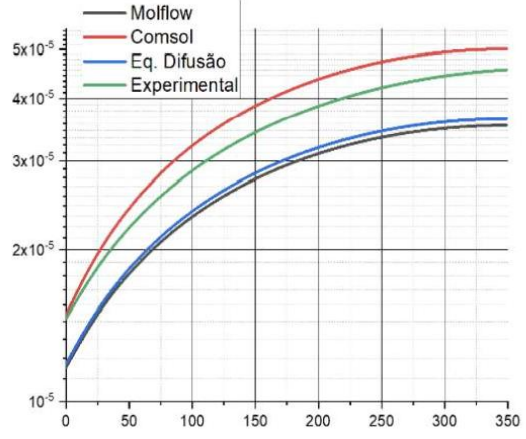


Fig. 2. Comparative graph of Pressure (mbar) versus Tube position (cm) with values obtained analytically, numerically, and experimentally on a logarithmic scale.

### 3. Results and Discussions

The values obtained analytically (diffusion equation) and by numerical simulation (Molflow) showed negligible deviation, while the values obtained by simulation in the COMSOL Multiphysics<sup>TM</sup> software and with the collection of experimental data were closer. Both the specific conductance and the outgassing rate per unit length of the tube are defined in order to achieve, by means of the diffusion equation, the pressure field obtained analytically. Despite the small variation between some values, the physical behavior presented excellent proximity, since experimental measurements also have the percentage error factor attributed to the equipment.

### 4. References

- [1] F. T. Degasperi, R. M. Ricotta, Vacuum, 188C, p. 1-30, (2021).
- [2] V. C. Morais, Estudo detalhado de um sistema de alto-vácuo tubular cilíndrico, TCC, Fatec-SP, 2024. R. Kersevan, J.-L. Pons, J. Vac. Sci. Technol. A 27, 1017 (2009).
- [3] F. T. Degasperi, R. M. Ricotta, Braz. J. Phys. 53 (2023) 44.

<sup>\*</sup>Corresponding author Francisco Tadeu Degasperi - ftd@fatecsp.br



# PHYSICAL AND MATHEMATICAL MODELING AND MEASUREMENT OF VACUUM LEAK DETECTION SYSTEM

Hernandes Miranda Alves<sup>1</sup>, Thiago Ricardo Braga Silva<sup>2</sup>, Francisco Tadeu Degasperi<sup>3</sup>,

<sup>1, 2, 3</sup>Departamento de Sistema Eletrônico - DSE

Faculdade de Tecnologia de São Paulo - FATEC-SP - CEETEPS

### 1. Introduction

Leak detection is a critical part of vacuum technology, with broad applications in industries and research that require vacuum to ensure the quality of their processes. It is also important in high-pressure systems, where leaks can contaminate the surrounding environment with harmful substances. In addition, the growing demand for technological innovations provides an opportunity for vacuum technology to improve and seek standards that are more precise.

Therefore, the creation of new methods and validation tools for leak detection is necessary. In this context, our project aims to calibrate leak detectors with an accuracy of (10<sup>-5</sup> to 10<sup>-6</sup>) mbar·L/s. Based on theory and the use of various mathematical methods to determine experimental curves.

### 2. Theory and Materials

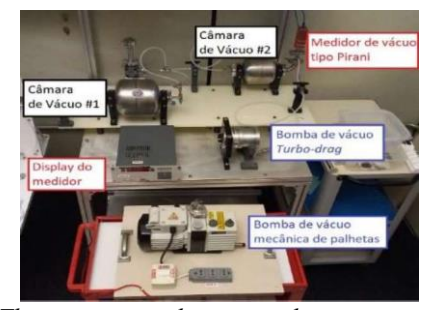
Based on vacuum technology theory, we model the throughput (Q) of a Leybold TL-4 capillary, which, through the choked flow effect, generates a continuous leak in the vacuum system, predetermined by the manufacturer. By analyzing the pressure in two chambers with the TL-4 capillary between them, a pressure difference will increase over time. This forms a graph of pressure over time. Because the manufacturer determines the throughput (Q), we can calculate the conductance (C) using the following equation:

$$C = \frac{Q}{\Delta p}$$

Initially, the throughput (Q) is determined only for helium (He) gas, but various other gases, such as N2 and CO2, will calibrated the TL-4 and the mathematical modeling of the system have been performed by the Scilab program. The assembly was made with two vacuum chambers (vacuum chamber #1 on the left and vacuum chamber #2 on the right), as shown in Figure 1. The experimental setup has been used two vacuum pumps, one being a vane pump and the other a turbodrag pump.

### 3. Results and Discussions (boldface Times New Roman 11 pt)

Using the gas accumulation method, in which the vacuum system is shut down and the pressure of the system is allowed to increase over a long period of time, it is possible to calculate the intrinsic leak rate of the system and test the simplest leak detection method, as shown in the graph obtained by plotting the pressure over time, as shown in Figure 2. The graph shows that there is linearity, which allows us to calculate the slope of the line and thus calculate the actual leak rate of our vacuum system.



Taxa de vazamento pela equação da reta Q = V entro de vazamento pela equação da reta Q = V entro de vazamento pela equação da reta Q = 1.8E - 4 mbar. L/s Q = 1.8E - 4 mbar. L/s y = 4E-05x + 0,0669

Fig. 1. The experimental setup used

Fig. 2. Gas accumulation method graph.

### 4. References

[1] A. Roth, Vacuum Technology, 3rd ed., Elsevier Science, 1990.

### Acknowledgments

We acknowledge the support of the CNPq through the PIBIC undergraduate research grant.

<sup>\*</sup>Corresponding author: place the e-mail of the corresponding author here (bookman old style 9 pt)



# NUMERICAL EVALUATION OF PEROVSKITE SOLAR CELLS USING NB2O5/AZO AS FRONT CONTACT LAYER

### CHRISTOF ZICKENHEINER<sup>1</sup>, RAUL RAMOS<sup>2</sup>, JOSÉ ROBERTO RIBEIRO BORTOLETO<sup>2\*</sup>

<sup>1</sup> Clausthal University of Technology, Clausthal-Zellerfeld, Germany

### 1. Introduction

To gain deeper insights into the impact of the optical properties of the AZO and Nb2O5 layers on the overall performance of the photovoltaic device, simulations with the software "OghmaNano" have been performed. This software employs a comprehensive numerical model which is capable of simultaneously simulating both the electrical and optical characteristics of the perovskite solar cell (PSC).

### 2. Experimental or Theory

For this simulation, a standard MAPbI3 PSC nip configuration was chosen. To simulate the transport and electrostatic effects within the device, the model solves Poisson's equation and the bipolar drift-diffusion equations in one dimension. Critical for this simulation are the device parameters, which serve as input for the model. These were extracted from literature to represent an ideal PSC [1]. To accurately represent the optical field distribution within the device, the model further employs the transfer matrix method [2]. This approach incorporates the wavelength dependent complex refractive index and the continuity condition to calculate reflections at material interfaces and optical losses for planar light waves at normal incidence. Several scenarios were simulated to shed light on the influence of the different material layers and interfaces on the optical behavior of the PSC.

### 3. Results and Discussions

Upon conducting this series of simulations, the resulting J-V curves (Fig. 1) exhibited a noticeable variation in short-circuit current (Jsc) when considering the optical parameters of the different layers, consequently impacting the power conversion efficiency (PCE) of the PSC. The drops in Jsc can be primarily attributed to reflections occurring at material interfaces, which can be concluded from the reflection profiles (Fig. 2). While the Nb2O5 layer initially increases the overall reflectivity of the stack, the subsequent addition of the AZO and SLG layers results in a reduction of reflectivity while introducing strong interference patterns. These patterns arise due to the superposition of a multitude of phase shifted reflected light waves. The phase changes are in turn caused by a difference in optical path length through the materials and reflection induced phase shifts at interfaces. This has a significant wavelength dependent impact on the quantum efficiency of the PSC. The gradual increase in refractive index of the material layers prevents an abrupt change in the optical properties at the interfaces, minimizing the reflection that would typically occur.

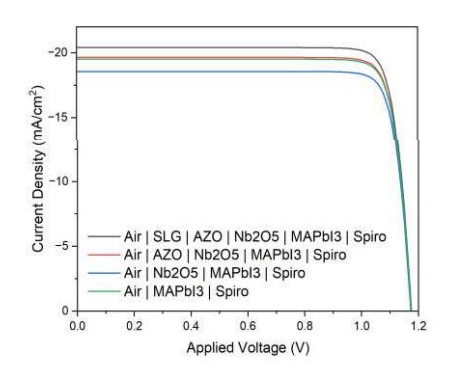


Fig. 1. J-V curves.

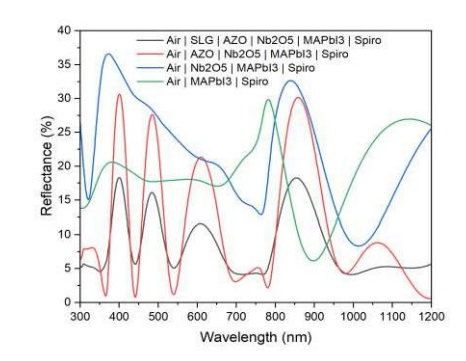


Fig. 2. Reflectance profiles.

### 4. References (bold face Times New Roman 11 pt)

[1]- Yassine Raoui et al, Solar Energy, 193, 948-955, 2019.

[2]- Sachchidanand, Anil Kumar, Pankaj Sharma, Solar Energy, 259, 63-71, 2023

### Acknowledgments (bold face Times New Roman 11 pt)

The authors thank CAPES, CNPq for financial support and CBMM Company for niobium metallic target.

<sup>&</sup>lt;sup>2</sup> Institute of Science and Technology, São Paulo State University (UNESP), Sorocaba, Brazil

<sup>\*</sup>Corresponding author: jose.rr.bortoleto@unesp.br



# ANALYSIS OF THE POTENTIAL FOR SUSTAINABLE GREEN HYDROGEN PRODUCTION USING BIOREFINERIES

Gustavo Henrique Romeu da Silva<sup>1\*</sup>, Andreas Nascimento<sup>1,2</sup>

<sup>1</sup>School of Engineering and Sciences, São Paulo State University, Guaratinguetá 12516-410, Brazil <sup>2</sup>Institute of Mechanical Engineering, Federal University of Itajubá, Itajubá 37500-903, Brazil

### 1. Introduction

Governments are seeking increasingly ambitious means to curb greenhouse gas emissions and decrease their dependence on fossil fuels or diversify their energy economies [1]. Thus, hydrogen has been highlighted for years as the energy source of the future - mainly from renewable sources (green hydrogen). This research aims to investigate the potential for sustainable green hydrogen production using biorefineries, with a specific focus on the feasibility of employing sugarcane biomass in Brazil.

### 2. Theory

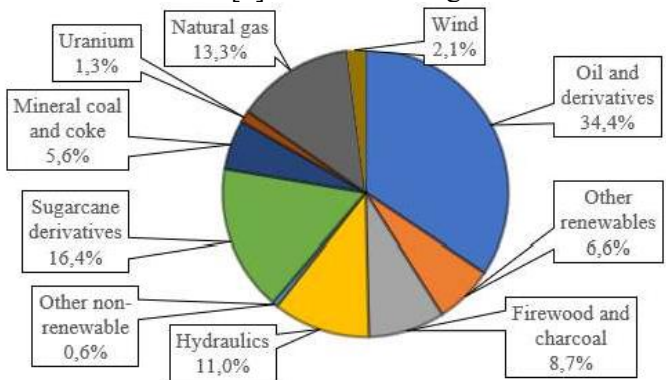
The work is developed from the bibliographic survey of technical-scientific articles related to the research theme found in the Scopus and Web of Science databases, using the R Language through the RStudio software. As seen in Table 1. The works were examined and criticized objectively.

Table 1. Bibliometric analysis of articles. Scopus and Web of Science (2018-August/2023).

One of the state o	Result in the number of "article" or "review"				
Query search string	Scopus	Web of Science	Union without duplicity		
"hydrogen" + "renewable energy" + "biorefinery"	38	145	158		
"green hydrogen" + "biorefinery"	12	22	24		
Total articles			174		

### 3. Results and Discussions

Currently, Brazil uses more renewable energy than the rest of the world. Adding firewood and charcoal, hydraulics, sugarcane derivatives and other renewables, it can be seen that 44.8% of the Brazilian energy matrix comes from renewable sources [2]. As noted in Figure 1.



Based on the analyses conducted in this study, it is concluded that the main objective has been achieved: the use of sugarcane biomass for green hydrogen production was evaluated, with biomass serving as a raw material for biofuel production in a biorefinery. The case study demonstrated the feasibility of producing green hydrogen through processes parallel to the production of second-generation ethanol, using the water-ethanol mixture, xylose, and circular biorefinery projects, making green hydrogen production in biorefineries viable.

### 4. References

- [1] ZHONG, M.; BAZILIAN, M. D., 2018. "Contours of the energy transition: investment by international oil and gas companies in renewable energy". Electricity Journal, Vol. 31, No. 1, pp. 82–91.
- [2] EMPRESA DE PESQUISA ENERGÉTICA. 2022. Balanço Energético Nacional. EPE: Rio de Janeiro, Brazil.

### Acknowledgments

This study was financed, in part, by the São Paulo Research Foundation (FAPESP), Brazil. Process Number 2024/10600-0; CNPq; ANP; FINEP; and MCTI through the PRH 34.1 FEG/UNESP program.

<sup>\*</sup>Corresponding author: gustavo.romeu@unesp.br



## DC-TRANSFERRED ARC THERMAL PLASMA TECHNOLOGY APPLIED TO SEWAGE SLUDGE TREATMENT FOR THE PRODUCTION OF GASES RICH IN H<sub>2</sub> AND CO.

Pedro William Paiva Moreira Júnior<sup>1\*</sup>, Felipe de Souza Miranda<sup>2</sup>, Nilton Francelosi Azevedo Neto<sup>1</sup>, Alexei Mikhailovich Essiptchouk<sup>2</sup>, Eduardo Sant Ana Petraconi Prado<sup>1</sup>, Antonio Carlos da Cruz<sup>1</sup>, Gilberto Petraconi Filho<sup>1</sup>

<sup>1</sup>Laboratório de Plasmas e Processos – LPP - Instituto Tecnológico de Aeronáutica – ITA/DCTA, São José dos Campos, SP, Brazil.

<sup>2</sup>São Paulo State University – Unesp - Instituto de Ciência e Tecnologia, São José dos Campos, SP, Brazil.

#### 1. Introduction

The increasing generation of sewage sludge due to urbanization and industrialization poses significant environmental and disposal challenges [1]. Conventional management methods like landfilling and incineration are becoming less viable due to stricter regulations and health concerns. Plasma processing technology offers a promising alternative, converting sewage sludge into valuable syngas and vitrified slag while minimizing harmful by-products. This high-temperature process efficiently breaks down organic materials, destroys pathogens, and recovers energy-rich gases [2]. However, challenges like high energy consumption and the need for pre-drying remain. This study investigates optimizing operational parameters in a DC-transferred arc plasma reactor to enhance syngas (H<sub>2</sub> and CO) production from sewage sludge, aiming for sustainable large-scale applications, such as in municipal wastewater treatment plants.

#### 2. Experimental

The plasma treatment reactor was specifically designed for the thermal treatment of materials, featuring a robust cooling system to continuously stabilize the reactor wall temperature. A DC supply powers it with a maximum output of 750 kW and operates at an average power of 20 kW, with a current of 200 A and a voltage of 100 V. The internal chamber, with a volume of 30 liters, maintains a controlled operating pressure via exhaust flow. The reactor's design includes a graphite cathode, which is adjustable via a mechanical armature, enabling arc length tuning and power dissipation adjustments. Additionally, an optical pyrometer measures the temperature near the arc through a quartz window. The system operates in a steady-state condition, maintaining relatively constant temperatures during treatment despite continuous sludge feeding and gas removal. The parameters explored were the working gas flow, the exhaustion speed, the feedstock supply rate, the reactor chamber operation temperature, and the plasma applied power. The sludge collected from a wastewater treatment plant (WWTP) was submitted to preliminary investigation, performed with Ultimate and Proximate analyses, X-ray fluorescent spectroscopy (XRF), and Fourier-transform infrared spectroscopy (FTIR). A syngas analyzer and mass spectrometer were utilized for gas analyses.

#### 3. Results and Discussions

The municipal wastewater treatment plant sludge presents an ash content of 40.5%, consisting mainly of Si, Al, Fe, and Ca (> 75%), and a complex organic fraction, including carbonyls, amines, and amides. X-ray fluorescence spectroscopy further confirmed these elemental compositions in the sludge ash. For a constant feedstock mass (without feed rate), plasma treatment produced gas with an 86% maximum syngas fraction and combustion heating of  $1.0 \times 10^4$  kJ/m³. However, when operating at a constant sludge feed rate of 300 g/min and an exhaust speed of 36 m³/min, the process significantly improved, with the volumetric fraction of syngas reaching up to 95% and combustion heating increasing to  $1.2 \times 10^4$  kJ/m³. These findings demonstrate the technique's potential as a direct single-stage solution for sewage sludge treatment, optimizing both the syngas yield and its energy content and contributing to developing a consistent methodology for fuel gas production from thermal plasma-treated sludge.

#### 4. References

[1]- Raheem A, Sikarwar VS, He J, et al. (2018) Opportunities and challenges in sustainable treatment and resource reuse of sewage sludge: A review. Chem Eng J 337: 616–641.

[2]- Cai X, Wei X, Du C (2020) Thermal Plasma Treatment and Co-processing of Sludge for Utilization of Energy and Material. Energy and Fuels 34: 7775–7805.

#### Acknowledgments

This work was supported by the São Paulo Research Foundation (FAPESP), grants 2023/02273-6 and 2022/03522-7.

<sup>\*</sup>Corresponding author: pedro\_kcond28@hotmail.com.

## MECHANICAL CHARACTERIZATION AND THERMAL STABILITY OF RECYCLED PLA FILAMENTS FOR 3D PRINTING

André Felipe Bizarri, Letícia da Rosa Carnin, Bruna Zappelino Camillo, Anderson de Carvalho Fernandes\*,
Andréa Loureiro Andrade\*

Centro Universitário SENAI/SC Campus Joinville

#### 1. Introduction

The PLA offers environmental advantages over petroleum-based plastics due to its origin from renewable agricultural sources, in addition to being recyclable and compostable. To overcome its mechanical limitations, the addition of new materials to create improved polymer blends is being explored [1]. Recycling plays a crucial role in reducing landfills and preserving natural resources, as indicated by [2]. In addition, improper management of plastic waste is associated with human health problems. [3] suggests replacing synthetic plastics with environmentally friendly materials, such as eco-composites, which are less harmful to the environment. This study aims to compare the properties of virgin and recycled PLA in different mass fractions, with 20%, 40% and 60% of recycled material.

#### 2. Experimental

To conduct the experiment, melt flow index and tensile tests were carried out for material characterization. A CEAST MF10 Plastometer was used for the melt flow index analysis, and the test parameters were in accordance with ASTM D1238. The tensile test was performed in an external laboratory at UFSC in Joinville, and adaptations of ASTM D638 were made with the help of an INSTRON EMIC 23-100 equipment.

#### 3. Results and Discussions

The Melt flow index (MFI) is crucial for measuring the ease of flow of a molten material and is essential for its processability. Virgin PLA initially has an MFI of 3.17 g, indicating high viscosity and low flowability. With the addition of 20% recycled PLA, the MFI increases to 4.47 g, suggesting lower viscosity due to thermal and mechanical degradation, facilitating extrusion and molding, but potentially compromising mechanical strength. By increasing to 40% recycled PLA, the MFI rises to 7.30 g, indicating greater flowability, which is beneficial for certain manufacturing processes but can result in a reduction in mechanical properties. With 60% recycled PLA, the MFI reaches 9.10 g, demonstrating even greater flowability, but indicating possible mechanical deterioration due to extensive polymer degradation.

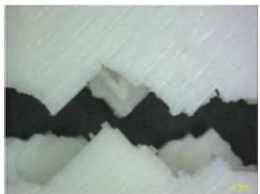




Fig. 1. Virgin PLA

Fig. 2. 20% Recycled PLA Fig. 3. 40%

Fig. 3. 40% Recycled PLA Fig. 4. 60% Recycled PLA

In summary, while higher fractions of recycled PLA increase material flowability, it is crucial to balance this characteristic with mechanical integrity. Further analysis showed that samples with 20%, 40%, and 60% recycled PLA exhibit a progressive reduction in mechanical strength, with losses of 20%, 65%, and 79%, respectively, compared to virgin PLA. Fracture surface analyses, Figures 1, 2, 3, and 4, also reveal that samples with higher recycled PLA content exhibit more spaced fibers and increased porosity, evidencing a deterioration of mechanical properties.

#### 4. References

- [1] Pereira, Renato Brisigueli; Morales, Ana Rita. Estudo do Comportamento Térmico e Mecânico do PLA Modificado com Aditivo Nucleante e Modificador de Impacto. *Polimeros, [s. l.]*, (2014).
- [2] Avelino, Guilherme Monteiro. A reciclagem química como alternativa ao tratamento de resíduos plásticos no Brasil, 64f, (2020).
- [3] Marinho, Vithória Alexandre Duarte et al. Aditivação e biodegradação de compósitos PHB/babaçu. **Revista Eletrônica de Materiais e Processos**, v. 13, n. 1, p. 37-41, (2018).

<sup>\*</sup>Corresponding author: andrea.loureiro@edu.sc.senai.br



## COMPARATIVE ANALYSIS OF MECHANICAL PROPERTIES BETWEEN MACHINING AND LASER POWDER BED FUSION (L-PBF) MANUFACTURING IN AISI 316L STAINLESS STEEL

Thiago Fernandes, Renan da Silva, Telmo Siqueira, Bruna Zappelino Camillo, Anderson de Carvalho Fernandes\*, Andréa Loureiro Andrade

Centro Universitário SENAI/SC Campus Joinville

#### 1. Introduction

While conventional machining processes mentioned by [1] are widely used in the industry for producing high-precision parts and components, additive manufacturing, as per [2] and [3], offers benefits such as the production of complex surfaces without the use of cutting tools, especially through L-PBF, which provides superior finish and dimensional accuracy. This study aims to analyze the mechanical properties of machining and L-PBF processes, presenting results of tensile and impact strength for both methods.

#### 2. Experimental

To conduct the tests, test specimens were fabricated using L-PBF and CNC machining processes. The material used was AISI 316L stainless steel, common to both processes. Four specimens were produced for each test type: tensile and impact. L-PBF specimens were manufactured using the Concept Laser M2 Cusing equipment. Conventional lathe and milling machines were employed for machining. CNC machining

#### 3. Results and Discussions

The test specimens manufactured by L-PBF and machining are shown in figures 01a and 01b, respectively.



Fig. 1. a) L-PBF, b) Usinagem

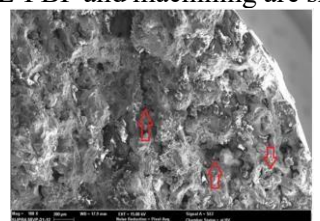


Fig. 2. Ampliação 100x

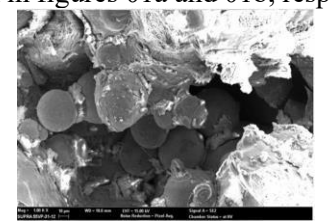


Fig. 3. Ampliação 1000x

Tensile and impact tests were conducted to analyze mechanical properties. L-PBF specimens exhibited yield strength of 29 MPa, ultimate strength of 493.2 MPa, modulus of elasticity of 121.3 GPa, 16% elongation, and 11.8% reduction in area. Machined specimens had yield strength of 260.5 MPa, ultimate strength of 501 MPa, modulus of elasticity of 180.4 GPa, 37.9% elongation, and 60.9% reduction in area. L-PBF specimens had comparable ultimate strength and higher yield strength than machined ones, but lower elongation, reduction in area, and modulus of elasticity, indicating greater fragility.

In impact tests, L-PBF specimens absorbed 45.4 J and expanded laterally by 0.203 mm, while machined ones absorbed 106 J and expanded by 0.651 mm. This confirmed machined specimens' higher impact absorption, typical of more ductile materials.

Micrographs (Figures 02 and 03) revealed cavities on L-PBF specimens' surfaces, indicating low density. Figure 03, an enlargement of a cavity from Figure 02, showed high concentrations of unfused particles and oxidized regions, likely due to the material's low density.

The results indicate that, although the samples produced by L-PBF exhibited comparable maximum strength and higher yield strength than the machined samples, they demonstrated brittleness due to lower elongation rates, area reduction, and elasticity modulus.

#### 4. References

- [1] Santos, Eduardo de Oliveira. **Efeito da prensagem em canais equiângulas (ECAP) sobre a microestrutura e dureza do alumínio reciclado obtido em processos de usinagem**, (2023). Dissertação Pós-Graduação em Ciência e Engenharia de Materiais da Universidade Federal de Sergipe.
- [2] Volpato, Neri. Manufatura Aditiva: Tecnologias e Aplicações da Impressão 3D. 1st ed. [S. 1.]: Blucher, (2017).
- [3] Denardi, Bruna et al. Otimização de parâmetros do processo de manufatura aditiva por fusão em leito de pó a laser da liga AISI 316l com foco em produtividade e propriedades mecânicas, (2021). Dissertação de Mestrado da Universidade Tecnológica Federal do Paraná.

<sup>\*</sup>Corresponding author: anderson.c.fernandes@edu.sc.senai.br



# SESSÃO DE PÔSTER 2

Terça-feira (12/11/2024)

XLV Congresso Brasileiro de Aplicações de Vácuo na Indústria e na Ciência

Balneário Camboriú - SC 11 a 13 de Novembro de 2024





#### VACCUM TECHNOLOGY: STATIC EXPANSION METHOD

João Pedro C. Andreatta<sup>1</sup>, Alicia Fernanda R. Pinheiro<sup>2</sup>, Francisco Tadeu Degasperi<sup>3</sup>,

<sup>1,2</sup>Faculdade de Tecnologia de São Paulo – Fatec-SP

<sup>3</sup> Doctor by electrical engineering and computer college UNICAMP, professor in FATEC-SP

#### 1. Introduction

Both in vacuum technology and in any other branch of the industrial sector, there must be a national standard to ensure a reliable unit of measurement, thereby guaranteeing quality and reliability in the processes conducted under vacuum. Analyzing the Brazilian metrological scenario, there is a noticeable gap in the field of measurements in vacuum technology, where there is not yet a national primary standard for conducting tests and calibrations for factory floor laboratories. Therefore, the method of static expansion is sought to create an experimental arrangement capable of determining a calibration standard.

#### 2. Experimental

The experimental points were taken by using an experimental arrangement assembled in the vacuum technology laboratory. By using a combination of multiple chambers as an initial volume, and a single large chamber as an expansion chamber, it's simple to predict and calculate what it will be the final pression on the system after the expansion of the nitrogen gas present on the initial volume to the single big chamber. Considering a conservative system, where the gas present on the initial volume is totally transferred to another volume, it's possible to describe this arrangement in one simple equation,  $p_1 * v_1 = p_2 * v_2$ , also known as Boyle's law. Where  $p_1$  is the initial pressure,  $v_1$  is the initial volume,  $p_2$  is the final pressure after the expansion, and  $v_2$  is the sum of the initial volume and the final volume, in this case the sum of the combinations of the 7 initial chambers, with the expansion chamber. Also, by using a tool present at the website of NIST institute, it's possible to determine the impact of uncertainties present in each part of the system.

#### 3. Results and Discussions

By using the experimental arrangement, it was possible to collect another round of experiments, those data were taken on May. With these points collected, a new graphic was designed on the figure 1, it's possible to see that the system is in perfect conditions to operate in an laboratory to calibrate other vacuum meters, since, knowing the initial values of  $p_1$ ,  $v_1$ , and  $v_2$ , it's possible to predict with a good accuracy an condition of pressure on the

Analyzing the figure 2, it's possible to visualize that the experimental arrangement have the value of  $v_l$  with an uncertain considerable high, and can be improved by using a new pressure sensor with a lower value in measurement uncertain, yet, when reducing the uncertainty of one of the values, other sources of uncertainty will increase and become more significant.

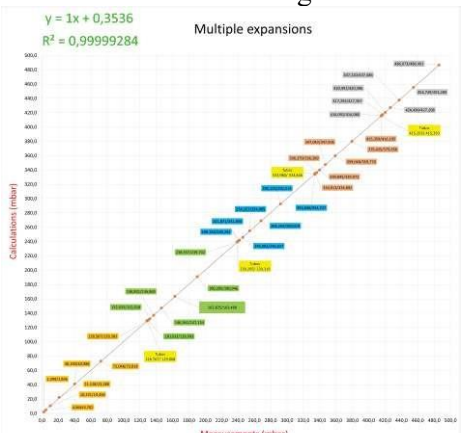


Fig. 1. (Latest experimental points taken in the experimental arrangement)

	w/out Residual	w/	Residual
pi	1.10		1.10
v1	70.63		70.63
v2	28.27		28.27
Residual	NA		0.00

ANOVA (% Contributions)

Fig. 2. (Uncertainty of each component of the experimental setup, taken on NIST Uncertain machine)

#### 4. References (bold face Times New Roman 11 pt)

[1] G. Dantas; K. Cesar. Criação do padrão primário de Vácuo no Brasil pelo método de Expansão Estática. Fatec São Paulo, São Paulo, 2022.

**Acknowledgments:** For the institution FATEC-SP for the support, the vacuum technology laboratory (LTV) and the CNPq institution for the scientific initiation scholarship.

Joao.andreatta@fatec.sp.gov.br

## GRAPHENE OXIDE DEPOSITION ON COPPER FOAM VIA CONVENTIONAL AND BIPOLAR ELECTROPHORETIC DEPOSITION WITH HIGH IMPULSE

Bruna Segat<sup>1\*</sup>, Julio. C. Sagás<sup>1</sup>, Luis. C. Fontana<sup>1</sup> and Daniela Becker<sup>1</sup>, <sup>1</sup>Laboratory of Plasmas, Films and Surfaces, Santa Catarina State University (UDESC), Joinville, Brazil.

#### 1. Introduction

Electrophoretic deposition (EPD) is an important technology for coating surfaces from suspensions. The versatility of this technique extends to various substrate morphologies, from flat to three-dimensional (3D) [1]. 3D structures like foams have advantages such as high surface area and easy electrolyte access, improving electrochemical performance. For this reason, the deposition of graphene derivatives has been studied for applications in supercapacitors, batteries and electrochemical hydrogen storage [2-3]. However, one of the challenges is the deposition inside of the foam. Therefore, this work aimed to evaluate the deposition of graphene oxide (GO) on a copper foam through conventional EPD and bipolar high impulse (HI) EPD, method that has been tested at UDESC's LabPlasma.

#### 2. Experimental

Before the EPD process, GO suspension was prepared in an aqueous medium with 1 mg/mL. The suspension was sonicated for 1 hour and 20 min. The Supplier DC Power Source (ABiPPS) electrical source was used for the depositions. The distance between the electrodes in the reactor was 1 cm. Conventional deposition was conducted under direct electric current with a voltage of 10 V. The bipolar HI deposition was conducted with alternating positive pulses of +600 V and negative pulses of -600 V. The pulse train was composed of two pulses (2p+ and 2p-) and lasted 1  $\mu$ s, with the interval between each pulse train being 20  $\mu$ s. Depositions were conducted for 5 min for bipolar HI and 10 min for conventional deposition. The best time was determined experimentally in other previous work. An ultrasonic bath at 30 kHz was used to stir the suspension during the EPD process. The samples were characterized by variation of the mass deposited in the samples and optical microscope.

#### 3. Results and Discussions

Fig 1. shows the copper foam before the deposition (Fig. 1A), after conventional deposition (Fig. 1B) and after bipolar HI deposition (Fig. 1C). Conventional deposition visually deposited only on the surface of the foam, while bipolar HI deposition deposited, in addition to the surface, inside the foam. This result corroborates the study of mass variation in which for conventional deposition, mass variation deposited was around  $0.0010 \pm 0.0006$  mg, while for bipolar HI the mass deposited was higher,  $0.0015 \pm 0.0005$  mg. This result may be related to the high intensity of the electric field. Then, the increase in voltage increases the applied field, and more intense fields accelerate the deposition rate and influence the movement of the particles [2]. Thus, this preliminary result indicates that using bipolar HI deposition can improve deposition inside the foam in a shorter time, overcoming the problems faced by conventional low-deposition EPD inside 3D structures.



**Fig. 1.)** Microscopic analysis of A) Copper foam, B) Copper foam after conventional deposition and C) Copper foam after bipolar HI deposition.

#### 4. References

- [1] A. Chavez-Valdez, M. S. P. Shaffer and A. R. Boccaccini, J. Phys. Chem. B, 117, 1502-1515, (2013).
- [2] H. Zhang, X. Zhang, D. Zhang, X. Sun, H. Lin, C. Wang and Y. Ma, J. Phys. Chem. B, 117, 1616-1627, (2013).
- [3] A. Shojaeinia, H. Aghajani and A. T. Tabrizi, International Journal of Hydrogen Energy, 48, 5836-5849, (2023).

#### Acknowledgments

This research was supported by CNPO, CAPES (code 001) and PAP-FAPESC (2023TR000258).

<sup>\*</sup>Corresponding author: brusegat@gmail.com

## ELECTROPHORETIC DEPOSITION OF TIO<sub>2</sub> NANOPARTICLES ON BACTERIAL CELLULOSE (BC) USING HIGH VOLTAGE BIPOLAR PULSES

Aline R. Almeida<sup>1\*</sup>, Julio César Sagás<sup>1</sup>, Cristiane Stegemann<sup>3</sup>, Jair Nunes<sup>2</sup>, Henrique de Souza Medeiros<sup>4</sup>, Luis César Fontana<sup>1</sup> and Daniela Becker<sup>1</sup>

<sup>1</sup>Laboratory of Plasmas, Films, and Surfaces, Santa Catarina State University (UDESC), Joinville, SC, Brazil

<sup>2</sup>Federal Institute of Santa Catarina (IFSC) - Jaraguá do Sul, SC, Brazil. <sup>3</sup>UniSENAI University Center - Jaraguá do Sul, SC, Brazil. <sup>4</sup>Catholic University Center of Santa Catarina - Jaraguá do Sul, SC, Brazil.

#### 1. Introduction

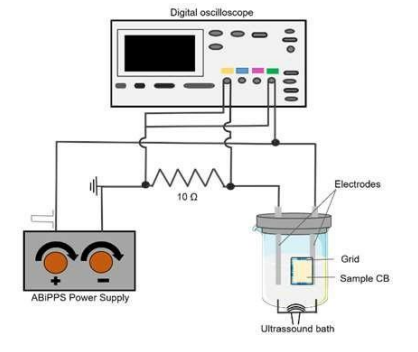
Bacterial cellulose (BC) is an environmentally friendly, biodegradable, and biocompatible raw material, similar to plant cellulose (PC), but with limitations in water affinity. To improve this characteristic, the incorporation of titanium dioxide (TiO<sub>2</sub>) is proposed due to its low cost and biocompatibility [1]. An innovative strategy involves the application of nanoparticles using modified electrophoretic deposition (EDP) [2]. This study aims to determine the optimal TiO<sub>2</sub> deposition parameters on BC and evaluate their impact on wettability.

#### 2. Experimental

A Central Composite Design (CCD) experiment was conducted with independent variables: TiO<sub>2</sub> concentration and deposition time. The dependent variable was the contact angle after drying the treated BC. The deposition used an asymmetric bipolar plasma power supply (ABiPPS), with the reactor built by the authors, as described in previous studies and illustrated in Figure 1 [3].

#### 3. Results and Discussions

The results for the contact angle are shown in Figure 2. With a variance of  $R^2 = 0.97$ , we found that the model provided good predictive capability and fit. Upon examining the results, it is evident that both time and concentration significantly influence the material's affinity for water. Specifically, as the deposition time increases, the material becomes less hydrophilic. Conversely, higher concentrations of  $TiO_2$  can enhance the hydrophilicity of the material, as demonstrated in experiment 4.



Samples	TiO <sub>2</sub> concentration (%)(m/v)	Time (min)	CA measure (°)
1	0,400 (-1)	10,00 (-1)	$13,6\pm0,1_a$
2	0,400 (-1)	20,00 (+1)	$41,1\pm0,3_b$
3	0,800 (+1)	10,00 (-1)	$20,\!4\pm0,\!2_a$
4	0,800 (+1)	20,00 (+1)	$11.8\pm0.1_a$
5	0,317 (-1,68)	15,00 (0)	$20,\!3\pm0,\!2_a$
6	0,882 (+1,68)	15,00 (0)	$13,\!5\pm0,\!4_a$
7	0,600 (0)	7,92 (-1,68)	$18,\!3\pm0,\!1_a$
8	0,600 (0)	22,07 (+1,68)	$30{,}7\pm0{,}2_b$
9 (C)	0,600 (0)	15,00 (0)	$37.7 \pm 0.3_b$
10 (C)	0,600 (0)	15,00 (0)	$34,1\pm0,\!2_b$
BC	-	-	$58,0\pm0,4_c$

**Fig. 1.** Schematic diagram of the experimental setup used

**Fig. 2.** Results of  $TiO_2$  deposition on dry bacterial cellulose (BC) and contact angle (CA)

#### 4. References

- [1]- S. Jafari et al., Int. J. Nanomedicine, 15, 3447-3470, (2020).
- [2]- K.M.K. Iwasaki et al., Appl. Surf. Sci., 611,155548, (2023).
- [3]- V. F. Dos Santos et al., J. Appl. Phys., 129, 123302 (2021).

#### Acknowledgments

The authors are thankful for the Multi-User Facility infrastructure from Santa Catarina State University's Technological Sciences Center and to the funding of CNPq (350722/2022-6) and FAPESC (2022TR001116).

<sup>\*</sup>Corresponding author: alinerosaufpr@gmail.com



## PLASMA TREATMENT IN CONTROLLED RELEASE SYSTEMS FOR INTEGRATED PEST MANAGEMENT

Maura de Almeida Bueno<sup>1</sup>, José Roberto Ribeiro Bortoleto<sup>1</sup>, Maria Carolina Blassioli Moraes<sup>2</sup>, Nilson C. Cruz<sup>1</sup>, Leonardo F Fraceto<sup>1</sup>,

<sup>1</sup>Universidade Estadual Paulista Júlio de Mesquita Filho (UNESP – Campus Sorocaba), <sup>2</sup>Empresa Brasileira de Pesquisa Agropecuária (Recursos genéticos e biotecnologia).

#### 1. Introduction

Butyl rubber, a copolymer of isobutylene and isoprene, is known for its excellent resistance to gas and liquid permeability, making it ideal for applications such as sealing rings and tires. In agriculture, it is used in septa as a pheromone releaser, offering a safer and more sustainable alternative to conventional pesticides [1]. To enhance the pheromone release rate, atmospheric plasma surface treatment is a promising technique. The KINPen IND plasma generator, an atmospheric plasma jet, is specifically designed for sensitive surface treatments at atmospheric pressure and room temperature, with optimized parameters for polymer materials.

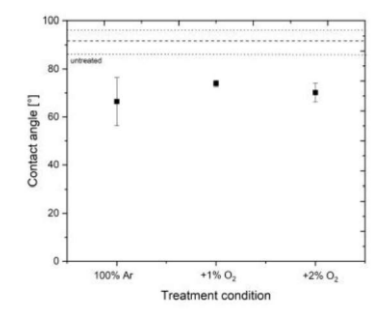
#### 2. Experimental

The project will use the atmospheric plasma jet equipment (KINPen IND, Neoplas GmbH, INP Greifswald) to modify the surface properties of the butyl rubber septum used as a pheromone release device in integrated pest management. The treatments were performed in pure Argon and a mixture with up to 2% Oxygen. The characterization techniques employed in this study include Scanning Electron Microscopy, Energy Dispersive X-Ray Spectroscopy, Fourier Transform Infrared Spectroscopy, Contact Angle, and Surface Energy measurements. These methods were applied both before and after treatment to compare and assess the surface modifications.

#### 3. Results and Discussions

The surface treatments addressed in this project alter the hydrophobic character of the butyl rubber septum. Argon plasma treatment reduced the original contact angle from  $91,63^{\circ} \pm 4,0^{\circ}$  to  $66,4^{\circ} \pm 9,98^{\circ}$ . Additionally, argon plasma with 2% oxygen resulted in a reduction of the contact angle to  $33,14^{\circ} \pm 8,16^{\circ}$ . The changes vary according to the gas conditions and exposure time to the treatment.

Although there were no significant changes in the FTIR spectra of the treated material, the increase in surface energy, related to the reduction in the contact angle, highlights the modification caused only in the surface layers of the material



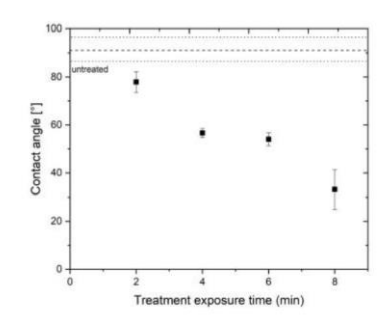


**Fig. 1. C**ontact angle after different treatment conditions.

**Fig. 2.** Contact angle after different exposure times to 98% Ar + 2% O<sub>2</sub>.

#### 4. References

[1] Borges M, Moraes MCB, Peixoto MF, Pires CSS, Sujii ER, Laumann RA. Monitoring the Neotropical brown stink bug Euschistus heros (F.) (Hemiptera: Pentatomidae) with pheromone-baited traps in soybean fields. Journal of Applied Entomology. 2011 Feb;135(1–2):68–80.

#### Acknowledgments

We thank the collaborating professors of the project, as well as the institutions, the State University of Júlio de Mesquita Filho (UNESP), Sorocaba campus, for providing their laboratories, and Embrapa for supplying research materials and expertise in the field.

<sup>\*</sup>Corresponding author: jose.rr.bortoleto@unesp.br



## PLASMA NITRIDING OF AISI 316L STAINLESS STEEL DEPOSITED BY PTA THROUGH ADDITIVE MANUFACTURING

Danielle Bond<sup>1\*</sup>, Ana Sofia C.M.D'Oliveira<sup>2</sup>, Abel André Cândido Recco<sup>1</sup>, Alícia Martins dos Santos Gonçalves<sup>1</sup>, Luiz César Fontana<sup>1</sup>

<sup>1</sup>Laboratory of Plasmas, Films and Surfaces, Santa Catarina State University (UDESC), Joinville, Brazil.

<sup>2</sup> Mechanical Engineering Department, Paraná Federal University (UFPR), Curitiba, Brazil.

#### 1. Introduction

The ASTM/ISO 52900 standard [1] defines additive manufacturing (AM) as "joining materials to produce objects from a 3D model through layer-by-layer processing, unlike subtractive manufacturing methodologies". Because of its layered approach, AM allows the production of customized parts on demand, but the deposited metals are exposed to complex thermal cycles [2]. Since the resulting microstructure of the additive metals is differentiated, they can respond differently to thermochemical surface treatments, such as nitriding [3], which are necessary in the post-processing stage of this manufacturing technique. Therefore, this work aims to analyze the nitriding of additive stainless steel.

#### 2. Experimental

The AISI 316L powder steel was deposited by plasma transferred arc (PTA) with the following parameters: current = 130 A; powder flow rate = 25 g/min; torch advance speed = 100 mm/min; gas flow rate: 0.1 L/min (plasma), 0.8 L/min (carrier), 15 L/min (shield). An 8.3 cm wall with 34 layers (16 cm length x 1 cm width) and an interpass temperature of 150 °C was constructed. Samples taken from the 316L PTA wall and 316L rolled steel samples were nitride under the following conditions: T = 380 °C; t = 3 h; working gas: 75% N2 + 25% H2; 350 V; 100 kHz; p = 3.0 Torr. The treated and untreated samples were characterized by XPS and SEM.

#### 3. Results and Discussions

XPS measurements (Fig. 1) show that the nitrogen concentration on the surface of the 316L PTA sample is higher than that on the conventional 316L sample (rolled steel). Figures 2-a and 2-b show the surface micrographs of the 316L PTA and conventional 316L samples, respectively. After the nitriding process, the microstructure of the 316L PTA sample (Fig. 2a) shows a surface topography, different from the conventional 316L sample (Fig. 2b), which shows well-defined grain boundaries. Considering that both have well-defined crystalline structures, it suggests that the 316L PTA sample has a higher N diffusion because of its typical melt structure.

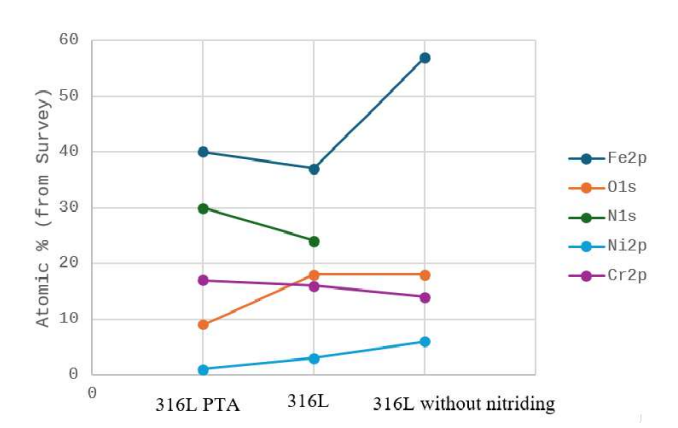


Fig. 1. XPS analysis

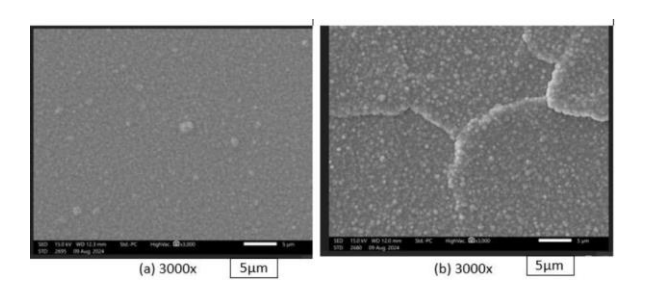


Fig. 2: (a) AISI 316L PTA. (b) AISI 316L rolled steel

#### 4. References

- [1]- ISO/ASTM 52900. "Additive manufacturing. General principles. Fundamentals and vocabular" (2021)
- [2]- I. Gibson et al. "Additive manufacturing technologies". Springer, Switzerland, (2021).
- [3]- J.S. Scholtz, et al. "Tecnologia em Metalurgia, Materiais e Mineração", 15.2 (2018).

#### Acknowledgments

This research was supported by FAPESC (2023TR000258).

<sup>\*</sup>Corresponding author: danielle.bond@udesc.br



#### STUDY OF MORPHOLOGY IN CARBON-CARBON COMPOSITE LASER CUT SURFACES.

L. Saito<sup>1\*</sup>, F.D. Origo<sup>2</sup>, M.S.F. Lima<sup>2</sup>, N. Monteiro<sup>2</sup>

<sup>1</sup> Instituto Tecnológico de Aeronáutica - Programa de Pós-graduação em Ciências e Tecnologias Espaciais; <sup>2</sup> Instituto de Estudos Avançados - Divisão de Fotônica;

#### 1. Introduction

In the context of hypersonic flight, the temperature on the surface of the aircraft is known to exceed 1800°C [1]. The aerospace industry is interested in exploring the potential of composite materials, such as carbon fiber reinforced composites, due to the vast array of mechanical, thermal, and chemical properties [2]. The use of lasers in carbon fiber composite processing is promising, as it eliminates the need of tool wear and offers a rapid processing time [3]. However, it is essential to understand the impact of high thermal input in this process on the structure of these composites. This work aims to discuss the causes of the undulated and globular morphology generated after the laser cutting.

#### 2. Experimental

The material used in this study is carbon-carbon composite, 7 mm thick, with random distribution of short fiber cloth. The samples were cut using a continuous Yb:fiber laser, model YLR-2000 IPG Photonics, with a cutting head coupled to the laser beam exit and a nitrogen gas feeder (20 L/min) to prevent oxidative reaction. Power and scanning speed were varied. The changes in the cut surface were analyzed using optical microscopy Olympus BX51 (bright and dark field) and scanning electron microscopy (SEM/FEG) conducted on a Tescan MIRA3 for a higher magnification and deeper insight, with an Energy-dispersive X-ray spectroscopy (EDS) Oxford model X-MAX 50 attached to obtain compositional information.

#### 3. Results and Discussions

Figure 1 illustrates micrographs of the laser cut surfaces using optical microscopy. Drag lines were observed all over the cut surface, with a greater degree of prominence at the lower edge of the cut and a corresponding increase in line density as the laser heat input increased. These drag lines may be the result of a complex mechanism that can be caused by irregularities in the laser irradiation process, such as deviations or disturbances. Figure 2 depicts a higher magnification of the surface using scanning electron microscopy, which reveals the formation of a globular structure with spheres between 10 and 20 µm in diameter. The globular morphology observed along the entire length of the cut face was caused by the laser processing, i.e., a consequence of a thermal transformation on the surface. This alteration suggests a melting of the carbon that is unconventional, but the higher temperature achieved by the laser could explain this phenomenon. The EDS analyses demonstrated the absence of contamination in the cut surface. This supplementary technique served to substantiate that all the material examined was, in fact, carbon.



Figure 1 - Micrograph of the cutting surface

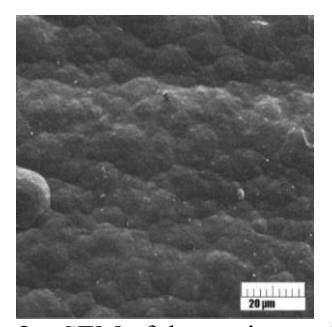


Figure 2 – SEM of the cutting surfaces.

#### 4. References

[1]- F. Costa, P. Camillo., A. Pivetta. "Brazilian 14-X Hypersonic Waverider Unpowered Scramjet Aerospace Vehicle Structural Analysis At Mach Number 7", 22 nd COBEM, (2013).

[2]- IYRS Blog. "The Many Exciting Uses of Carbon Fiber in Composites Manufacturing", IRYS SCHOOL OF TECHNOLOGY & TRADES. (2021).

[3] H. Dittmara, F. Gäblerb, U. Stutea. "UV-laser ablation of fibre reinforced composites with ns- pulses." Physics Procedia, 41, 266-275, (2013).

#### Acknowledgments

This work was carried out with the support of the Coordenação de Aperfeiçoamento de Pessoal de Nível Superior - Brasil (CAPES).

<sup>\*</sup>lucassaitosantos4@gmail.com



## ANALYSIS OF MECHANICAL PROPERTIES CAUSED BY HOT FORGING IN THE SAE 1040 STEEL

Pedro Augusto de Brito Inácio<sup>1</sup>, Marcos Dorigão Manfrinato<sup>1</sup>, Luciana Sgarbi Rossino<sup>1,2</sup> *<sup>1</sup>FATEC Sorocaba*, <sup>2</sup>UFSCAR Campus Sorocaba

#### 1. Introduction

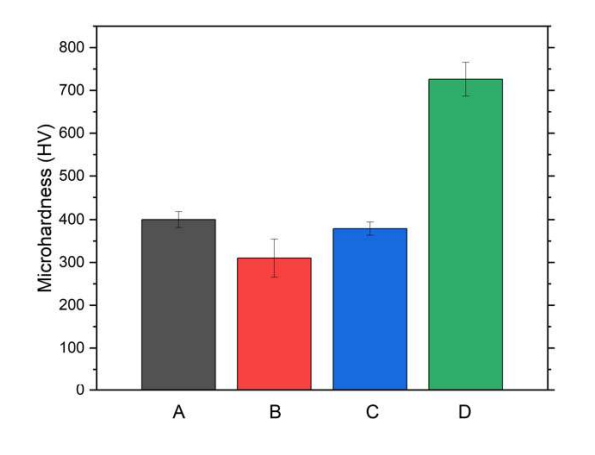
Well-established by the metallurgical industries, the mechanical manufacturing process by hot forging is widely used today, mainly in the automotive area, due to the improvement in the mechanical properties of parts in this sector, or to produce large parts, such as ship axles. In this work, it was possible to analyze the influence of the different cooling carried out in the hot forging process on the mechanical properties of the SAE 1040 steel.

#### 2. Experimental

The as-received SAE 1040 (A) in Ø16x10mm dimension and with a polished surface finish was submitted to a hot open forging process using a 1kg non-hardened commercial sled. The specimens were heated in the range of 800°C to 1000°C, forged for 1 hour to reduce the thickness from 16 mm to 10 mm, and treated with different matter: one sample was cooled in the air (B), another sample was normalized (C), and the other sample was cooled in the water (D). After that, the sample with dimensions of 16 x 10 x 10 mm with polished surface finish was produced. The as-received and forged materials were characterized by Vickers microhardness testing and microwear testing by rotative fixed ball.

#### 3. Results and Discussions

It is possible to observe (**Fig. 1**) a hardness decrease for the sample (B) forged and cooled in the air, in relation to the sample of the base material (A) due to a long time kept at high temperature, which produces a gross microstructure. It is noted that the normalizing heat treatment (C) refined the microstructure and influenced the hardness of the material. The forged and quenched sample (D) **shows** the highest hardness due to the martensite formation. It is possible to observe (**Fig. 2**) that the hot forging process was effective in increasing the wear resistance of the material for samples (C) and (D). Also, the hardness influenced the wear results, in that the forged specimen (B) had a lower wear resistance due to the lower hardness. The forging process was able to change the mechanical properties of the hardness and wear resistance of the material, with differences in each stage of the heat treatment.



0.016 В 0.014 C /olume de desgaste (mm³) D 0.012 0,010 0.008 0,006 0,004 0.002 0.000 100 120 140 Distância percorrida (m)

**Fig. 1.** Microhardness results for the as received and forged samples

**Fig. 2.** Wear volume at function of sliding distance for as received and forged samples

#### 4. References

[1]- KAYNAR, A.; et al.. Materials & Design, v. 51, p. 819–825, out. 2013.

[2]- JAHAZI, M.; EGHBALI, B.. Journal of Materials Processing Technology, v. 113, n. 1-3, p. 594–598, jun. 2001.

<sup>\*</sup>Corresponding author: place the e-mail of the corresponding author here (bookman old style 9 pt)



## A PROSPECTIVE STUDY OF THE ADDITION OF GRAPHENE OXIDE TO LEAD-FREE SOLDER PASTE

Caio Cavadas<sup>1\*</sup>, Ana Neilde Rodrigues da Silva<sup>2</sup>, Bruno Soares de Lima<sup>1</sup>, Marcos Massi<sup>1</sup> Escola de Engenharia Mackenzie, <sup>2</sup>Faculdade de Tecnologia de São Paulo, Fatec São Paulo

#### 1. Introduction

As electronic devices have become more complex and smaller, the processes for electronic assemblies have improved in recent years. As a result of the elimination of lead, new solder alloys have been developed in response to this new reality. Intermetallic, the thin layer that forms between the solder joint and the surface of printed circuit board (PCB) in ternary SAC solder compositions, can lead to serious reliability problems if the process parameters are not controlled. To reduce intermetallic formation, various types of particles has been researched aiming at being mixed into the solder paste, among then graphene. However, several authors have reported that it may not be incorporated into the solder joint and may form agglomerates. A prospective study of the addition of graphene oxide to SAC 305 solder paste was conducted in this paper to study the interaction between the solder alloy powder and the graphene oxide before mixing with the flux.

#### 2. Experimental

Initially, 1 g of solder alloy powder (SnAgCu alloy 305, T3) and 0.004 g (0.4% by mass) of graphene oxide were mixed manually. Two different tests were carried out, first the flux was put over the substrate and immediately adding the powder mixture, and second the powder mixture was placed on the substrate and then adding flux. The substrates were bare copper, PCI with OSP finish, and alumina, to observe the influence of the flux and avoid the wetting effect. The fluxes were no-clean paste flux and RMA flux. The substrates were heated on a hot plate at 220°C but the environment is not controlled. The samples were evaluated using an optical microscope.

#### 3. Results and Discussions

The results showed that the alloy only melts when flux is added. When the powder mixture is added to the flux, a solder joint is formed, and the graphene oxide remains on the surface of the flux. However, when the flux is added to the powder, several small solder balls are formed suggesting that the solder powder oxidizes when heated. The presence of oxide hinders the melting process and the formation of the solder joint, thus in the presence of flux, the oxide is removed allowing fusion and the joint formation. The formation of small, scattered solder balls when flux is added after the powder is heated confirms oxidation during heating. In all the tests performed, the graphene oxide was not incorporated into the solder alloy during melting, but always remained dissolved in the flux. So, there are two hypotheses: first the oxide that forms on the surface of the solder particles avoids the graphene oxide to be dissolved in the melted solder, or second as it is lighter than the solder the graphene oxide dissolves in the flux. Also, the thickness of the intermetallic may be influenced by the presence of graphene oxide in the solder. In the analyses performed there was no significant variation in the thickness of the intermetallic layer, indicating that the graphene oxide had not been incorporated.



**Fig. 1.** a) Flux added to the powder - small solder balls are formed - the solder powder oxidizes when heated. b) Metallographic analysis. Graphene oxide agglomerates on the solder joint surface. Intermetallic  $\sim 1.5 \mu m$ .



**Fig. 2.** a) Powder added to the heated flux, b) Metallographic analysis. Graphene oxide agglomerates on the solder joint surface. Intermetallic  $\sim 1,7\mu m$ .

#### 4. References

[1]- Li, Y.; Yu, S.; Li, L.; Song, S.; Qin,W; Qi, D.; Yang, W.; Zhan, Y. Metals **2023**, 13, 1209. https://doi.org/10.3390/met13071209

#### Acknowledgments

The author acknowledge to Laboratórios de Confiabilidade em Eletrônicos (LCE) of Eldorado Institute.

<sup>\*</sup>Corresponding author: place the e-mail of the corresponding author here (bookman old style 9 pt)

#### SOIL REMEDIATION BY HYDROGEL AND EARTHWORMS AS SOIL QUALITY INDICATORS

Alana Maria Corá<sup>1\*</sup>, Francisco Tadeu Degasperi<sup>2</sup>, Silvia Pierre Irazusta<sup>1,2</sup>

<sup>1</sup>Faculdade de Tecnologia de Sorocaba; <sup>2</sup>Unidade de Pós-Graduação, Extensão a Pesquisa do Centro

Estadual de Educação Tecnológica Paula Souza

#### 1. Introduction

The increasing soil contamination by metallic waste, mainly arising from industrial activities may result in environmental liabilities, that are understood as contaminated deposits and sites that present risks to public health and/or to environment [1, 2]. The present work aimed to use sodium polyacrylate (PAS) as tool to remove metal contamination and establish a reliable bioindicator system to evaluate soil quality.

#### 2. Experimental

A leaching assay was carried out constituted, respectively, by three vertical layers of metal contaminated soil, PAS in powder and swollen, and standard soil, to leach the toxic metals to the inferior layers a water flow was used and after the precipitation all the layers were separated and frozen for posterior Inductively Coupled Plasma (ICP) analysis. An ecotoxicological test, to demonstrate the environmental hazard, was conducted in triplicates using boric acid as reference substance and contaminated soil for 14 days using 10 earthworms in each recipient as soil bioindicator, after that they were removed and analyzed for avoidance, mass loss and metallothionein protein, then lyophilized and metalized with Au/Pd for Scanning Electron Microscopy (SEM) analysis.

#### 3. Results and Discussions

The ICP results (Fig. 1) shows that the polymer was effective in retain metals from soil, with some differences in specie efficiency, a higher adsorption occurred for Fe and Al, while Cu was one of the least retained, such as Cr, Ba and Mn. There was no difference in SEM-EDS analysis (Fig. 2 A, B, C, d, E and F) performed on organisms, the cuticle was preserved in both cases, without rigidity or cuticle injury, only dehydration resulting from freeze-drying. The avoidance of earthworms in the contaminated soil was observed since the first day of the test exposure until the final of 14 days, without death, but the bioindicators expose to contaminants demonstrated a significative mass loss (Fig. 3 B). The Fig. 4 show the metallothionein protein test performed on the organisms from the avoidance test, the result shows that the protein increased on the exposed earthworms. The protein increases among with the mass loss represent a stress induced by metabolic damage, probably due to the attempt of metal decontamination by the earthworm's organism.

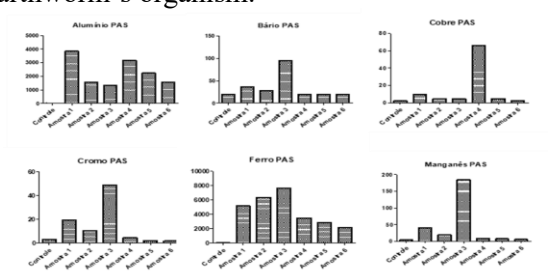


**Fig. 1.** ICP result of the PAS after the leaching assay.

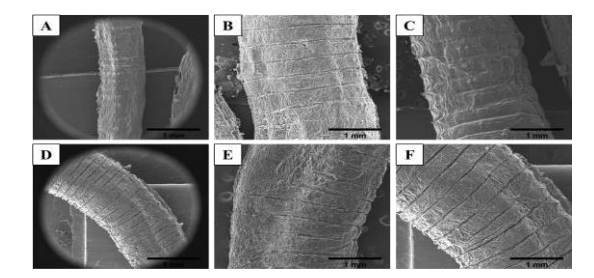


**Fig. 2.** Avoidance test SEM analysis. A, B and C, earthworms in control soil. D, E and F, earthworms in contaminated soil.

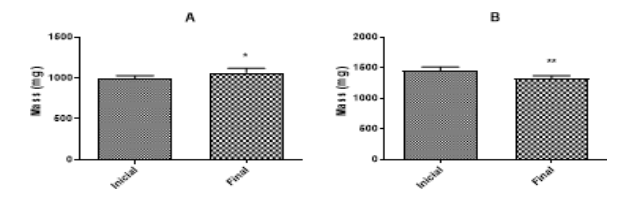
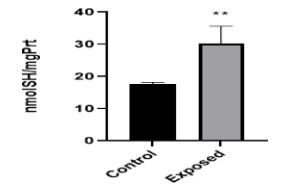


Fig. 3. Mass loss graphic of the avoidance test. A, control soil. B, contaminated soil.



**Fig. 4.** Metallothionein protein test of the avoidance test earthworms.

#### 4. References

- [1] M. Andrea, M. Acta Zoológica Mexicana, 2, 95-107, (2010).
- [2] C. Galdino, et al. Revista Produção, 14, 54-63, (2004).

#### Acknowledgments

To FAPESP for the Process No. 2022/49136-3 and to Poli-USP for providing the SEM analysis.

<sup>\*</sup>Corresponding author: alana.cora@fatec.sp.gov.br



## CHARACTERIZATION OF THERMAL BARRIER COATINGS PRODUCED BY AIR PLASMA SPRAY ON TITANIUM ALLOY SUBSTRATES

## A. C. Corrêa<sup>1</sup>, J. Mascarello<sup>3</sup>, V.L.O. de Brito<sup>1</sup>, D.A.P. Reis<sup>2</sup>, R.J.Takahashi<sup>2</sup>, M.S.F. Lima<sup>1</sup>, D.C. Silva<sup>2</sup>, C.W.S. Barbosa<sup>2</sup>, N.M. Santos<sup>1\*</sup>

<sup>1</sup>Institute for Advanced Studies, IEAv/DCTA, São José dos Campos, SP. <sup>2</sup>Federal University of São Paulo, UNIFESP, São José dos Campos, SP. <sup>3</sup>Alpha Metalização LTDA, Barueri, SP.

#### 1. Introduction

Thermal barrier coating (TBC) is fundamental to thermal insulation technology. It finds applications in devices that are subject to high temperatures, such as turbine components, protecting them from thermal exposure that can cause their degradation. A typical TBC system consists of a metallic bond layer (bond coat), in contact with the metallic substrate, and an external ceramic layer (top coat), applied over the bond layer [1, 2].

#### 2. Experimental

In this work, TBC samples with NiCrAlY as bond coat and YSZ as top coat were produced on Ti-6Al-4V substrates using Atmospheric Plasma Spraying (APS). The elemental mappings of the NiCrAlY and YSZ powders, as well as the elemental line profile and cross-section micrograph of the bonding (BC) and top-coating (TC) layers of the samples, were analyzed by scanning electron microscopy (SEM) equipped with a field emission gun (FEG) and energy-dispersive X-ray spectroscopy (EDS).

#### 3. Results and Discussions

According to the results obtained, the coating presented the coexistence of fused and dense ceramic particles, in addition to semi-fused particles with a more porous structure and fine grains. The metal bonding layer (BC) presented the characteristic elements (Ni, Cr, Al and Y), with small amounts of Ti and V. The presence of the constituent elements of the substrate (Ti, V, Al) indicates that the BC layer did not completely cover the substrate surface, despite its thickness of approximately 360  $\mu$ m. The TC layer presented a thickness of 1062  $\mu$ m and the presence of the main elements of the ceramic coating, zirconium (Zr) and yttrium (Y), with the presence of aluminum (Al), nickel (Ni) and chromium (Cr) diffused in the BC/TC interface.

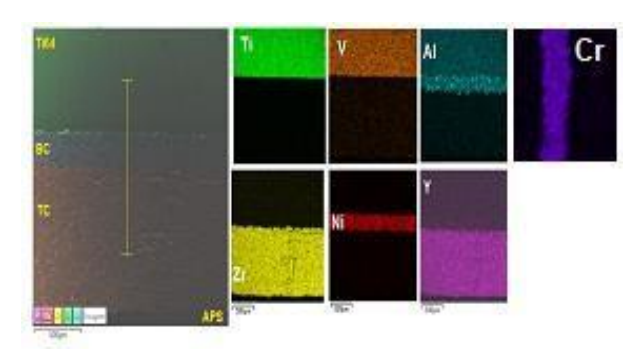


**Fig. 1.** Cross-section micrograph showing the elements of the Ti64 substrate, metal bonding and top TBC layers.

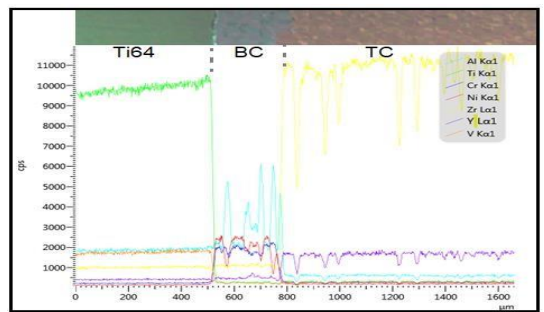


**Fig. 2.** Elemental line profile of the elements of the Ti64 substrate, metal bonding and top TBC layers.

#### 4. References

- [1] S. T. Vagge and S. Ghogare, Materials Today: Proceedings 56 (3), 1201-1216 (2022).
- [2] B. A. Yalçınyüz et al., Journal of Thermal Spray Technology 32, 2636-2646 (2023).

#### Acknowledgments

This work was supported by the IEAv 001/2019 SCV Prosolo and Proc. 125229/2024-0 CNPq.

<sup>\*</sup>Corresponding author: <a href="mailto:nazirmonteiro@gmail.com">nazirmonteiro@gmail.com</a>



#### CHARACTERIZATION OF Ti-Nb-Zr COATINGS

Sidney C. Z. Costa<sup>1\*</sup>, Angelo L. Gobbi<sup>2</sup>, Valmor R. Mastelaro<sup>3</sup>, Pedro A. P. Nascente<sup>1</sup>, 
<sup>1</sup>Federal University of Sao Carlos, Department of Materials Engineering, 13565-905, Sao Carlos, SP, 
Brazil.

<sup>2</sup>Brazilian Center for Research in Energy and Materials, Brazilian Nanotechnology National Laboratory, 13083-970, Campinas, SP, Brazil.

<sup>1</sup>University of Sao Paulo, Sao Carlos Institute of Physics, 13560-590, Sao Carlos, SP, Brazil.

#### 1. Introduction

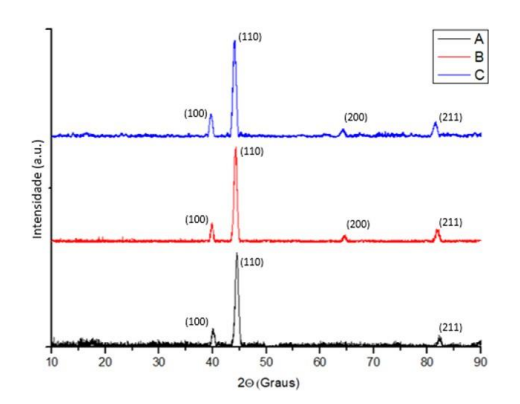
Ti, Nb, and Zr are biocompatible, non-toxic, and non-allergenic biocompatible metals, and the addition of Nb and Zr to Ti favors the stabilization of the  $\beta$  (bcc) phase. This phase is more adequate for biomedical applications since it exhibits a low elastic modulus, a shape memory effect, and superelastic characteristics. However, these alloys are significantly more expensive than 316L stainless steel (SS) that is commonly used as implants, and an economical approach is to coat an 316L SS implant with a thin film of Ti-Nb-Zr that has appropriate composition and thickness [1]. In this study, three Ti-Nb-Zr coatings having approximately the same amount of Nb were deposited by magnetron sputtering on 316L substrates.

#### 2. Experimental

Ti, Nb, and Zr disks with a 2-inch diameter, 3 mm thickness, and 99.99% purity were used as targets. For the substrates, 15 mm diameter disks made of 1 mm thick AISI 316L SS were utilized. An AJA Orion 8 Phase II J magnetron sputtering system was employed to deposit three coatings with different compositions. The physicochemical characteristics of the Ti-Nb-Zr coatings were characterized using X-ray fluorescence spectroscopy (XRFS), X-ray diffraction (XRD), X-ray photoelectron spectroscopy (XPS), and polarization testing, utilizing a Shimadzu 720 spectrometer, a Shimadzu XRD-6100 diffractometer, a Scienta-Omicron spectrometer, and an AUTOLAB potentiostat, respectively.

#### 3. Results and Discussions

Elemental analysis was conducted using XRFS, yielding the following compositions (at%):  $Ti_{66}Nb_{21}Zr_{13}$ ,  $Ti_{62}Nb_{20}Zr_{18}$ , and  $Ti_{59}Nb_{19}Zr_{22}$ . Fig. 1 displays the XRD diffractograms for the three coatings, revealing a predominance of the  $\beta$  phase and a minor contribution of the  $\alpha$  (HCP) phase. Surface analysis by XPS indicated that the coating surfaces were oxidized and a surface enrichment of Zr and a depletion of Ti. Fig. 2 shows the polarization testing in Simulated Body Fluid (SBF), indicating improved corrosion resistance of the coatings. The oxidized surface layers provide enhanced corrosion protection and thus are beneficial for implant materials.



10 - 0.5 - 0

**Fig. 1.** XRD diffractogram for the (A)  $Ti_{66}Nb_{21}Zr_{13}$ , (B)  $Ti_{62}Nb_{20}Zr_{18}$ , and (C)  $Ti_{59}Nb_{19}Zr_{22}$  coatings.

**Fig. 2.** Polarization curves of 316L steel, Grade IV Ti, and (A)  $Ti_{66}Nb_{21}Zr_{13}$ , (B)  $Ti_{62}Nb_{20}Zr_{18}$ , and (C)  $Ti_{59}Nb_{19}Zr_{22}$  coatings in SBF.

#### 4. Reference

[1] E.D. Gonzalez *et al.*, Thin Solid Films, **721**, 138565 (2021).

#### Acknowledgments

This work was supported by FAPESP (process 2017/25983-8), CNPq (process 302450/2017-3), CAPES (Finance Code 001), and CNPEM/LNLS.

<sup>\*</sup>Corresponding author: sidneycherman@gmail.com



## SIMULAÇÃO E DEPOSIÇÃO DE TITÂNIO POR MAGNETRON SPUTTERING EM CÂMARAS CERÂMICAS PARA ACELERADORES DE PARTÍCULAS

KAKIZAKI D.Y.<sup>1\*</sup>, DORETTO D.S.<sup>1</sup>, RIBEIRO R.D.<sup>1</sup>, LANCINI I.C.<sup>1</sup>, PEREIRA V.F.<sup>1</sup>, MENDES L.M.<sup>1</sup>, FRANCISCO F.R.<sup>1</sup>, TERADA M.<sup>1</sup>, DEFAVARI R.<sup>1</sup>

<sup>1</sup>Centro Nacional de Pesquisa em Energia e Materiais (CNPEM)

#### 1. Introdução

Componentes do sistema de injeção pulsada presentes em aceleradores de partículas, requerem modelos específicos de câmaras de vácuo para aplicação de campos eletromagnéticos específicos, como câmaras cerâmicas com *coating* metálico no interior do componente. Um dos processos utilizados para a deposição é o *magnetron sputtering*. Para uma performance do componente que atenda aos requisitos de projeto, a deposição do *coating* metálico requer uma distribuição e espessuras bem definidas, para não causar alteração no campo elétricomagnético criado, e a formação de corrente parasita no dispositivo, que ocasionar perturbação no feixe do acelerador. Portanto, é fundamental realizar simulações para definir a geometria e posição do cátodo, visando atender os requisitos de distribuição da espessura do *coating* metálico na seção transversal ao longo do perímetro interno da câmara de vácuo.

#### 2. Experimental

Para o entendimento da distribuição da deposição do *coating* metálico, foi utilizado o software de simulação desenvolvido pelos pesquisadores da Organização Europeia para a Investigação Nuclear (CERN) denominada MolFlow+ [1], que trabalha com o método de Monte Carlo. Para isso, foram simuladas três condições de cátodos em uma câmara com perfil transversal interno oblongo de 40x16mm com 500mm de comprimento, sendo: condição I - Ø2,00mm centralizado na seção transversal da câmara; II - oblongo 2,6x1,4mm posicionado na vertical na seção transversal da câmara e III oblongo 2,6x1,4mm posicionado na horizontal na seção transversal da câmara. Para comprobação das simulações foi utilizado um equipamento de *magnetron sputtering* para deposição no interior da câmara de vácuo cerâmica via RF (radiofrequência). O material do cátodo utilizado foi o material titânio GR2 (UNS R50400), e as análises da morfologia das deposições foram feitas através de microscopia eletrônica de varredura (MEV).

#### 3. Resultados e Discussões

As simulações realizadas no Molflow+ utilizando as diferentes geometrias de cátodos, representadas pela Fig. 1, proporcionaram diferentes comportamentos de distribuição da deposição ao longo do perímetro da câmara de vácuo, conforme o gráfico representado pela Fig.2. Desta forma, foi possível identificar que a simulação no cátodo do modelo III, apresentou uma distribuição mais homogênea de deposição em relação aos modelos I e II. Para validações das simulações, foram realizadas análises dimensionais da espessura de deposição nas regiões de maior e menor espessura, comparando com os resultados obtidos no estudo teórico. As simulações se mostraram ferramentas importantes para o desenvolvimento de *coating* com características especificas para aplicações especiais.

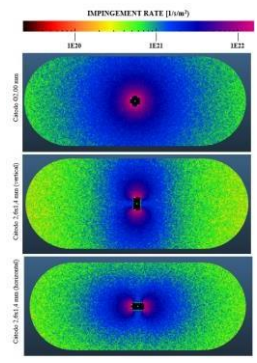


**Fig. 1.** Simulação realizada no Molflow+, utilizando diferentes geométricas de cátodos.

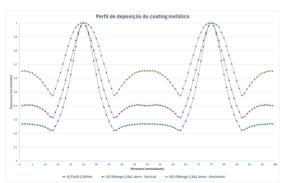


Fig. 2. Perfil de deposição ao longo do perímetro normalizado da câmara de vácuo.

#### 4. Referência

[1]- R. Kersevan, M.Ady In: 10th Int. Particle Accelerator Conf., Melbourne, Australia -doi:10.18429/JACoW-IPAC2019-TUPMP037 (2019)

<sup>\*</sup>Corresponding author: daniel.kakizaki@cnpem.br



## SURFACE CHARACTERIZATION OF Ti-Nb-Zr COATINGS DEPOSITED ON Si (100) WAFER SUBSTRATE

Ana L. C. Garcia<sup>1</sup>, Angelo L. Gobbi<sup>2</sup>, Valmor R. Mastelaro<sup>3</sup>, Pedro A. P. Nascente<sup>1\*</sup>, 
<sup>1</sup>Federal University of Sao Carlos, Department of Materials Engineering, 13565-905, Sao Carlos, SP, 
Brazil.

<sup>2</sup>Brazilian Center for Research in Energy and Materials, Brazilian Nanotechnology National Laboratory, 13083-970, Campinas, SP, Brazil.

<sup>1</sup>University of Sao Paulo, Sao Carlos Institute of Physics, 13560-590, Sao Carlos, SP, Brazil.

#### 1. Introduction

The medical grade stainless steel (SS) type AISI 316L (ASTM F138-10) is commonly used as prosthetic materials; however, the cytotoxicity caused by the release of Cr and Ni ions is harmful to health. In comparison, Ti-based alloys having bcc structure ( $\beta$  phase) exhibits lower elastic moduli, adequate mechanical properties for load-bearing implant applications, excellent biocompatibility, low density, and wear and corrosion resistance in biological environments. Among the  $\beta$ -Ti alloys, the Ti-Nb-Zr ternary system has been one of the most studied metallic biomedical materials. The addition of Nb and Zr to Ti favors the stabilization of the  $\beta$  phase and offer excellent biocompatibility [1]. A main disadvantage of bulk Ti-Nb-Zr alloys is its high cost compared to SS. An economical option would be to coat an SS implant with a Ti-Nb-Zr thin film with adequate composition to improve the material biocompatibility [2]. However, the ideal Ti-Nb-Zr composition is uncertain. Combinatorial strategies allow for the production of many alloys simultaneously, and magnetron sputtering has shown to be an adequate technique to deposit alloy coatings [2]. The objective of this study is to establish the optimal composition of the Ti-Nb-Zr system.

#### 2. Experimental

The substrate was a Si (100) wafer having a diameter of 4 inches and a thickness of 0.5 mm. Ti, Nb, and Zr disks having a diameter of 2 inches and a thickness of 6 mm, with a purity of 99.99%, were used as targets, which were positioned 40 cm below the substrate in a triangular geometry to yield a composition gradient over the wafer area. The deposition was performed using an AJA Orion 8 Phase IIJ magnetron sputtering equipment. Characterization was carried out by EDS, XRD, AFM, and XPS.

#### 3. Results and Discussions

Elemental composition obtained from EDS analysis gave the following compositions (in at. %):  $Ti_{49}Nb_{13}Zr_{38}$  (for the sample near the Ti target),  $Ti_{22}Nb_{58}Zr_{20}$  (for the sample near the Nb target),  $Ti_{43}Nb_{42}Zr_{15}$  (for the sample in the wafer center),  $Ti_{67}Nb_{21}Zr_{12}$  (for the sample near the Zr target), and  $Ti_{36}Nb_{59}Zr_{5}$  (for the sample opposite to the Ti target). XRD structural analysis indicated mainly the presence of the  $\beta$  phase, with a minor contribution of the  $\alpha$  phase that has hcp structure.

The AFM analysis revealed the following grain sizes: 72.3, 51.7, 83.1, 74.5, and 84.2 nm for the Ti<sub>49</sub>Nb<sub>13</sub>Zr<sub>38</sub>, Ti<sub>22</sub>Nb<sub>58</sub>Zr<sub>20</sub>, Ti<sub>43</sub>Nb<sub>42</sub>Zr<sub>15</sub>, Ti<sub>67</sub>Nb<sub>21</sub>Zr<sub>12</sub>, and Ti<sub>36</sub>Nb<sub>59</sub>Zr<sub>5</sub> coatings, respectively. For the same sequence, the roughness values are: 2.0, 1.2, 0.6, 1.3, 0.9 nm; for comparison, the roughness of the Si (100) substrate is 0.1 nm.

XPS surface analysis showed the formation of oxidized layers that have a predominance of TiO<sub>2</sub>, Nb<sub>2</sub>O<sub>5</sub>, and ZrO<sub>2</sub> phases. Comparison between EDS and XPs results indicated a surface enrichment of both Ti and Zr concomitant with a surface depletion of Nb on the oxide surface layer for all five coatings. These nanostructured and oxidized surfaces provide high corrosion protection and are thus advantageous for implant materials.

#### 4. Reference

- [1] E.D. Gonzalez et al., Mater. Today Comm. **32**, 104069 (2022).
- [2] E.D. Gonzalez et al., Thin Solid Films **721**, 138565 (2021).

#### Acknowledgments

This work was supported by FAPESP (process 2017/25983-8), CNPq (process 302450/2017-3), CAPES (Finance Code 001), and CNPEM/LNLS.

<sup>\*</sup>Corresponding author: nascente@ufscar.br



### MAGNETIC PROPERTIES OF AISI 1006 STEEL COATED WITH CO:TI DEPOSITED BY TRIODE MAGNETRON SPUTTERING

Salézio Francisco Momm<sup>1,3</sup> Joel Stryhalski<sup>1</sup>, Alexandre Werner Arins<sup>1</sup>, Jaison Vieira da Maia<sup>1</sup>, Andre Avelino Pasa<sup>2</sup>, Cristiani Campos Plá Cid<sup>2</sup>, Abel André C. Recco<sup>3</sup>, Carla Dalmolin<sup>4</sup>, and Luis César Fontana<sup>3</sup>

<sup>1</sup>Departament of Physics, Instituto Federal de Santa Catarina, Santa Catarina, 88103-902, Brasil

<sup>2</sup>Departament of Physics, Universidade Federal de Santa Catarina, Florianópolis, SC, 88040-900, Brasil

<sup>3</sup>Department of Physics, Universidade do Estado de Santa Catarina, Joinville, 89219-710, Brasil

<sup>4</sup>Department of Chemistry, Universidade do Estado de Santa Catarina, Joinville, 89219-710, Brasil

#### 1. Introduction

AISI 1006 electrical steel is commonly used in the manufacture of electric motors, and enhancing its electrical and magnetic properties [1] is of fundamental interest to the industry. On the one hand, titanium provides corrosion protection and has notable electrical properties [2]. On the other hand, cobalt offers both good electrical and magnetic properties [3] and the combination of these two elements holds promise for improving the substrate.

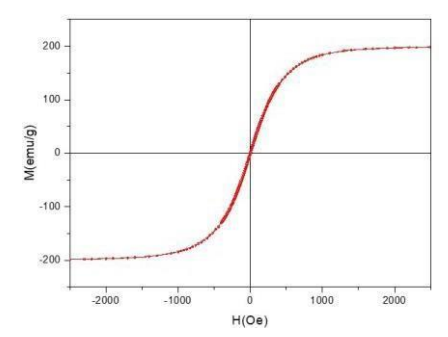
#### 2. Experimental

The metal film was deposited on the AISI 1006 substrate using triode magnetron sputtering. EDS analysis and SEM images were performed with Neo Scope equipment, model JCM-7000. Magnetic analysis was carried out using VSM (Microsense, EZ9).

#### 3. Results and Discussions

The metallic Ti-Co film was obtained after 20 minutes of deposition and had a thickness of 360 nm. EDS analysis revealed an relative percentage of 91% Ti and 9% Co. SEM images showed a homogeneous film that preserved the original irregularities of the electrical steel surface. A sample coated with metallic film was analyzed using the VSM, weighed 11.7 mg while the reference AISI 1006 sample weighed 21.1 mg. Comparing the sample with Ti-Co film and the electrical steel without film, we observed a decrease in the saturation magnetic field of approximately 17.2%, an increase of 188.9% in remanent magnetization, an increase of 38.1% in the coercive field and reduction in the magnetic hysteresis loop area and power loss of 32.4%. Additionally, there was an increase in the mass magnetic susceptibility of around 13.9%.

In conclusion, from a magnetic perspective, the metal film deposited on the electrical steel led to a reduction in hysteresis loss and power per unit mass, as well as an increase in the sample's magnetic susceptibility. Both characteristics are beneficial for improving the magnetic properties of materials used in electromagnetic machines such as motors and transformers.



200 - 100 - 1000 2000 H(Oe)

Figure 1. Magnetic hysteresis of the metal film.

Figure 2.
Magnetic hysteresis of AISI 1006 steel.

#### 4. References

[1]- LANDGRAF, F. J. (Julho de 2012). Nonoriented Electrical Steels. Jom, 64, pp. 764-771.

[2]-BRAZ, D. C., BARBOSA, J. C., NUNES FILHO, A., ROCHA, R. C., SILVA, D. R., & ALVES JUNIOR, C. (2012). Influência das espécies do plasma na modificação das propriedades superficiais do titânio tratado por plasma de N2 - Ar - O2. *Matéria*, pp. 1035-1044.

[3]- SARGENTELLI, V., & FERREIRA, A. A. (27 de Dezembro de 2010). Nanopartículas magnéticas: o cobalto. Eclética Química, 35, pp. 153-163.

#### Acknowledgments

This research was supported by FAPESC/CNPq – PRONEM 2020TR730 and FAPESC-PAP 2023TR000258

<sup>\*</sup>Corresponding author: <a href="mailto:salezio.momm@ifsc.edu.br">salezio.momm@ifsc.edu.br</a>



## TRIBOLOGICAL PERFORMANCE OF GD-DLC AND EU-DLC COATINGS IMPROVED BY IONIC LIQUID ADDITIVES IN SYNTHETIC OILS

Marcos Alves Fontes<sup>1\*</sup>, Omiya Takeru<sup>2</sup>, Fabio Emanuel de Souza Ferreira<sup>2</sup>, Albano Cavaleiro<sup>2</sup>

<sup>1</sup>Instituto Federal de Educação, Ciência e Tecnologia de São Paulo, campus Sertãozinho.

<sup>2</sup>Universidade de Coimbra, CEMMPRE (Centre for Mechanical Engineering Materials and Processes, Department of Mechanical Engineering).

#### 1. Introduction

Diamond-like carbon (DLC) coatings have been employed due to their excellent tribological performance and mechanical properties, including high hardness, high wear resistance, and a low coefficient of friction (CoF) [1]. To ensure optimal performance under aggressive conditions, effective interactions between the coatings and lubricants are essential for sustained low wear and friction over the long term. However, DLC coatings are considered "inert" due to their low surface energy [2]. This means they do not interact with various oil additives or attract the polar groups of the additives and oil, which are the typical mechanisms for lubricating steels and other metals [3]. In recent years, ionic liquids (ILs) have attracted significant interest among various lubricant additives, due to their unique properties, including high thermal stability, low flammability and low vapor pressure [4]. In this study, it was investigated the mechanical and tribological properties of gadolinium and europium-doped diamond-like carbon (Gd-DLC and Eu-DLC) coatings, comparing samples lubricated with ionic liquids (ILs) and base oil (BO). The purpose was to demonstrate the effectiveness of the doping process on the lubrication performance of the ILs.

#### 2. Experimental

DLC films were deposited using High-Power Impulse Magnetron Sputtering (HiPIMS) technology. Two different atomic concentrations of gadolinium (1.7% and 2.3% at. concentration) and europium (1.7% and 2.4% at. concentration) were incorporated into the DLC coatings. It was used the PAO 8 as base lubricant, and PAO 8 with 1 wt% of Trihexyltetradecylphosphonium bis(2-ethylhexyl) phosphate [P<sub>66614</sub>][DEHP] as ionic liquid. Tribological experiments were performed using a ball-on-disk tribometer in reciprocating motion. The load applied was 3 N, and the frequency range of 0.2-to-5.0 Hz over a 15 mm stroke length at 80 °C. Hardness and reduced Young's modulus were measured via nano-indentation.

#### 3. Results and Discussions

Figures 1 and 2 show the CoF as a function of sliding speed for Gd-DLC and Eu-DLC coatings, respectively, lubricated with BO or IL. For both coatings, incorporating IL into the BO reduces the CoF under boundary lubrication conditions.

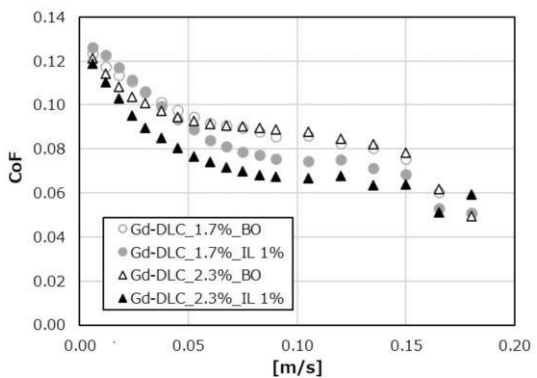


**Fig. 1.** CoF as a function of sliding speed for Gd-DLC coatings lubricated with BO or IL.

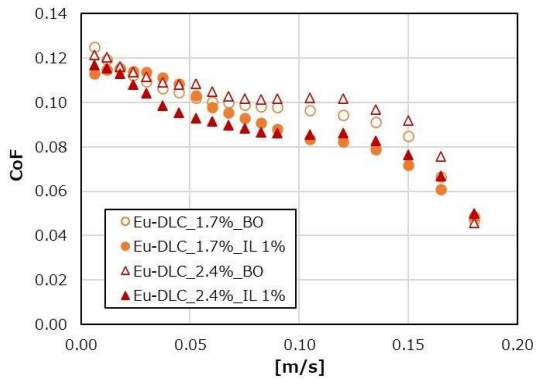


**Fig. 2.** CoF as a function of sliding speed for Eu-DLC coatings lubricated with BO or IL.

A higher atomic concentration of Gd and Eu improves the friction reduction effect. This effect, particularly for Gd-DLC coatings, was observed at velocities above 0.05 m/s, suggesting an interaction between the IL and the coating.

#### 4. References

- [1] P. S. Martins et al., Wear 498–499, 204326 (2022).
- [2] J. C. Sanchez-Lopez et al., Surf. Coat. Technol. 163, 444–450 (2003).
- [3] I. Velkavrh, M. Kalin, J. Vizintin, Stroj Vestn-J. Mech. E 54, 189–206 (2008).
- [4] Y. Zhou, J. Qu, ACS Appl. Mater. Interfaces 9, 3209–3222 (2017).

<sup>\*</sup>Corresponding author: marcos.fontes@ifsp.edu.br



## TRIBOLOGICAL AND CORROSION PROPERTIES OF TIALN AND ALTIN COATINGS DEPOSITED ON TITANIUM ALLOY

Thiago de Lima Gontarski<sup>1</sup>\*, Luciane Sopchenski Santos<sup>2</sup>, Luis Henrique Gaio<sup>1</sup>, Bruno Leandro Pereira<sup>1</sup>, Luis Cesar Fontana<sup>3</sup>, Ricardo Diego Torres<sup>1</sup> and Paulo Soares<sup>1</sup>

<sup>1</sup>Department of Mechanical Engineering, Pontifical Catholic University of Paraná, Brazil <sup>2</sup>Vrije Universiteit Brussel, VUB, Belgium

Laboratory of Plasma, Films and Surfaces Center for Technological Science, UDESC, Brazil

#### 1. Introduction

Titanium alloy Ti6Al4V is widely used in the aerospace, biomedical, and automotive sectors due to its superior strength-to-weight ratio, outstanding corrosion resistance, and excellent biocompatibility [1]. However, when the alloy is exposed to aggressive environments, improved corrosion and wear resistance become essential for reliable performance [2]. So, the deposition of thin films plays a crucial role in enhancing these properties. Therefore, the objective of this study is to analyze the effect of the Ti/Al ratio in Ti-Al-N ternary coatings on their tribological properties and corrosion resistance.

#### 2. Experimental

Samples of FUTURA Nano® (TiAlN) and LATUMA® (AlTiN) coatings were deposited on Ti6Al4V titanium alloy using cathodic arc physical vapor deposition (CAE/PVD) by Oerlikon Balzers Revestimentos Metálicos LTDA. The morphology and chemical composition of both the substrate and the thin films were analyzed using Scanning Electron Microscopy (SEM) and Energy Dispersive Spectroscopy (EDS). X-ray Diffraction (XRD) was used to identify the crystalline phases of the materials. The friction and wear properties of the samples were assessed through dry linear reciprocating sliding tests in a ball-on-plate configuration, employing an Anton-Paar universal tribometer. In the potentiodynamic polarization test, the Biologic SP-300 potentiostat was utilized to measure the electrochemical behavior. The sample was immersed in 70 mL of a 3.5% NaCl solution at room temperature. The potential was scanned from -500 to +500 mV relative to the open circuit potential (OCP) at a scan rate of 1 mV/s. A platinum counter electrode and an Ag/AgCl(sat) reference electrode were employed to ensure accurate measurements.

#### 3. Partial Results

The potentiodynamic polarization curves of the substrate, Latuma, and Futura coatings in a 3.5% NaCl solution are illustrated in Figure 1, and their data are described in Table 1. The Ecorr of the substrate is -282.4 mV, and Icorr is 0.317 μA/cm2. The Ecorr value of the Latuma coating (AlTiN) shows a shift towards the positive side (more noble). Despite the Futura coating (TiAlN) demonstrating the lowest corrosion potential, it exhibited the highest Icorr value. The term Icorr is frequently used as a standard measure to assess the kinetics of a corrosion process. Therefore, it can be inferred that all the coatings can effectively act as protective barriers, isolating the substrate from the corrosive electrolyte.

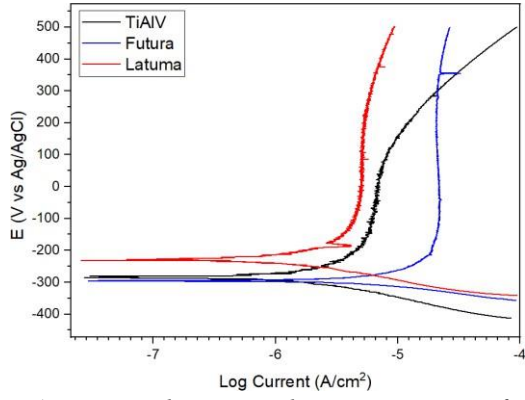


**Fig. 1.** Potentiodynamic polarization curves of the bare TiAlV substrate, Futura, and Latuma coatings.

Sample	Ecorr (mV vs Ag/AgCl)	Icorr (μΑ/cm²)
TiAlV	-282.4	0.317
Latuma	-223.2	0.501
Futura	-294.2	0.750

**Tab. 1.** Potentiodynamic polarization data of the TiAlV substrate, Futura, and Latuma coatings.

#### 4. References

- [1]- C. Leyens, and M. Peters, Wiley-vch, (2006).
- [2]- ASM International Handbook Committee. ASM Handbook: Volume 13 Corrosion (1990).

#### Acknowledgments

The authors would like to acknowledge the CNPq/CT-AERO (Grant 405747/2022-5) and CAPES/PROEX. \*Corresponding author: Thiago.gontarski@pucpr.edu.br



## CHARACTERIZATION OF THE CORROSION RATE OF AA2024 ALUMINUM ALLOY TREATED BY PLASMA ELECTROLYTIC OXIDATION WITH DIFFERENT DUTY CYCLES

Rogério P. Mota<sup>1\*</sup>, Emanuelle R.R. Silva<sup>1</sup>, Luís F.B. Marques<sup>1</sup>, Miguel O.L. Vieira<sup>1,2</sup>, Luís R.O. Hein<sup>1</sup>, Francisco J.G. Silva<sup>3</sup>, Rita C.M. Sales-Contini<sup>3,4</sup>, Rafael R. Lucas<sup>1,3</sup>

<sup>1</sup>São Paulo State University (UNESP), School of Engineering and Sciences, Guaratinguetá/SP, Brazil

<sup>2</sup>University of São Paulo (USP), School of Engineering, Lorena/SP, Brazil

<sup>3</sup>CIDEM, ISEP Polytechnic of Porto, Porto, Portugal.

<sup>4</sup>Technological College of São José dos Campos (FATEC), São José dos Campos/SP, Brazil

#### 1. Introduction

The Plasma Electrolytic Oxidation (PEO) process is recognized as a sustainable methodology that involves the application of elevated voltages (ranging from 100 to 600 volts) to establish a defensive oxide coating on various metal surfaces. Implemented either singularly or through a concise series of actions, PEO diminishes the duration of processing while amplifying the ability to withstand corrosion. Particularly for the aluminum alloy 2024, composed of copper and other components that undermine its resistance to corrosion owing to intermetallic particles, PEO offers a proficient shield by curtailing the occurrence of localized corrosion [1, 2].

#### 2. Experimental

In this study, the AA2024-O alloy was treated with a Na<sub>2</sub>SiO<sub>3</sub> solution (15 g/L) at different duty cycles (40%, 55%, 70%, 90%), using a constant current of 60 mA/cm<sup>2</sup> for 600 seconds. Corrosion resistance was evaluated according to ASTM G31 by immersing the treated and control samples in a 3.5% NaCl solution. After 30 days, the samples were weighed to measure mass loss.

#### 3. Results and Discussions

The significant improvement in the corrosion resistance of the AA2024 alloy, reducing the corrosion rate from 0.099 mm/year to 0.002 mm/year, representing an approximately 98% enhancement, can be attributed to the inert nature of the oxide coating  $(Al_2O_3)$  formed during the treatment process. This oxide coating acts as a barrier layer, preventing direct contact between the saline environment and the substrate pores, and inhibiting interaction with the Al-Cu intermetallic particles.

	AA2024-O	40%	55%	70%	90%
Mass loss	- 27.8 mg	- 0.5 mg	- 0.8 mg	- 0.7 mg	- 0.7 mg
Corrosion Rate	0.099 mm/y	0.002  mm/y	0.004  mm/y	0.003  mm/y	0.003  mm/y

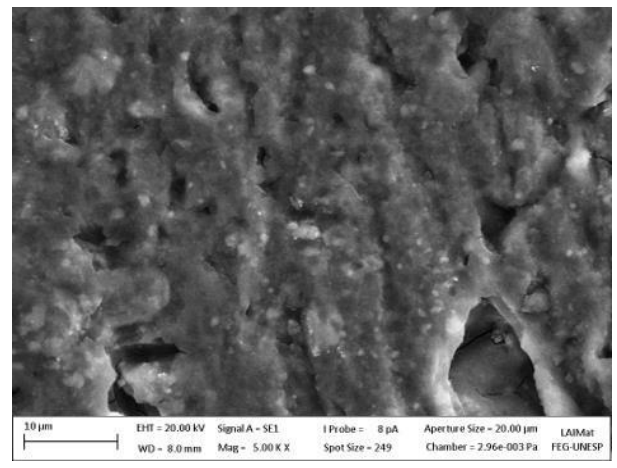


Fig. 1. Untreated AA2024 alloy sample

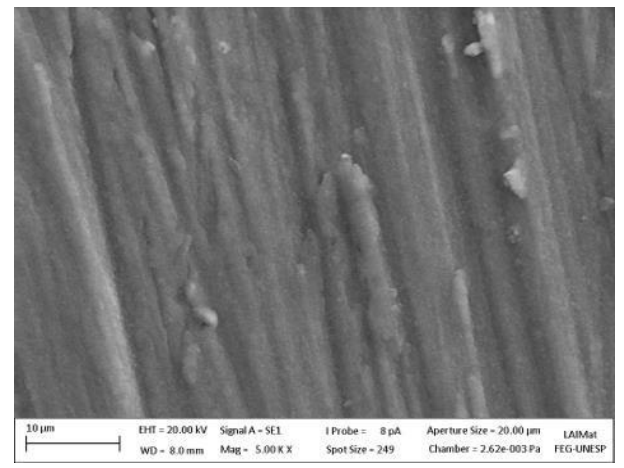


Fig. 2. AA2024 alloy sample with PEO treatment

#### 4. References

- [1]- K. Kamarska. Proc. Bulg. Acad. Sci., 75, 422-427, (2022).
- [2]- R. Lucas, R. Sales-Contini, L. Marques, et al. AIMS Mater. Sci., 11, 585-601, (2024)

#### Acknowledgments

The authors would like to thank the CAPES agency for providing financial support in the form of a doctoral scholarship (88881.933644/2024-1)

<sup>\*</sup>Corresponding author: rogerio.mota@unesp.br



#### PREPARATION AND CHARACTERIZATION OF ACRYLONITRILE-BUTADIENE-STYRENE AND STAINLESS STEEL HYBRID

Abel André Cândido Recco <sup>1</sup>\*, Daniela Becker <sup>1</sup>, and Marcio Luiz Moretti <sup>1</sup> Centro de Ciências Tecnológicas, Universidade do Estado de Santa Catarina, Joinville, SC, Brasil

#### 1. Introduction

Chen et al. [1] and Zou et al. [2] highlight that polymer-metal hybrids combine the physicochemical properties of both materials, enhancing their industrial applications. In this context, the study aimed to prepare and characterize acrylonitrile-butadiene-styrene (ABS) and stainless steel (SS) hybrid using direct current magnetron sputtering (DC-MS). The thermal degradation of ABS and ABS-SS, as well as the adhesion of ABS-SS to the film and substrate, were analyzed. The results showed no significant degradation of ABS. Additionally, the adhesion between the metal and polymer was deemed acceptable (B4 index). These findings suggest that the DC-MS technique and process parameters are well-suited for producing these hybrid materials.

#### 2. Experimental

The deposition of SS films onto the ABS substrate was carried out using DC-MS. The process conditions were as follows: power of 100 W at  $(425 \pm 5) \text{ V}$  and  $(0.24 \pm 0.01) \text{ A}$ , working pressure of  $(0.50 \pm 0.01) \text{ Pa}$ , argon flow rate of  $(5.0 \pm 0.1) \text{ sccm}$ , deposition rate of  $(10.0 \pm 0.5) \text{ nm/min}$ , and deposition temperature of  $(28 \pm 5) ^{\circ}\text{C}$ . Thermal degradation of ABS and ABS-SS was analyzed by thermogravimetry (TGA) using a Netzsch STA 449C, which was programmed to heat the samples from  $(25 \text{ to } 600) ^{\circ}\text{C}$  at a rate of  $10 ^{\circ}\text{C/min}$  in a nitrogen atmosphere with a flow rate of  $20 ^{\circ}\text{ml/min}$ . Film-substrate adhesion was qualitatively evaluated using the cross-cut method B according to ASTM D3359.

#### 3. Results and Discussions

Figure 1 shows that both ABS and ABS-SS experienced only one significant mass loss event. It is noteworthy that there was no significant thermal degradation of the ABS during the SS film deposition process. Additionally, Figure 2 demonstrates that the hybrid sample exhibited no significant film delamination and received a B4 rating, indicating that the film-substrate adhesion was acceptable. These results confirm that the deposition technique and parameters used are suitable for producing the ABS-SS hybrid, consistent with the studies by Moretti, Recco, and Becker [3].

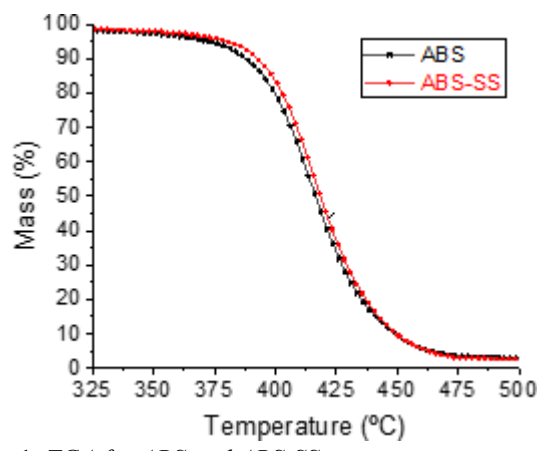
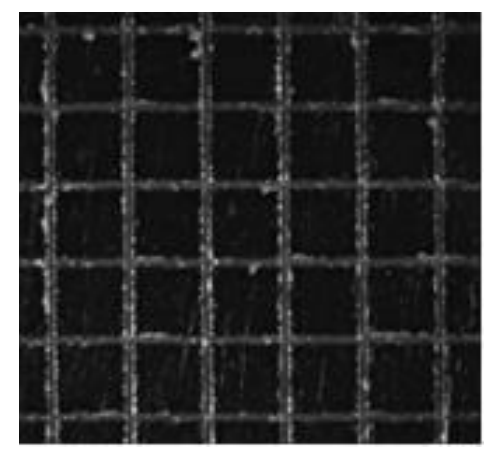


Fig. 1. TGA for ABS and ABS-SS in mass percentage.



**Fig. 2.** Surface of the ABS-SS revealed via optical stereoscopy with image enlarged in a 7:1 ratio.

#### 4. References

- [1] Chen J. et al, Appl. Surf. Sci., **489**, 392-402 (2019).
- [2] Zou, X. et al., Met., 11, 567, (2021).
- [3] Moretti, M. L., Recco, A. A. C., and Becker, D., J. Appl. Polym. Sci., 141, e54888, (2023).

#### Acknowledgments

This research was supported by FAPESC-PAP 2023TR000258. Part of the funding for this study came from the UNIEDU/FUMDES graduate program. The authors are thankful for the Multi-User and Plasma Lab Facility infrastructure of Udesc.

<sup>\*</sup>Corresponding author: abel.recco@udesc.br



## EFFECTIVENESS OF THE NATIVE OXIDE REMOVAL PROCEDURE FROM SILICON WAFERS

Josieli Honorato, Luis Guilherme Silva Rosa, Julio César Sagás Laboratory of Plasmas, Films and Surfaces, Universidade do Estado de Santa Catarina, Joinville-SC, Brazil

#### 1. Introduction

Monocrystalline silicon wafers are used not only in microelectronics but also as a standard substrate for fundamental studies about thin film deposition. Depending on the properties to be analyzed, it is necessary to remove the native oxide from the silicon surface, i.e. the wafer must be free of chemical contaminants and particles while maintaining the integrity of the substrate [1]. To perform this cleaning, one of the most commonly used processes is the RCA process, which involves the consecutive application of two hot solutions containing pure and volatile reagents. In this work, we evaluate the effectiveness of the RCA process through measurements of surface composition using a X-ray photoelectron spectrometer (XPS).

#### 2. Experimental

The silicon samples cut from a Si (100) wafer, measuring 1 cm x 1 cm, were initially placed in an ultrasonic bath with distilled water for 10 minutes. Subsequently, the samples were immersed in a "piranha" solution, consisting in 2:1 of sulfuric acid (H<sub>2</sub>SO<sub>4</sub>) and hydrogen peroxide (H<sub>2</sub>O<sub>2</sub>), for 10 minutes to remove organic contaminants. After, the samples underwent a second 10-minute ultrasonic bath and were then thoroughly rinsed with deionized water to ensure complete removal of the viscous piranha solution. Finally, to eliminate the thin native silicon oxide layer, the samples were submerged in a diluted HF solution (1:10) at room temperature. The immersion process was repeated ten times for 30 seconds each, and the visual change of the surface from hydrophilic to hydrophobic. Then, one as-received sample and one cleaned sample were analyzed in a Thermo Scientific K-Alpha XPS using Al Kα (1486.6 eV) as radiation source. The spot was 400 μm and a flood gun was used to neutralize induced surface charges. For the curve fitting, a Gaussian (70%) and Lorentzian (30%) sum function was used, and we constrained the spin-orbit split to 0.6 eV for Si-Si bond.

#### 3. Results and Discussions

Figure 1 shows the as-received sample, while Figure 2 displays the sample that underwent the cleaning process. A significant reduction in the atomic percentage of oxygen is observed, decreasing from 24.7% to 2.6% after the application of the cleaning process. A strong reduction in the peak corresponding to SiO<sub>2</sub> is also observed, but the oxide is not eliminated. However, it must be pointed out that between the cleaning process and the measurement, the samples remained exposed to air, which can cause minor surface oxidation.

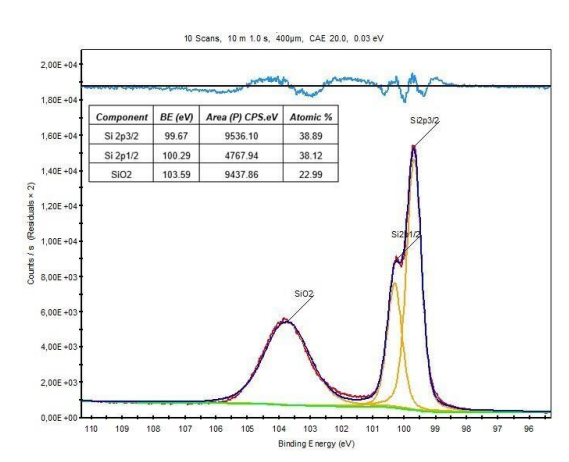


**Fig. 1.** Si 2p fitting in XPS for the sample without cleaning process.

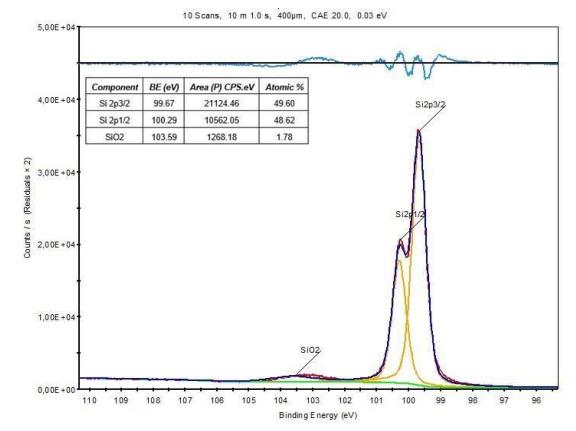


**Fig. 2.** Si 2p fitting in XPS for the sample with RCA cleaning process.

#### 4. References

[1] Kern, W.; Reinhardt, K. A. Handbook of Silicon Wafer Cleaning Technology. Third Edition, William Andrew Inc, 2018.

#### Acknowledgments

The authors are thankful for the Multi-User Facility infrastructure from Santa Catarina State University's Technological Sciences Center, to FAPESC (grant 2024TR000258), and CNPq (grant 304053/2021-0).

<sup>\*</sup>Corresponding author: julio.sagas@udesc.br



#### GENERATION OF POLYMERIC LAYERS ON 1006 STEEL PLATES THROUGH ACETYLENE PLASMA POLYMERIZATION

Thassiana Camargo\*, Abel Andre Candido Recco, Carla Dalmolin and Luis Cesar Fontana Universidade do Estado de Santa Catarina – UDESC

#### 1. Introduction

Plasma polymerized  $C_xH_y$  thin films, deposited on metallic substrates, is discussed in this paper. The plasma polymerization method provided an effective, dry, and simpler process, which can result in dense thin films with the thickness of a few hundred nanometers, but with undefined chemical structure and varying compositions. Furthermore, this process brings some properties and improvements to the metallic sample, such as greater durability, corrosion resistance, shrinkage, etc. [1] Formation of acetylene by plasma produced numerous radicals in its deposits, and an energy-related dose factor was proposed to compare different plasma conditions and search for methodologies to produce regular films with good adhesion to the substrate. [2]

#### 2. Experimental

The films were prepared through C<sub>2</sub>H<sub>2</sub> plasma generated by a 100 kHz pulsed power supply. The substrate was low carbon AISI 1006 steel. The depositions were carried out through plasma of gas Ar/C<sub>2</sub>H<sub>2</sub> low pressure plasma, the deposition time was between 1 min and 15 min, and the substrate temperature was kept at 150°C. The substrates surface were previously functionalized through ion bombardment in Ar/N<sub>2</sub> plasma, just to improve the adhesion of the polymeric films. The film thickness and adhesion can be correlated with the plasma parameters and deposition time. The physico-chemical properties of the thin films were evaluated by field-emission scanning electron microscope (FE-SEM), water contact angle (WCA), Fourier Transform Infrared Spectroscopy (FTIR), and corrosion resistance measured by potentiodynamic polarization tests.

#### 3. Results and Discussions

Optical microscopy images (Figure 1) show that the films are homogeneous. However, there may be peeling of the films due to residual stresses generated during deposition (Figure 2).



**Fig. 1.** Optical microscopy image (1000x) of the polymeric film formed on AISI 1006 steel surface, showing the homogeneous surface.

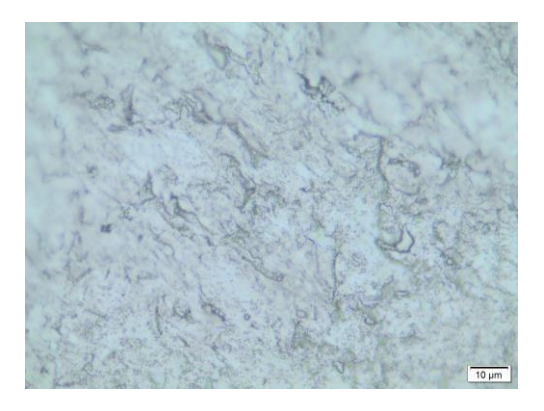


**Fig. 2.** Optical microscopy image (1000x) of the polymeric film formed on AISI 1006 steel surface, showing a region with peeling.

FT-IR analyses were compared with data from the NIST library for polyethylene and ethylene, and the films formed showed some bands typical of the polymer, but also bands indicating the formation of oligomers or intermediated structures.

#### 4. References

[1]- J. Friedrich, Plasma Process. Polym., **8**, 783–802, (2011).

[2]- H. Yasuda, T. Hirotsu, J. Polym. Sci. Polym. Chem. Ed. 16, 743, (1973)

#### Acknowledgments

## CONSTRUCTION AND VALIDATION OF A TEMPERATURE GRADIENT SAMPLE HOLDER SYSTEM FOR PLASMA NITRIDING

Julio César de Oliveira Fermino<sup>1\*</sup>, Laurita Istéfani da S. Teles<sup>1</sup>, Luis Cesar Fontana<sup>1</sup>, Abél A. Cândido Recco<sup>1</sup> *Universidade do Estado de Santa Catarina, Laboratório de Plasmas, Filmes e Superficies, Joinville-SC* 

#### 1. Introduction

Plasma nitriding is a thermo-chemical treatment applied for surface modification, allowing for improvements in both the mechanical characteristics and microstructural properties of the formed layer. The compounds formed and the thickness of the added layer are strongly influenced by the process temperature [1]. In this work, a sample holder with a temperature gradient was developed. It is a configurable heat exchanger, enabling the evaluation of the effect of nitriding the sample at varying temperatures in a single test, making the treatment faster and more accurate regarding the other parameters used during the nitriding process.

#### 2. Experimental

The experiment was conducted in a cylindrical nitriding chamber where the sample holder was adapted. The temperature gradient sample holder (Figure 1-a) can be thermodynamically simplified as a heat exchanger composed of two heat sources at different temperatures connected by a sample that, through thermal conduction, allows the study of nitriding over a temperature range between 300°C and 700°C (Figure 1-b). To ensure that the O-rings are not exposed to high temperature beyond their tolerance, a cooling system consisting of a fluid circuit near the O-rings was implemented. Heating is achieved using a Xenon lamps HLX64655 with adjustable power from 0 to 250W (0-24V). To meet the requirements of electrical insulation and good thermal conductivity, mica was used between the heating module and the sample's mounting bushing. Ceramic centering bushings were employed to position and electrically insulate the sample.

#### 3. Results and Discussions

According to studies, different configurations of the compound layer and diffusion zone are expected in the isochronal series, as nitrogen penetration is sensitive to the nitriding temperature [2]. The implementation of the temperature gradient sample holder makes it possible to treat the sample at various temperatures while keeping other parameters unchanged: pressure, duration, and mixture composition. A sample of SAE 1045 steel will be studied, and after treatment, characterizations will be performed to identify the present phases and reveal the formation of layers, as well as the quantity, size, and shape of the nitride precipitates in a single test.

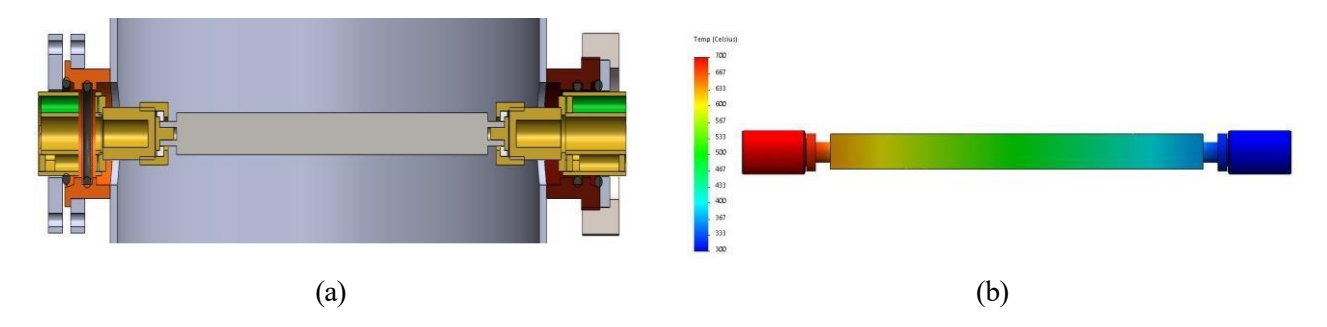


Figure 1: a) Sample holder with temperature gradient in the nitriding reactor; b) Temperature gradient to which the sample will be exposed.

#### 4. References

- [1] L.F. Zagonel, C.A. Figueroa, R. Droppa, F. Alvarez, Influence of the process temperature on the steel microstructure and hardening in pulsed plasma nitriding, Surface and Coatings Technology, Volume 201, Issues 1–2, 2006.
- [2] Pinedo, Carlos & Monteiro, Waldemar. (2011). Tratamento térmico e de nitretação sob plasma do aço inoxidável martensítico AISI 420. Tecnologia em Metalurgia Materiais e Mineração. 8. 86-90.

#### Acknowledgments

The authors thank FAPESC (PAP-UDESC 2023 TR1363) for financial support.

<sup>\*</sup>Corresponding author: julio.fermino@udesc.br



## ATOMIC LAYER DEPOSITED TITANIUM DIOXIDE ON CARBON FIBER FABRICS: MATERIAL PROPERTIES AND THERMAL / OXIDATIVE RESISTANCE ASSAYS

T. M. Vieira<sup>1\*</sup>, V. M. Dias<sup>1</sup>, F. S. Miranda<sup>1</sup>, W. Chiappim<sup>2</sup>, A. S. da Silva Sobrinho<sup>1</sup>, G. Petraconi<sup>1</sup>, H. S. Maciel<sup>1</sup>, R. S. Pessoa<sup>1</sup>

<sup>1</sup>Laboratório de Plasmas e Processos, Instituto Tecnológico de Aeronáutica (ITA), São José dos Campos, SP, 12228-900, Brazil.

<sup>2</sup>Faculty of Engineering in Guaratinguetá, Universidade Estadual Paulista (UNESP), Guaratiguetá, SP, 12516-410, Brazil.

#### 1. Introduction

Carbon fiber fabrics (CFFs) are widely used in industries due to their high tensile strength, low weight, and chemical resistance. However, their low oxidation resistance limits their application in high-temperature environments [1]. Atomic Layer Deposition (ALD) offers a promising solution to enhance the oxidation and thermal resistance of CFFs by applying thin and conformal coatings. In this study, titanium dioxide (TiO<sub>2</sub>) thin films were deposited on CFFs using the thermal ALD technique to improve their thermal and oxidative stability in harsh environments [2].

#### 2. Experimental

The TiO<sub>2</sub> films were deposited on CFFs using a Beneq TFS-200 ALD system at 100°C, with TiCl<sub>4</sub> and H<sub>2</sub>O as precursors. The number of reaction cycles varied from 500 to 3000 to control film thickness. Characterization of the coated CFFs included mechanical profilometry, Field Emission Scanning Electron Microscopy (FESEM), Energy-dispersive X-ray spectroscopy (EDS), Raman spectroscopy, and X-ray diffraction (XRD). Thermogravimetric analysis (TGA) was performed under both inert (nitrogen) and oxidative (synthetic air) environments to assess the thermal and oxidation resistance.

#### 3. Results and Discussions

The TiO<sub>2</sub> coatings achieved a growth rate of 0.067 nm/cycle, resulting in amorphous films that uniformly covered the carbon fibers. TGA results indicated that the TiO<sub>2</sub>-coated CFFs showed significant improvements in thermal stability, with reduced mass loss between 600 and 900°C compared to uncoated samples. In oxidative environments, thicker TiO<sub>2</sub> coatings improved resistance to degradation, although some cracking was observed in the films. Overall, the TiO<sub>2</sub> coatings enhanced both the thermal and oxidative resistance of CFFs, demonstrating the potential of ALD for advanced textile applications.

#### 4. References

[1]- B. Jones and C. Lee, *Materials Engineering*, 22, 456-462, (2018).

[2]- P. Lin and L. Zhao, *Applied Surface Science*, 493, 1027-1033, (2022).

#### Acknowledgments

This research was funded by FAPESP, grant number 2018/01265-1, and CNPq, grant number 313482/2021-7 and 405637/2022-5. Thais Vieira thanks CAPES (Finance Code 001).

<sup>\*</sup>Corresponding author: vieira.macedothais@gmail.com

## ELECTROPHORETIC DEPOSITION OF TIO<sub>2</sub> NANOPARTICLES ON BACTERIAL CELLULOSE (BC) USING HIGH VOLTAGE BIPOLAR PULSES

Aline R. Almeida<sup>1\*</sup>, Julio César Sagás<sup>1</sup>, Cristiane Stegemann<sup>3</sup>, Jair Nunes<sup>2</sup>, Henrique de Souza Medeiros<sup>4</sup>, Luis César Fontana<sup>1</sup> and Daniela Becker<sup>1</sup>

<sup>1</sup>Laboratory of Plasmas, Films, and Surfaces, Santa Catarina State University (UDESC), Joinville, SC, Brazil

<sup>2</sup>Federal Institute of Santa Catarina (IFSC) - Jaraguá do Sul, SC, Brazil. <sup>3</sup>UniSENAI University Center - Jaraguá do Sul, SC, Brazil. <sup>4</sup>Catholic University Center of Santa Catarina - Jaraguá do Sul, SC, Brazil.

#### 1. Introduction

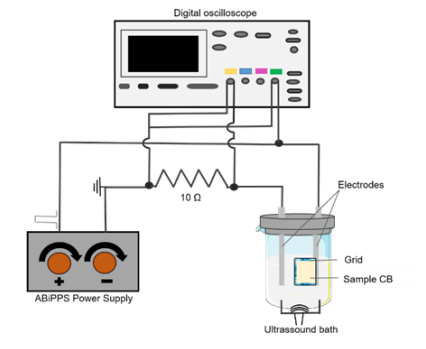
Bacterial cellulose (BC) is an environmentally friendly, biodegradable, and biocompatible raw material, similar to plant cellulose (PC), but with limitations in water affinity. To improve this characteristic, the incorporation of titanium dioxide (TiO<sub>2</sub>) is proposed due to its low cost and biocompatibility [1]. An innovative strategy involves the application of nanoparticles using modified electrophoretic deposition (EDP) [2]. This study aims to determine the optimal TiO<sub>2</sub> deposition parameters on BC and evaluate their impact on wettability.

#### 2. Experimental

A Central Composite Design (CCD) experiment was conducted with independent variables: TiO<sub>2</sub> concentration and deposition time. The dependent variable was the contact angle after drying the treated BC. The deposition used an asymmetric bipolar plasma power supply (ABiPPS), with the reactor built by the authors, as described in previous studies and illustrated in Figure 1 [3].

#### 3. Results and Discussions

The results for the contact angle are shown in Figure 2. With a variance of  $R^2 = 0.97$ , we found that the model provided good predictive capability and fit. Upon examining the results, it is evident that both time and concentration significantly influence the material's affinity for water. Specifically, as the deposition time increases, the material becomes less hydrophilic. Conversely, higher concentrations of  $TiO_2$  can enhance the hydrophilicity of the material, as demonstrated in experiment 4.



Samples	TiO <sub>2</sub> concentration (%)(m/v)	Time (min)	CA measure (°)
1	0,400 (-1)	10,00 (-1)	$13,\!6\pm0,\!1_a$
2	0,400 (-1)	20,00 (+1)	$41,1\pm0,3_b$
3	0,800 (+1)	10,00 (-1)	$20,\!4\pm0,\!2_a$
4	0,800 (+1)	20,00 (+1)	$11,\!8\pm0,\!1_a$
5	0,317 (-1,68)	15,00 (0)	$20,\!3\pm0,\!2_a$
6	0,882 (+1,68)	15,00 (0)	$13,\!5\pm0,\!4_a$
7	0,600 (0)	7,92 (-1,68)	$18,3\pm0,1_a$
8	0,600 (0)	22,07 (+1,68)	$30,7\pm0,2_b$
9 (C)	0,600 (0)	15,00 (0)	$37{,}7\pm0{,}3_b$
10 (C)	0,600 (0)	15,00 (0)	$34,1\pm0,2_b$
BC	-	-	$58,0\pm0,4_c$

**Fig. 1.** Schematic diagram of the experimental setup used

**Fig. 2.** Results of  $TiO_2$  deposition on dry bacterial cellulose (BC) and contact angle (CA)

#### 4. References

- [1]- S. Jafari et al., Int. J. Nanomedicine, 15, 3447–3470, (2020).
- [2]- K.M.K. Iwasaki et al., Appl. Surf. Sci., 611,155548, (2023).
- [3]- V. F. Dos Santos et al., J. Appl. Phys., 129, 123302 (2021).

#### Acknowledgments

The authors are thankful for the Multi-User Facility infrastructure from Santa Catarina State University's Technological Sciences Center and to the funding of CNPq (350722/2022-6) and FAPESC (2022TR001116).

<sup>\*</sup>Corresponding author: alinerosaufpr@gmail.com



## INFLUENCE OF PLASMA NITRIDING OF THE PRODUCTUVITY OF HIGH SPEED STEEL HOLE SAW

Marcos Dorigão Manfrinato<sup>1</sup>\*, Leandro Barbosa<sup>1</sup>, Leandro Almeida Silva<sup>2</sup>, Larissa Solano de Almeida<sup>2</sup>, Rogério Varavallo<sup>3</sup>, Luciana Sgarbi Rossino<sup>1,2</sup>

<sup>1</sup>Sorocaba Technological College – FATEC, Sorocaba, SP, Brazil <sup>2</sup>Federal University of São Carlos - -UFSCar, Sorocaba Campi, Sorocaba, SP, Brazil <sup>3</sup>Etec Sylvio de Mattos Carvalho, Matão, SP, Brazil

#### 1. Introduction

Hole saws, manufactured from quenched and tempered high-speed steel, are widely used in the furniture industry, industrial assemblies, and electrical installations, and in these applications, wear resistance is required to these parts. Plasma nitriding can improve the wear resistance of metals due to a formed layer of high hardness and compressive residual stresses [1]. The objective of this work is to study the influence of the plasma nitriding temperature on the drilling capacity of a bimetallic hole saw made from high-speed steel with a diameter of 37 mm.

#### 2. Experimental

The quenched and tempered (TR) hole saws were plasma nitrided at 380°C (TRN 380°C) and 450°C (TRN 450°C) for 4 hours with a gas mixture of 80% N2 and 20% H2. The microhardness profile of the saw teeth was determined, and metallographic analysis was carried out to verify the structure and thickness of the layer formed. The cutting test was performed on a bench drill with a load of 38 kgf and the time of each cut was measured until completing 100 repetitions to verify the productivity of the hole saws with and without treatment. A 3 mm thick AISI 304L stainless steel plate was used for the cutting test. The greater effectiveness of the tool is determined by the shorter time required to drill the plate.

#### 3. Results and Discussions

As shown in Fig. 1, the maximum hardness values were 720 HV, 820 HV, and 665 HV for the TR, TRN380°C and TRN 450°C samples, respectively. The nitriding temperature of 450°C decreased the material microhardness due to the dissolution of tempering carbides [2]. It did not occur at 380°C, and the nitrogen diffusion increased the microhardness of the studied material in this treatment condition. The hole saw nitrided at 380°C showed a shorter drilling time than the commercial tool, TR, as illustrated in Fig. 2. The hole saw nitrided at 450°C showed the longest drilling time, due to the lower hardness obtained. Thus, the TRN380°C condition showed the highest productivity for the hole saw application.

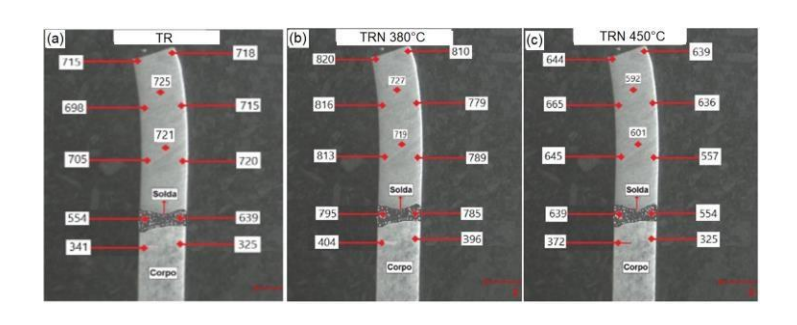


**Fig. 1.** Microhardness profile of hole saw (a) TR, (b) TRN 380°C, and (c) TRN 450°C.

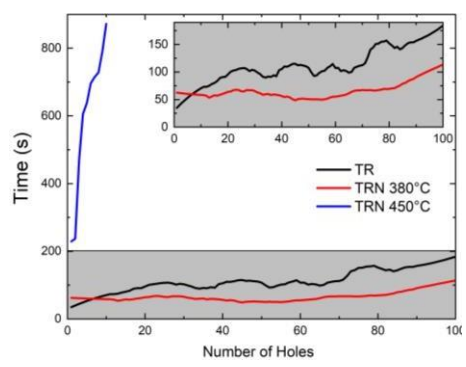


**Fig. 2.** *Drilling time at function of number of holes for treated and untreated material* 

#### 4. References

[1]- M.D. Manfrinato "Estudo do Comportamento do Aço Inoxidável Austenítico AISI 321 Nitretado e Nitrocementado a Plasma sob Solicitações de Desgaste, Corrosão e Fadiga", Tese Doutorado, UFSCar (2023).

[2]- C.E.Pinedo "Tratamento Térrmico e Superficiais dos Aços", 1º edição, Blucher, Brasil. (2021)

<sup>\*</sup>Corresponding author: marcos.manfrinato@fatec.sp.gov.br



## DEVELOPMENT AND CHARACTERIZATION OF PLASMA BORIDING TREATMENT USING TRIMETHYL BORATE

Crislaine Pereira da Rocha<sup>1</sup>, Marcos Dorigão Manfrinato<sup>1</sup>, Luciana Sgarbi Rossino<sup>1,2</sup>

<sup>1</sup>UFSCAR Campus de Sorocaba <sup>2</sup>FATEC Sorocaba

#### 1. Introduction

Titanium alloys, such as Ti6Al4V, are widely used in sectors that require corrosion resistance, biocompatibility, high rigidity, and toughness. However, this alloy presents low wear resistance that can be improved with plasma boriding treatment [1]. Boriding is a thermochemical process that introduces boron atoms into the surface of the material, forming hard and resistant layers [2]. This work aims to develop the plasma boriding treatment using trimethyl borate (TMB) as a precursor and evaluate the effect of the layer formed on the hardness and wear resistance of the Ti6Al4V alloy.

#### 2. Experimental

The plasma boriding treatment started with the plasma ablation step with 80% Ar and 20% H<sub>2</sub> for 1 hour at 730°C. After that, boriding was carried out with TMB flow of 0.2 torr for 60, 80 and 180 minutes, and 0.1 torr for 180 and 300 minutes, using a mixture of 200 sccm of N<sub>2</sub>, 200 sccm of H<sub>2</sub>, and 1 torr of Ar, at 730°C. The samples were analyzed for metallography, microhardness and, microwear tests.

#### 3. Results and Discussions

Continuous and dense layers were formed under all treatment conditions, evidencing the effectiveness of boron diffusion using TMB as a precursor (Figs. 1 and 2). A significant increase in the hardness of the borided samples was also observed with increasing treatment time (Fig. 3), with a reduction in the wear volume for all treated samples compared to the untreated material (Fig. 4). The highest wear resistance was obtained for the treatment carried out for 30 min. using 0.1 torr of TMB. Thus, it is concluded that TMB, a highly volatile, low-cost, and non-toxic organic liquid, was efficient in forming boride layers, increasing the hardness and wear resistance of the plasma borided Ti6Al7V alloy.

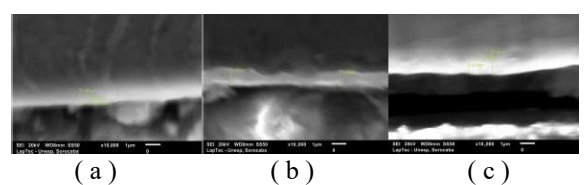
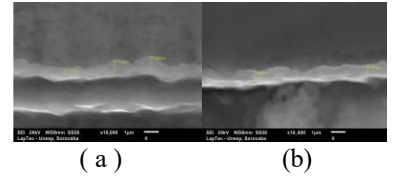
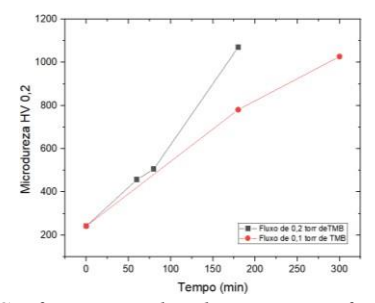


Fig. 1. Compound layer formed in plasma boriding using 0.2 torr of TMB for times of a) 60 min. b) 80 min. c) 180



**Fig. 2.** Compound layer formed in plasma boriding using 0.1 torr of TMB for times of a) 180 min. and b) 300 min.



**Fig. 3.** Surface microhardness as a function of treatment time

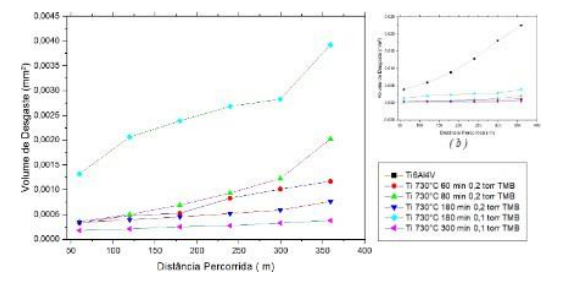


**Fig. 4.** Wear volume for a) borided samples b) Ti6Al4V samples with and without treatment

#### 4. References

[1]- MAKUCH, N. et al. Growth kinetics and mechanical properties of two-phase boride layers produced on commercially pure titanium by plasma paste boriding. Thin Solid Films, v. 626, p. 25-37, 2017.

[2]- BELKIN, K.; KUSMANOV, A. Plasma electrolytic boriding of steels and titanium alloys. Surface Engineering and Applied Electrochemistry, v. 55, n. 1, p. 1-30, 2019.

#### Acknowledgments

We would like to thank Capes (code 001)

<sup>\*</sup>Corresponding author: crislaineprocha@gmail.com



#### DEVELOPMENT OF BORON-DOPED DLC USING TRIMETHYLBORATE

Leandro Almeida Silva<sup>1</sup>, Luciana Sgarbi Rossino<sup>1,2</sup>

<sup>1</sup>UFSCAR Campus Sorocaba, <sup>2</sup>Fatec Sorocaba

#### 1. Introduction

The scientific interest in diamond-like carbon (DLC) films has increased due to their exceptional properties, such as low friction coefficient, high hardness, chemical inertness, and wear resistance. The versatility in depositing these films on metallic substrates and their various applications, such as solid lubricants and protective coatings in space environments, make them even more attractive. Additionally, their biocompatibility them to be used in orthopedic prosthetics and catheters. These properties can be improved with film doping using elements such as nitrogen, fluorine, and boron.

The objective of this work was the development of DLC films doped with boron by plasma-enhanced chemical vapor deposition (PECVD) using trimethylborate (TMB) as a precursor on titanium alloy substrates (Ti6Al4V).

#### 2. Experimental

Ti6Al4V was treated with the deposition of DLC films with and without doping with boron element. Initially, the plasma ablation process was carried out using a gas mixture of 80% Ar and 20% H<sub>2</sub> for 1 hour at 490°C. Next, a silicon-based interlayer was deposited using hexamethyldisiloxane (HMDSO) in a ratio of 70% HMDSO and 30% Ar, with a voltage of 500 V for 15 minutes at 300°C. After that, the DLC or DLC-B films were deposited. For the deposition of pure DLC, 90% CH<sub>4</sub> and 10% Ar were used, with a voltage of 500 V at 200°C for 2 hours. In the case of DLC-B, 90% CH4 and 10% Ar were used, varying the TMB pressure of 0.025 torr, 0.050 torr, and 0.075 torr, maintaining a voltage of 500 V at 200°C for 2 hours.

#### 3. Results and Discussions

The semi-quantitative composition analyses of the surface films were carried out by energy dispersive X-ray spectroscopy (EDS) via scanning electron microscopy (SEM). Tab. 1 shows the increase in the percentage of boron content with the increase in the pressure of TMB. The presence of boron content in the DLC film without doping is explained due to the similarity in the peak presence of carbon and boron. We can conclude that the TMB, a highly volatile, low-cost, and non-toxic organic liquid, was efficient in forming DLC film with the presence of boron using the PECVD technique on Ti6Al4V alloy.

Table 1 – Atomic Composition (%at) of the DLC films with end without doping with boron element							element
	TREATMENT	(% <u>at</u> )	(%at)				

TREATMENT	(% <u>at</u> ) BORON	(% <u>at</u> ) CARBON	(% <u>at</u> ) TITANIUM	(% <u>at</u> ) SILICON	(% <u>at</u> ) ALUMINUM	(% <u>at</u> ) VANADIUM
Ti6Al4V	2,6	11,4	74,9	0,2	8,6	1,9
DLC	10,7	86,8	1,5	0,5	0,2	0,1
DLC - 0,025 - TMB	6,6	92,1	0,7	0,4	0,1	0,1
DLC - 0,050 - TMB	10,4	87,2	1,1	1,0	0,1	0,2
DLC - 0,075 - TMB	9,2	79,0	7,4	3,2	0,8	0,1

#### 4. References

[1]- DANELON, M. R. Study of the effect of duplex treatments of nitrocarburizing and deposition of nitrogen and silicon-doped DLC films on the tribological properties of M2 steel. 2023.

[2]- FERREIRA, S. R. et al. Study of the influence of boron-doped DLC film at different growth voltages in PECVD system with additional cathode. Published by, v. 12328, p. 26, 2023.

#### Acknowledgments

We would like to thank Capes (code 001).

<sup>\*</sup>Corresponding author: place the e-mail of the corresponding author here (bookman old style 9 pt)



#### HEAT TREATMENT EFFECT ON THE NITRIDED LAYER OF SUPER DUPLEX STEEL

Bruna Corina Emanuely Schibicheski Kurelo<sup>1\*</sup>, João Frederico Haas Leandro Monteiro<sup>2</sup>, Francisco Carlos Serbena<sup>1</sup>, Gelson Biscaia de Souza<sup>1</sup> e Carlos Maurício Lepienski<sup>3</sup>.

<sup>1</sup>Universidade Estadual de Ponta Grossa, Ponta Grossa (PR).

<sup>2</sup>Núcleo Interdisciplinar de Dinâmica dos Fluidos, UFRJ, Rio de Janeiro (RJ).

<sup>3</sup>Universidade Tecnológica Federal do Paraná, Curitiba (PR).

#### 1. Introduction

The UNS S32750 super duplex steel is used in valves and pipelines for oil extraction in the Pre-Salt layer. An alternative to increase the wear resistance of this material without compromising its high corrosion resistance is to apply plasma nitriding treatment. The Plasma Immersion Ion Implantation (PIII) nitriding technique was used to form a nitrided layer in this material, and the thermal stability of this layer was investigated through in-situ XRD heat treatment, in a similar manner to that discussed in a previous work [1].

#### 2. Material and Methods

The samples with chemical composition measured by WDS (wt%): 61.8Fe, 25.6 Cr, 6.4Ni, 3.9 Mo, 0.8Mn, 0.3Si, 0.2 Cu, 0.03P, 1C; were cut, mechanically polished and ultrasonically cleaned. Then, PIII nitriding was performed in two steps: 1° sputtering with Ar (1.75 sccm) and H<sub>2</sub> (0.75 sccm) atmosphere at 250 °C for 20 min; 2° nitriding was carried out in N<sub>2</sub> (2.85sccm) and H<sub>2</sub> (1.90sccm) atmosphere, pressure of 3Pa, voltage of 10kV at 350 °C for 4h and these samples were named 350-4. The samples were heat treated at the XRD2 line of the National Synchrotron Light Laboratory in a furnace with an inert He atmosphere and a heating rate of 20°C/min and analyzed by in situ XRD with energy of 7kV and incidence angle fixed at 2° and 10°. The isothermal treatments were performed at temperatures of 450 °C (TT450 sample) and 550 °C (TT550 sample) for 124 and 94 min respectively. Using the Fityk software (curve fitting and peak fitting software) [2], peak deconvolution was performed with the pseudo-Voigt function. Before and after the treatments, nanoindentation tests were performed using the quasi-continuous stiffness measurement method to analyze the hardness and the maximum load used was 400 mN. The morphologies and compositions of the modified layers before and after the heat treatments were analyzed by SEM and EDS.

#### 3. Results and Discussions

The XRD analyses showed that after nitriding, in addition to the austenite and ferrite phases present in the untreated sample, the nitrogen-expanded austenite  $(\gamma_N)$ , nitrogen-expanded ferrite  $(\alpha_N)$ , and CrN phases were identified. In heat treatments, during the heating stage, it is observed in the diffractograms that the peaks related to the  $\alpha$  and  $\gamma$  phases shift to lower 20 values with heating due to the thermal expansion of the crystalline structure and consequent increase in the lattice parameter. It is also observed that the crystalline structure of the γ<sub>N</sub> phase expands thermally up to a temperature of 350 °C and, above this temperature, a reduction in the lattice parameter is observed due to the diffusion of nitrogen into the substrate. During the isothermal heating step, the gradual diffusion of nitrogen from the modified layer to the substrate continues and the lattice parameter of the  $\gamma_N$  phase decreases. As this effect occurs, the peaks related to the CrN phase become more evident and there is also a broadening of the peak associated with the  $\alpha$  phase due to the increase in the contribution of the  $\alpha_N$  phase in the diffractograms. This effect is related to decomposing the  $\gamma_N$  phase into CrN+ $\alpha$  [1]. The layer thickness of sample 350-4 was estimated to be 3.7  $\pm$  0.3  $\mu m$  in ferritic grains and  $2.9 \pm 0.4 \,\mu m$  in austenitic grains. After heat treatment, the modified layer thickness is homogenized between the different grains. In sample TT450, the layer thickness was estimated at  $5.1 \pm 0.2$  $\mu m$ , and with the increase in the treatment temperature to 550 °C (TT550), the layer thickness increased to  $5.9 \pm 0.7$ . The SEM-EDS analyses on the cross sections of the modified layers indicate a reduction in the N concentration at the surface and an increase in the thickness of these layers after the heat treatments. In the nitrided sample, the hardness values reach 15 GPa, while after heat treatments, according to EDS and XRD analyses, the hardness values close to the surface become lower.

#### 4. References

[1]-Kurelo, B. C. E.S, Lepienski, C. M., et. al., Metals, 13, 1744, (2023).

[2]- Wojdyr, M. Fityk: J. Appl. Crystallogr., 43, 1126–1128, (2010).

#### Acknowledgments

This work was part of the NESAP project (PRONEX CNPq/Fundação Araucária 15/2017). The authors thank the CAPES for the postdoctoral research scholarship and the LNLS for the synchrotron XRD analyses (proposal 20190153).

<sup>\*</sup>Corresponding author: bruna\_schibicheski@hotmail.com.

## STUDY OF THE EFFECT ON TRIBOLOGICAL BEHAVIOUR OF VARYING THE CHEMICAL COMPOSITION OF THERMOCHEMICAL TETRABORATE IN AISI 420 STEEL

Jucielton Alves Batista<sup>1</sup>, Leandro Almeida Silva<sup>2</sup>, Marcos Dorigão Manfrinato<sup>2</sup>, Luciana Sgarbi Rossino<sup>2</sup>, Rogério Varavallo<sup>1</sup>

<sup>1</sup>Escola Técnica Estadual Sylvio de Mattos Carvalho, ETEC <sup>2</sup>Faculdade de Tecnologia de Sorocaba, FATEC

#### 1. Introduction

AISI 420 martensitic steel is widely used in the production of polymer injection moulds and in glass moulding. This type of steel combines high hardness with resistance to corrosion. The boriding heat treatment process is a technique used to increase the wear and corrosion resistance of metal surfaces[1]. It involves the diffusion of boron atoms into the surface of the metal, creating a protective layer of borides[2]. This layer significantly improves the material's mechanical properties, such as resistance to abrasion and oxidation at high temperatures. The treatment is carried out in specific furnaces, where the parts are subjected to high temperatures, usually between 800°C and 1000°C. The research aims to analyse the behaviour of AISI 420 steel in the boriding process.

#### 2. Experimental

AISI 420 stainless steel was used in this work. The materials were cut to 26x26x12 mm and heat-treated at 950°C for 5 hours in different chemical compositions of tetraborates. Microstructural analyses were carried out using scanning electron microscopy, energy dispersive spectroscopy, wear tests and microhardness tests. Table 1 shows the compositions used.

rable 1 - Spraying agents, temperature and treatment time					
Temperature	re Time Buttering Agent				
950°C	5 Horas	25% Na <sub>2</sub> B <sub>4</sub> O <sub>7</sub> – 10H <sub>2</sub> O desidratado + 75% SiC			
		50% Na <sub>2</sub> B <sub>4</sub> O <sub>7</sub> – 10H <sub>2</sub> O desidratado + 50% SiC			
		75% Na <sub>2</sub> B <sub>4</sub> O <sub>7</sub> – 10H <sub>2</sub> O desidratado + 25% SiC			
		10% Na <sub>2</sub> B <sub>4</sub> O <sub>7</sub> – 10H <sub>2</sub> O desidratado + 90% SiC			

Table 1 - Spraying agents, temperature and treatment time

#### 3. Results and Discussions

Figure 1 shows the results of the wear test for all the materials studied. The material with the best wear resistance was EKBOR, due to the formation of precipitates in the heat treatment.

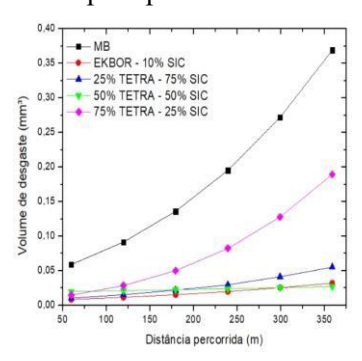


Figure 1 - Wear test, all samples..

#### 4. References

[1] Silva, R. F., & Gomes, P. H. (2016). Tratamento térmico por boretação: Aplicações e vantagens. Revista de Engenharia Metalúrgica, 29(2), 112-118.

[2] Oliveira, L. M. (2019). Processos de boretação em materiais metálicos. Jornal de Ciência dos Materiais, 52(1), 68-75.

#### Acknowledgments

Thanks to the paula souza centre, especially FATEC Sorocaba.

<sup>\*</sup>Corresponding author: place the email of the corresponding author here (bookman old style 9 pt)



#### CHARACTERIZATION OF Ti-Nb-Mo COATINGS DEPOSITED ON STAINLESS STEEL

Bruno B. Aquino<sup>1\*</sup>, Angelo L. Gobbi<sup>2</sup>, Abner de Siervo<sup>3</sup>, Pedro A. P. Nascente<sup>1</sup>,

<sup>1</sup>Federal University of Sao Carlos, Graduate Program in Materials Science and Engineering, 13565-905, Sao Carlos, SP, Brazil.

<sup>2</sup>Brazilian Center for Research in Energy and Materials, Brazilian Nanotechnology National Laboratory, 13083-970, Campinas, SP, Brazil.

#### 1. Introduction

 $\beta$ -Ti-based alloys are widely studied in biomaterials due to their biological performance in the body. This  $\beta$  (BCC) phase can be stabilized by the addition of alloying elements such as Nb, Zr, Ta, or Mo. Ti-Nb-Mo alloys are biocompatible and have low elastic modulus, high strength, shape memory behavior, and high corrosion resistance [1]. Ti-based alloys in the form of coatings have been investigated for improving the biocompatibility and mechanical properties of the AISI 316L stainless steel (SS), which is commonly used as implant material [1]. In this study, three Ti-Nb-Mo coatings were deposited on AISI 316L SS substrates by magnetron sputtering, and the effects of Mo content on the phase formation, morphology, and surface composition were evaluated.

#### 2. Experimental

Ti, Nb, and Mo disks with a 2-inch diameter, 3 mm thickness, and 99.99% purity were used as targets. For the substrates, 15 mm diameter disks made of 3 mm thick AISI 316L SS were utilized. An AJA Orion 8 Phase II J magnetron sputtering system was employed to deposit three coatings with different compositions. Mechanical characterizations were carried out by nanoindentation tests. Chemical and structural characterizations were carried out by X-ray fluorescence spectroscopy (XRFS), energy dispersive X-ray spectroscopy (EDS), X-ray diffraction (XRD), scanning electron microscopy (SEM), and X-ray photoelectron spectroscopy (XPS).

#### 3. Results and Discussions

Elemental analysis by XRFS and EDS determined the following compositions (at%): Ti<sub>78</sub>Nb<sub>15</sub>Mo<sub>7</sub>, Ti<sub>74</sub>Nb<sub>14</sub>Mo<sub>12</sub>, and Ti<sub>72</sub>Nb<sub>13</sub>Mo<sub>15</sub>. Fig. 1 displays the XRD diffractograms for the three coatings, revealing a predominance of the β phase with a minor contribution of the α (HCP) phase. SEM microstructural analysis indicates that the coatings are homogeneous and continuous. Fig. 2 shows a cross-section micrograph for the Ti<sub>78</sub>Nb<sub>15</sub>Mo<sub>7</sub> coating. Nanoindentation test results revealed that all three coatings had higher hardness than AISI 316L SS and lower elastic moduli than AISI 316L SS. Surface analysis by XPS indicated the formation of oxidized surface layers on the coating, comprising mainly of TiO<sub>2</sub>, Nb<sub>2</sub>O<sub>5</sub>, and MoO<sub>3</sub>. These oxidized surface layers are highly advantageous for implant materials since they provide greater corrosion protection.

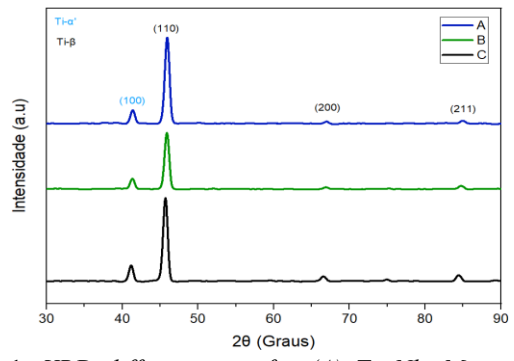


**Fig. 1.** XRD diffractogram for (A)  $Ti_{72}Nb_{13}Mo_{15}$ , (B)  $Ti_{74}Nb_{14}Mo_{12}$ , and (C)  $Ti_{78}Nb_{15}Mo_7$  coatings.

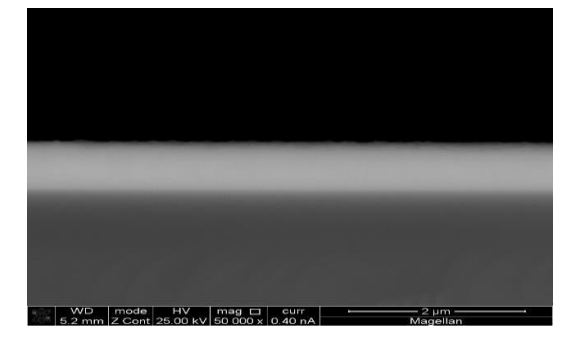


**Fig. 2.** *SEM cross-section micrograph for the* Ti<sub>78</sub>Nb<sub>15</sub>Mo<sub>7</sub> *coating*.

#### 4. Reference

[1] E.D. Gonzalez et al., Thin Solid Films, **721**, 138565 (2021).

#### **Acknowledgments**

This work was supported by FAPESP (process 2017/25983-8), CNPq (process 302450/2017-3), CAPES (Finance Code 001), and CNPEM/LNLS.

<sup>&</sup>lt;sup>3</sup> University of Campinas, "Gleb Wataghin" Institute of Physics, 13083-859, Campinas, SP, Brazil.

<sup>\*</sup>Corresponding author: brunoba@estudante.ufscar.br

## ELECTROSPINNING TO OBTAIN POLYETHYLENE OXIDE AND ZEIN NANOFIBERS LOADED WITH SILVER NANOPARTICLES OBTAINED BY GREEN SYNTHESIS

Matheus Vinicius de Oliveira Brisola Maciel<sup>1,2,3</sup>, Aline R. Almeida<sup>4</sup>\*and Pedro Luiz Manique Barreto<sup>1</sup>

<sup>1</sup>Department of Food Science and Technology, Graduate Program in Food Science, Federal University of Santa Catarina (UFSC), Florianópolis, SC, Brazil

<sup>2</sup>Catholic University Center of Santa Catarina - Joinville, SC, Brazil.

<sup>3</sup>Bom Jesus Lutheran Higher Institute and Educational Center (IELUSC), 89221-665 Joinville, SC, Brazil

<sup>4</sup>Laboratory of Plasmas, Films, and Surfaces, Santa Catarina State University (UDESC), Joinville, SC, Brazil

#### 1. Introduction

Electrospinning is a technique that produces micro or nanometric fibers from polymer solutions. Several polymers are used in this process. Research focuses on the incorporation of active ingredients such as fungicides, antimicrobials and antioxidants for applications in agriculture and the food industry [1].

#### 2. Experimental

Polymeric solutions were prepared with PEO and zein at different concentrations and molar mass. AgNPs at 2% (w/w) were added and the solution parameters were evaluated. The electrospinning voltages ranged from 7.33 to 9.5 kV. The presence and distribution of AgNPs in the nanofibers were confirmed by transmission electron microscopy (TEM).

#### 3. Results and Discussions

Increasing the polymer molar mass increased the consistency index and all solutions exhibited pseudoplastic behavior. The addition of AgNP and zein increased the electrical conductivity, and lower voltages were required for solutions with 1000 kDa PEO (Fig. 1). The nanofibers obtained with PEO or PEO/AgNP were uniform and smooth, with diameters between  $335.9 \pm 1.7$  and  $843.1 \pm 6.1$  nm. The zein nanofibers were more irregular, with no visible interference from AgNPs, which, according to TEM analysis, were concentrated at some points along the fibers (Fig. 2).

	Amostra	Diâmetro±desv. Padrão (nm)	Voltagem (kV)	Fluxo (mL/h)	Distância (cm)
1	PEO1	745,4±6,4	7,33	1,0	12
2	PEO1/AgNP	$843,1\pm6,1$	7,33	1,3	12
3	PEO1/Z	$765,5\pm7,6$	7,33	0,7	12
4	PEO1/Z/AgNP	$688,1\pm7,1$	7,33	0,7	12
5	PEO5	$570,8\pm14,5$	8,52	1,0	14
6	PEO5/AgNP	$335,9\pm1,7$	8,52	1,0	14
7	PEO5/Z	$870,7\pm19,2$	9,50	1,0	12
8	PEO5/Z/AgNP	822,8±9,6	7,33	1,0	14

**Fig. 1.** Results for the average diameters of nanofibers and their electrospinning parameters

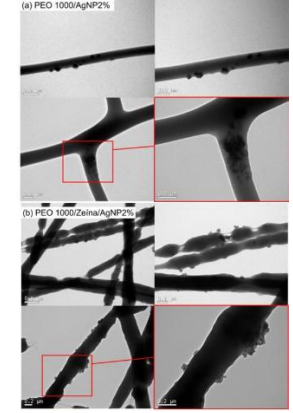


**Fig. 2.** (a) Nanofibers with PEO 1000 kDa and impregnated with AgNP 2% (b) Nanofibers with PEO 1000 kDa, zein 10% and AgNP 2%

#### 4. References

[1]-R. ASMATULU and W. S. KHAN, Synthesis and Applications of Electrospun Nanofibers, p.89–109. (2019).

#### Acknowledgments

The LCME - Central Laboratory of Electron Microscopy. CAPES.

<sup>\*</sup>Corresponding author: alinerosaufpr@gmail.com







# XLV Congresso Brasileiro de Aplicações de Vácuo na Indústria e na Ciência

Balneário Camboriú - SC 11 a 13 de Novembro de 2024

